Steam Reheat in Nuclear Power Plants

A Dissertation Presented for the
Doctor of Philosophy
Degree
The University of Tennessee, Knoxville

Paul John Marotta
December 2012

Acknowledgements

I would like to thank everyone that supported the pursuit of this work at the expense of other priorities.

First and foremost, thank you to my wife Margaret, and also my children Katie, Nick, Molly, Adam and Grace, to whom I am grateful for their understanding through this extensive process. I only hope that my endeavor somehow inspires them to follow their dreams.

Thank you to Dr. Basil Antar, my mentor and major professor throughout this process. Hopefully he has enjoyed working with me as much as I with him. To my committee lead by Dr. Antar, Dr. Trevor Moeller, Dr. Arthur Ruggles and Dr. Christian Parigger, I truly appreciate your time investment, guidance and commitment to my learning process.

Finally, thank you to my current employer Mike Corn, President of AquAeTer Inc., for providing the flexibility in my work life to pursue this important personal goal.

You all have played a supportive role in this accomplishment.

Abstract

In this work, reheating steam from a commercial nuclear power plant is explored in order to increase efficiency and power output. A thermal source in the form of a High Temperature Gas Reactor (HTGR) is considered. Engineering challenges include proof-of-principle, reactor sizing, evaluation, and feasibility.

The proposed thermodynamic process modifications have been evaluated for a range of inlet steam quality conditions. The evaluation of the steam tube dimensions and number of optimal tubes have been calculated utilizing the so-called Log Mean Temperature Difference method. Subsequently, the performance of the steam tubes was further analyzed within a water vapor and liquid fluid model to investigate two phase boiling flow thermal phenomena. Detailed calculations include a non-uniform axial heat flux distribution based on published results for the tri-structural isotropic fuel system. Non-uniform axial heat flux served as the non-uniform heat source boundary condition in the computer model for the High Temperature Gas Reactor. The calculations validate improvement in system thermal performance. Moreover, thermal radiation transport between the tube wall surface and the steam flow was evaluated for optically thick steam.

The work shows that the proposed modifications are not only feasible but also show increase of the power cycle efficiency of over 10%. Significant improvement is concluded for power output and exergy in the amount of over 50%.

Table of Contents

List of Tables

List of Figures

Abbreviations and Symbols

* (superscript)	Property associated with the bulk interface
$^{`}$ (superscript)	Property associated with the wall or boundary layer
A	Area, (m^2)
^{B} (superscript)	Bulk flow
B_x	Body force in the x-direction, (m/s^2)
C	Coefficient of virtual mass, (1/K·s)
^{o}C	Temperature, degrees Celsius
c_p	Heat capacity, (kJ/kg K)
D	Inside tube diameter, (m)
DISS	Energy dissipation function, (W/m^3)
E_b	Black body emissive power in a vacuum, (W/m^2)
f	Friction factor
FIF, FIG	Interphase drag coefficients (liquid, vapor), (s^{-1})
$\boldsymbol{\mathcal{F}}_{\nu}$	Radiant energy flux vector, (W/m^2)
FWF, FWG	Wall drag coefficients (liquid, vapor), (s^{-1})
g	Gravitational field vector, (m/s^2)
G	Mass flux, (kg/m^2 s)
GW_{th}	Thermal Power Output, (GW, Giga Watts)
g (subscript)	Gas or Vapor
$h_{\#}$	Enthalpy at state #, (kJ/kg)
$I_{b,\nu}$	Intensity of radiation of a black body, (W/μm sr m^2)
$_{il}$ (subscript)	Interface, liquid phase
$_{ig}$ (subscript)	Interface, gas/vapor phase
I_{ν}	Intensity of radiation, (W/μm sr m^2)
K	Absolute Temperature, (Kelvin)
k	Thermal conductivity, (W/m K)
k_r	Steam thermal conductivity (Rosseland Approx.), (W/m K)
k_{steam}	Steam thermal conductivity, (W/m K)

k_{total}	Total steam thermal conductivity, (W/m K)
l (subscript)	Liquid
ℓ	Length of tube element, (cm)
L	Tube length, (m)
□	Mass flow, (kg/s)
n	Surface normal vector
N	Number of tubes
Nu_D	Nusselt Number
n_ω	Index of refraction for frequency range
P	Normal pressure stress component or pressure, (Pa)
$P(z)$	Power Density at location z, (W/cm^3)
P_{avg}	Average Power Density, (W/cm^3)
$PF(z)$	Power Factor at location z (non-dimensional)
Pr	Prandtl Number
Q	Volumetric heat addition rate, (W/m^3)
Q	Heat transferred to the steam, (kJ/s)
q”	Heat flux, (kJ/kg cm^2)
Q_{in}	Total Heat Input, (kJ/s)
r	Spatial dimension in cylindrical radius direction, (m)
Re	Reynolds Number
s	Unit vector in the direction of the pencil rays
S	Control volume surface, (m^2)
^{s} (superscript)	Saturated conditions at local thermodynamic pressure
T	Absolute Temperature, (Kelvin)
T_c	Local Temperature of the steam, (K)
T_h	Local Temperature of nuclear fuel, (K)
u	Internal Energy (specific), (kJ/kg)
U	Overall heat transfer coefficient, (kJ/s K m^2)
ω	frequency, (s^{-1})

V	Control volume, (m^3)
$\boldsymbol{v}$	Velocity, (m/s)
$\vec{v}_k$	Phase *k* velocity, (m/s)
^{w} (superscript)	Wall or boundary layer
$_{wl}$ (subscript)	Wall, liquid phase
$_{wg}$ (subscript)	Wall, gas/vapor phase
W_{net}	Net Work Output from system, (kJ/s)
x	Steam quality, (fraction)
x	Spatial dimension in x-direction, (m)
Z	Non-dimensional axial location
z	Axial dimension, (cm)
z_{max}	Maximum axial dimension, (cm)
α	Void fraction
β_R	Rosseland mean extinction coefficient, $(atm \cdot m)^{-1}$
$\beta_{\boldsymbol{u}}$	Mean extinction coefficient, (m^{-1})
Γ	Interfacial mass transfer, (kg/s)
ΔT	$T_h - T_c$, (K)
ε	Wall vapor generation/condensation flag
η	Bulk saturation enthalpy flag
$\eta_{thermal}$	Thermodynamic power cycle thermal efficiency
θ	Non –dimensional temperature, (T (K) / 555)
μ	Viscosity, (kg/m s)
ρ	Density, (kg/m^3)
σ	Stefan-Boltzmann constant, 5.6704E-8 ($W/m^2\ K^4$)
$\boldsymbol{\tau}$	Surface shear stress component, (Pa)
$\boldsymbol{\psi}$	Exergy (specific), (kJ/kg)
Ω	Solid Angle, (sr)
ΔT_1	$T_{hi} - T_{ci}$, (K)
ΔT_2	$T_{ho} - T_{co}$, (K)

Chapter 1

Introduction and Problem Definition

The objective of this research is to attain improved thermodynamic power cycle efficiency for commercial Pressurized Water Reactors (PWR); or, Boiling Water Reactors (BWR) with the addition of steam "reheat". The Problem Definition: "Investigate the integration of a state-of-the-art High Temperature Gas Reactor (HTGR) and fuel system as a steam reheat thermal source, and quantify the resulting thermodynamic power cycle improvements."

HTGR technology will be used to "reheat" steam generated from commercial Pressurized Water Reactor (PWR), or, Boiling Water Reactor (BWR), nuclear power plants to attain improved thermodynamic power cycle efficiency. Similar reheat processes are already in use successfully in modern fossil fire power plants (Bendixen 2003) resulting in higher thermodynamic power cycle efficiency (Iwamoto 2001), and reduced maintenance and operational issues due to the resulting improvements in steam conditions (Jonas 2008). The HTGR is capable of producing gas temperatures in excess of 1000^{o}C (Ball 2010). This is made possible primarily with the use of newly developed nuclear fuel systems. The TRi-structural ISOtropic (TRISO) fuel system, for example, is capable of withstanding temperatures in excess of 1600^{o}C without fuel failure and subsequent release of fission products. TRISO fuel is comprised of small (0.9 mm in diameter) spherical fuel "micro-spheres" encapsulated with a high temperature resistance pyrolytic and silicon carbide coatings. The fuel pellets can then be compressed into fuel "compacts" and arranged in larger fuel assemblies which can be placed as required by the

specific reactor design. Such a new fuel technology provides the ability to achieve temperatures in the range of modern fossil fuel fired power plants. As a result, such high temperatures provide the opportunity for boosting the maximum thermodynamic power cycle efficiencies up to the order of 50% (Leizerovich 2005). Commercial PWR and BWR thermodynamic power cycle efficiencies are usually in the range of 30% to 35% (Leizerovich 2005). Therefore, a significant thermal efficiency performance improvement opportunity of >40% exists.

The current HTGR designs are in the conceptual and initial testing phases (Ball 2010). The designs incorporating the TRISO fuel system utilize helium as the primary heat transfer fluid. The helium flows through the HTGR reactor core achieving temperatures >1000^{o}C. The high temperature helium flow is then used to generate electric power and process heat. Helium is preferred in the new HTGR designs due to its inherently inert, non-corrosive, chemical qualities. Helium is also very expensive and in short supply

This research focuses on using steam generated from a commercial PWR or BWR as the primary heat transfer fluid in the HTGR. This concept represents a significant departure from the typical HTGR design, however, reheat processes in use in modern fossil fuel fired power plants are currently in operation successfully at these high temperatures using steam (ASME 2010). Based on the significant opportunity for thermal power cycle improvement, this novel reheat concept will now be further developed.

The Rankine Power Cycle with Reheat

Figure 1 illustrates a comparison of the typical Rankine steam power cycle with reheat (blue), and without reheat (red). The reheat process is initiated at state point (**1**), which is schematically representative of typical PWR/BWR steam. The HTGR is utilized as the reheat thermal source to increase the steam temperature beyond the saturated region and into the superheated region to state point (**1'**).

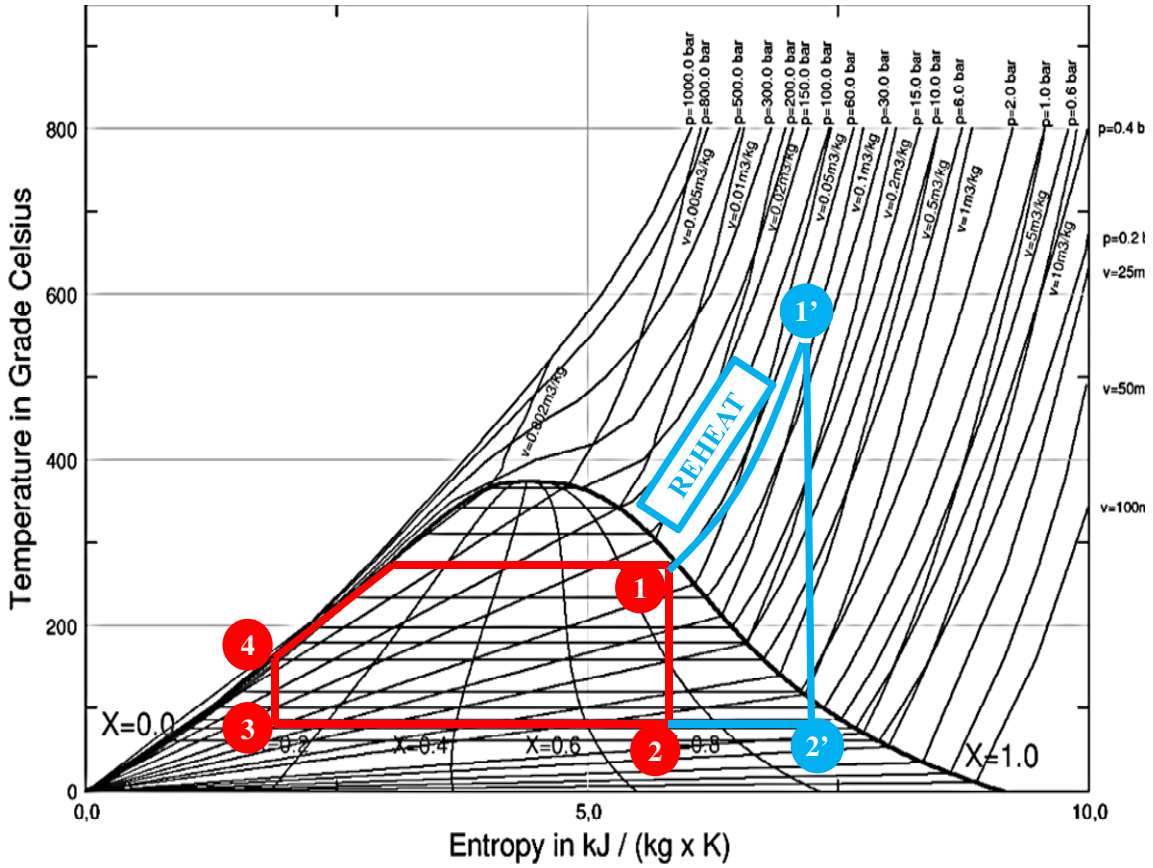

Figure 1. Rankine Power Cycle with Reheat-Superheat Illustrated on a T-S Diagram (Wikimedia)

The addition of superheating to the power cycle accomplishes two very significant improvements. First, as can be seen, state (**1'**) is at an increased temperature,

which increases the overall thermodynamic efficiency. Second, it results in a super-heated state with less opportunity for liquid droplet formation as the steam expands across the multiple stages of the steam turbine. High moisture (low "quality") steam flows, characteristic of commercial PWR and BWR power plants, require more attention and design consideration since the droplets are propelled by the steam flow at very high velocities (Jonas 2008) increasing the potential for erosion. It should be noted that the turbine expansion and pump compression are assumed to be isentropic processes for illustrative purposes.

The change in state from liquid water through saturated water to saturated vapor is denoted as the change from state **(4)** to state **(1)**. The steam expands across the multiple stages of the steam turbine generator, and is represented by changing from states **(1)** to **(2)**. Mechanical work (W) is extracted in this process, and W drives the electrical generator. Residual heat is removed and rejected to the environment in the condenser. The steam vapor is condensed from the vapor to the liquid phase as illustrated in states changing from **(2)** to **(3)**. The liquid is pumped back up to the working pressure, states **(3)** to **(4)**, completing the cycle.

The heat rejection temperature at state **(2)** is typically set by the local environmental conditions. The state **(2)** temperature approaches either the ambient air temperature, if cooling towers are utilized for heat rejection, or, the ocean, river, or, the lake water temperature if a heat exchanger is used for heat rejection. Since the temperature at state **(4)** is also dependent on the heat rejection temperature, state **(2)**, and

the energy input from the pump to raise the working fluid pressure, the overall thermal efficiency is essentially determined by the maximum temperature in the cycle, state **(1)**.

The following data presented in Table 1 quantifies typical steam properties defined by the thermodynamic states found in modern steam plant designs including information from boiler and steam turbine manufacturers. Conditions are provided for the boiler super heater outlet (boiler manufacturer), High Pressure (HP) steam turbine inlet (steam turbine manufacturer), reheat section outlet (boiler manufacturer) and inlet to the Intermediate Pressure (IP) and Low Pressure (LP) steam turbines.

Table 1. Reheat Process

State Point	Boiler Designer/Manufacturer	Temperature (degree C)	Pressure (MPa)	Reference
1 - Boiler Superheater Outlet	Mitsubishi (CFE Pacifico 700 MW)	542	25.1	(Fujita 2010)
	Babcock-Hitachi K.K.(Tachibana-Wan Thermal Power Station No.2 - 1,050 MW)	600	25.0	(Iwamoto 2001)
	American Electric Power and Babcock and Wilcox (Superheater upgrade 250 MW)	566	15.9	(Planta 1997)
	Foster-Wheeler Benson Vertical Tube	540	24.1	(FosterWheeler 2002)
1 - HP Steam Turbine Inlet Steam	General Electric	593	31.0	(Retzlaff 1996)
	Siemens-Westinghouse	600	25.4	(Hurd 2005)
1' - Reheat Outlet	Mitsubishi (CFE Pacifico 700 MW)	568	-	(Fujita 2010)
	Babcock-Hitachi K.K.(Tachibana-Wan Thermal Power Station No.2 - 1,050 MW)	610	-	(Iwamoto 2001)
	American Electric Power and Babcock and Wilcox (Superheater upgrade 250 MW)	566	3.62	(Planta 1997)
	Foster-Wheeler Benson Vertical Tube	568		(FosterWheeler 2002)
1' - IP/LP Turbine Inlet Steam	General Electric	621	-	(Retzlaff 1996)
	Siemens-Westinghouse	600	-	(Hurd 2005)

(Retzlaff 1996; Planta 1997; Iwamoto 2001; FosterWheeler 2002; Hurd 2005; Fujita 2010)

Boiler and turbine designers manufacture equipment to fit design target ranges of capability so that they can be integrated into a variety of different power plant design scenarios. Design data from both turbine and boiler design/manufactures is presented in Table 1 to illustrate this point for a couple of examples. As mentioned previously, steam enters the high pressure turbine and work is extracted. This extraction process results in the steam exiting the high pressure turbine at a lower energy level (temperature, pressure and enthalpy). The exact state of the exiting steam depends on the specific turbine design (i.e., number of turbine stages in the HP turbine), and condenser conditions. For the purposes of this analysis, the exact exiting steam conditions are not critical to the reheat concept discussion. Based on the data provided in Table 1, a reasonable benchmark steam condition to consider exiting the boiler superheater section and entering the HP turbine is 600 ^{o}C and 28 MPa. This steam condition is referred to as ultra-supercritical (USC) (ASME 2010). The term being used to describe power plant designs with HP turbine steam inlet temperature to the between 700 and 760 ^{o}C is Advanced Ultra-Supercritical (A-USC). Conditions beyond USC are not considered in this study.

Reheat Applied to Nuclear Power Cycles

This section describes the most prevalent commercial nuclear power cycles, identifies how the reheat concept could be applied to the power cycles, and finally, describes the benefits of this application. The development of nuclear power plants has occurred over the past fifty years and has encompassed a design evolution that has been characterized as Generations I through IV. Most of the Generation I designs are no

longer operating and were designed in the 1950 to 1960 time frame (Article 2011). Generation II reactors represent the majority of the reactors in operation today, and ~85% of their designs are similar to those developed for use on large naval ships and submarines. Generation III and III+ are considered the advanced reactor designs. A few are currently in operation in Japan, and several are under construction worldwide. The Generation III reactor designs include many safety and efficiency improvements such as passive natural circulation cooling system designs, simplified standardized designs for expedited licensing, and 60 year operating life (Article 2011). The Generation IV designs are still in the conceptual and early design/testing feasibility phases. The following provides an overview of the generic PWR and BWR designs. In concept, this overview is sufficient for a basic understanding of reactor designs up to and including Generation III designs.

Nuclear Power Cycles – Pressurized Water Reactors and Boiling Water Reactors

The Pressurized Water Reactor (PWR) and Boiling Water Reactor (BWR) power plants utilize heat generated from the nuclear fission process to produce steam. For commercial nuclear power plants, the steam is used to drive a turbine generator to produce electric power. Figure 2 illustrates the main components employed by the PWR and BWR commercial designs, with the addition of the HTGR thermal source for reheat.

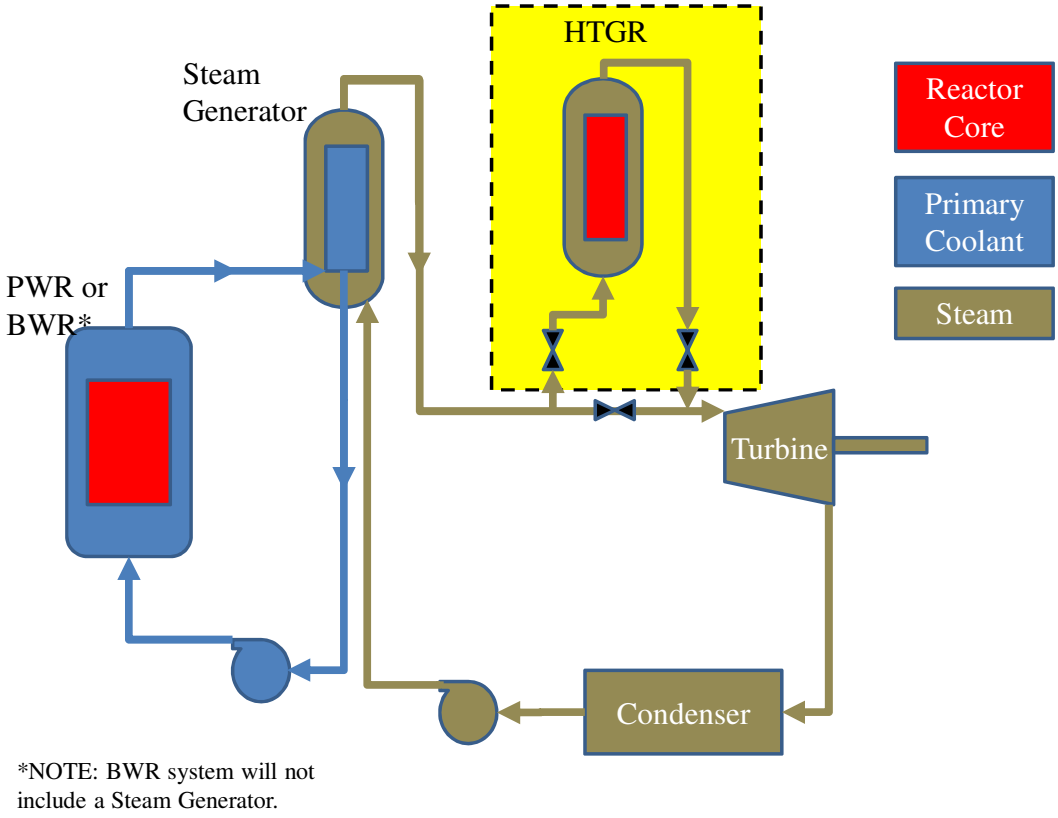

Figure 2. PWR/BWR Power Cycle Schematic with HTGR Reheat

The primary coolant, water, is circulated through the core by the reactor coolant pump (RCP), where the fission heat is removed from the reactor core raising the primary coolant temperature. The high temperature primary coolant passes through the steam generator (S/G) tubes where it indirectly heats the feedwater in the S/G. The primary coolant exits the S/G at a lower temperature and returns to the RCP to complete the primary coolant circuit. The heat input to the S/G results in the formation of steam.

Steam exiting the S/G enters the turbine generator and produces electricity. Therefore, for the PWR, there are the primary and secondary (steam) fluid circuits.

The BWR design, utilizes a single fluid circuit. The pressure is somewhat lower in the BWR system, about half, allowing liquid in the BWR to reach boiling conditions within the reactor while sustaining the fission reaction. This eliminates the secondary S/G circuit. Steam produced, within the BWR, is processed by moisture separators and dryers within the reactor vessel. The steam is then utilized in the turbine generator in the same manner as the PWR. The important point here is, regardless of reactor design, PWR or BWR, the steam produced is essentially at the same thermodynamic state (temperature and pressure).

As discussed previously, the overall thermal efficiency of either PWR or BWR is set based on the practical upper temperature, T_H. For light water reactors of either PWR or BWR design, the water is required to be in liquid form in the main fuel region to act both as an effective neutron moderator, for maintaining the fission reaction, and to effectively remove heat from the reactor core fuel region. The critical temperature for water is 375 ^{o}C (Knief 1992). Above this temperature, regardless of working pressure in the reactor, the sub-cooled liquid condition could not exist in the core fuel region. The fission process and effective heat removal would not be sustained. Therefore, the light water reactor T_H is set by this fact.

The reactor core temperature is also limited based on the specific materials utilized to construct the fuel matrix and the core structure. The nuclear fission heat generated as a result of the neutrons interacting with fissionable material, typically

enriched uranium, is generated within an enclosure that separates the fissile material from the reactor coolant water. This enclosure is typically a long cylindrical shape and is referred to as a fuel rod. The fuel rod contains fuel pellets comprised of the uranium fuel material. As the fissions occur, radioactive daughter fission products are produced. The purpose of the fuel rod is to prevent the fuel and fission products from being released into the reactor coolant. Radioactive materials released to the coolant are circulated throughout the coolant circuit and can produce areas of high radiation dose rate. The radiation dose rate of the power facilities employees is controlled by shielding, distance and time of exposure. In high dose rate areas, routine maintenance activities become very challenging to plan and execute, and result in higher costs. Some high dose rate areas preclude human activity, and robotic equipment (Moore 1985) is relied upon to perform maintenance and repair activities. Consequently, the design of the fuel rod must accomplish containment of the radioactive materials while at the same time maximize the heat transfer from the fission process to the reactor coolant. These competing design objectives result in limiting the maximum nuclear power cycle temperature to 290 ^{o}C (Knief 1992). Based on previous discussions, this is less than half the maximum fossil fueled power cycle temperature of 600 ^{o}C. Many improvements have been made in the reactor core design in order to increase the T_H such as improved fuel systems, metallurgy and fabrication techniques. Even though there may be future improvement opportunities in the core design area, results will most likely provide incremental improvements.

The steam properties for conditions at state points **(1)** and **(1')** are compared in Table 2.

Table 2. Steam Conditions at States **(1)** and **(1')**(Holman 1980)

		T	P	h	u	spec.vol.	s	Deg. Superheat
State Point	Condition	(^{o}C)	(MPa)	(kJ/kg)	(kJ/kg)	(cm^3/g)	(kJ/kg^{o}K)	(^{o}C)
1	Saturated	295	8.0	2758.0	2569.8	23.5	5.7432	0
1'	Superheated	600	8.0	3642.0	3254.4	48.5	7.0206	305

The potential improvement opportunity is to increase the actual power cycle thermodynamic efficiencies of 30 to 35% for PWR/BWR power plants, to the range of 45 to 50% for modern fossil fuel power plants (Naidin 2009). The objective of this research is to determine the feasibility of capturing this thermodynamic power cycle efficiency improvement with the application of the HTGR reheat concept from a thermodynamic, heat transfer and fluid mechanics standpoint.

Beyond the benefits of improved thermodynamic power cycle efficiency, are the improvement opportunities in the areas of operations, maintenance and design. The challenges associated with "wet" steam nuclear turbines are well documented (Leizerovich 2005). Training programs designed to educate technicians are very clear to point out the differences between wet nuclear and dry fossil steam turbine designs (Zirn 2008). High moisture content of steam is cited as a root cause for steam turbine flow-accelerated corrosion, for example (Jonas 2008). New computational models are being used to analyze designs to minimize degradation of the later stages of nuclear power plant turbines such as hollow stationary blades with suction slots (TAN 2009).

HTGR Technology – Application to the PWR/BWR Reheat Process

The opportunity for improving power cycle thermodynamic efficiency and eliminating the operational disadvantages due to wet steam in a PWR/BWR is significant. The concept proposed in this study is the reheat of wet steam generated by a PWR or BWR using a Generation IV High Temperature Gas Reactor (HTGR).

The new nuclear reactor power plant designs are referred to as Generation IV (Article 2011), since they are considered the fourth significant iteration of power plants utilizing heat from the uranium fission process. There are many design variants currently in different stages of development (Article 2011); however, a consistent theme within the designs is the objective of increasing the working fluid maximum temperature in order to achieve the efficiency and operational improvements that result.

The HTGR design selected for consideration as a basis to develop the integrated reheat concept is the modular HTGR. Its modular design fits the overall concept of either retrofitting an existing PWR/BWR power plant with the HTGR, or, adding it to the design of a new Generation III reactor plant which are currently being constructed internationally and are currently planned for the United States. The modular HTGR design features are illustrated schematically in Figure 3.

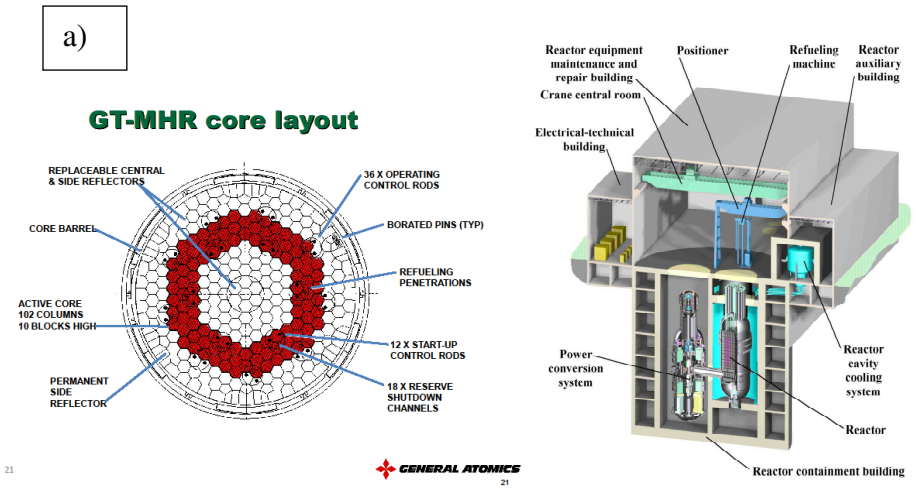

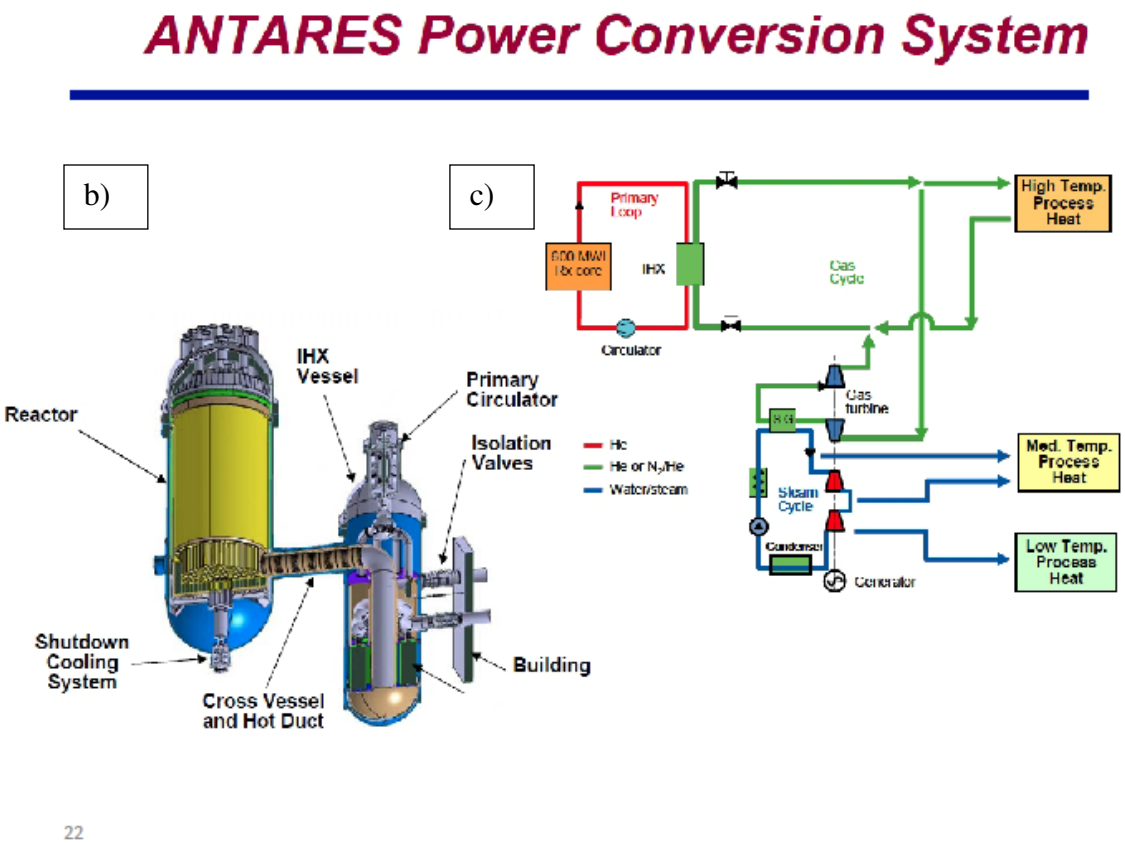

Figure 3. Modular HTGR Design Schematics – a) Reactor Core Cross Section, b) Three Dimensional Plant View, and c) Close-up of Reactor/Generator Equipment and Associated Thermodynamic Schematic. (Ball 2010)

There are several features of this design that will be retained for use in this study and others will not. The modular HTGR utilizes helium as the primary working fluid. The motive force to provided fluid motion required for the convective mode of heat removal from the core to the gas turbine is a circulator (compressor). The flowing helium moves through the core and is heated, and it is ducted to a gas turbine which extracts the work from the helium to drive the electric generator. The medium/low thermal energy steam cycle will not be included as part of this study. Only the main reactor gas heating portion of the design will be integrated.

The advantages to using helium are its inert properties and single phase. It is non-reactive and therefore not corrosive. However, corrosion mechanisms for reactor component materials, primarily due to impurities in the helium, are currently being studied for high temperature application in the HTGR (Cabet, Terlain et al. 2006). Also, since helium is a single phase gas throughout the power cycle process, there is no phase change and no issues associated with droplet formation.

The heat in the modular HTGR is provided by the core which uses a fuel design called TRISO. TRISO fuel is illustrated in Figure 4.

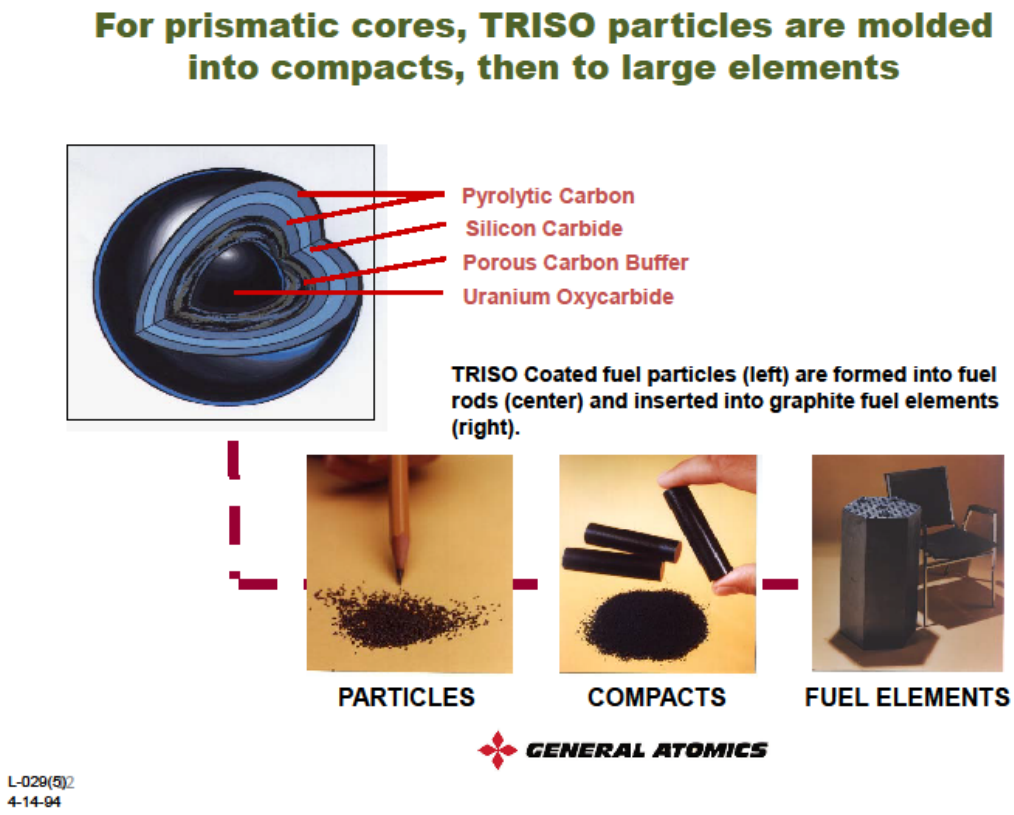

Figure 4. TRISO Fuel System (Ball 2010)

The most significant attribute of this fuel system, and the reason for its use in this study application, is it can achieve temperatures in excess of 1600 ^{o}C (Ball 2010) without fuel system failure and the release of fission products or fuel. This makes the TRISO fuel system an excellent choice to achieve the temperature objectives of the Generation IV reactor concepts, but, due to its high temperature capacity, it is intrinsically safe which simplifies accident transient analyses. Also, it provides the opportunity to increase steam temperatures well beyond 600 ^{o}C used in the previous base case thermodynamic calculations, and could potentially offer an increase in thermodynamic cycle efficiency approaching the 50% range.

The modular HTGR design assumptions for this study are as follows:

1. The primary working fluid will be steam generated by a standard PWR/BWR instead of helium;
2. The driving force for the steam "primary coolant" in the modular HTGR will be provided by the existing pressure drop between the S/G and the turbine condenser. No additional moving equipment such as a circulator, pump, compressor or blower is required;
3. The steam "primary coolant" will flow in tubes passing through the core. Steam will flow through the inside of the tubes, and the nuclear fueled heat source provided by the TRISO fuel, will be located on the outside of the tubes within the core; and
4. The outer vessel containing the TRISO fuel will be pressurized with argon in order to provide an inert atmosphere for the graphite/fuel matrix and to provide mechanical stress relief on the steam tubes by equalizing internal and external pressure loads, thereby relieving concerns associated with alloy steel tube creep at elevated temperatures (ASME 2010).

A schematic illustrating this conceptual design is provided in Figure 5.

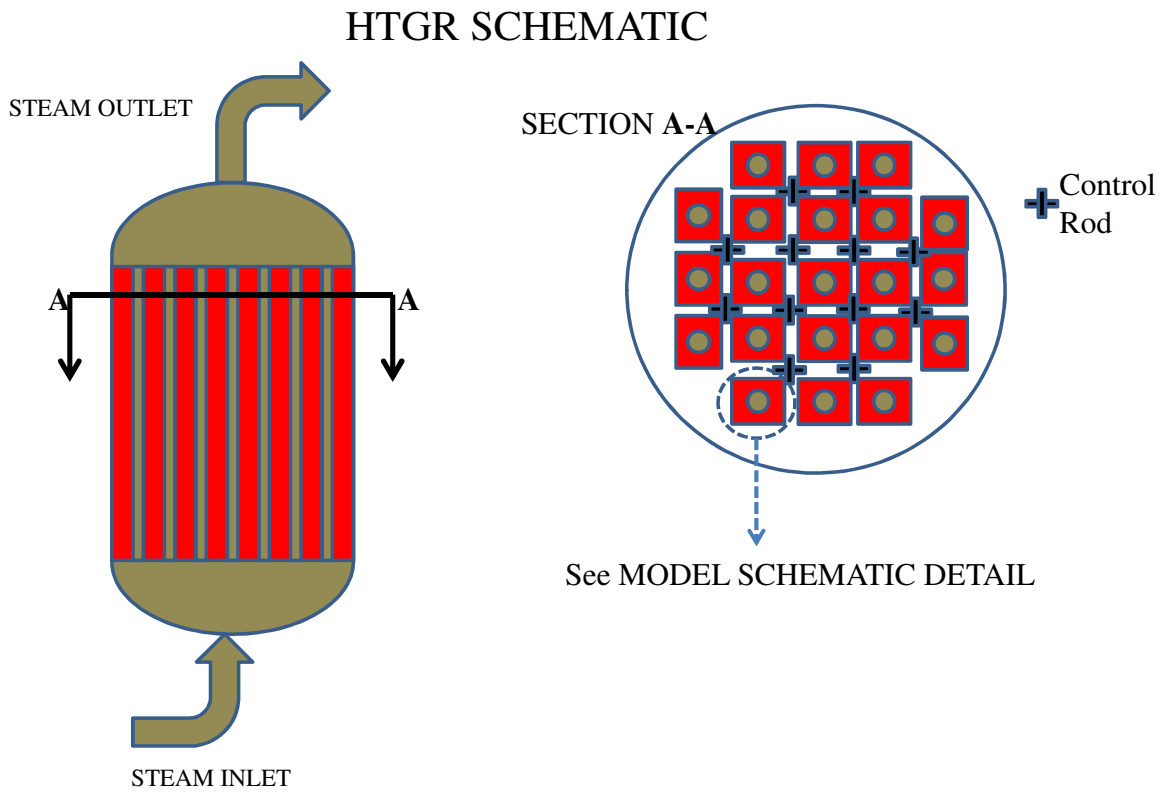

Figure 5. HTGR Vessel and Core Layout Schematic for Reheat

This concept offers several significant advantages over the modular HTGR. First, helium is an inert gas which is extracted from mining operations and cannot be manufactured. Therefore it is a limited resource (Fitzpatrick 2007), and reliance on this material as a coolant in rather large quantities does not appear to be a sustainable option. Steam/water, on the other hand, is an abundant commodity and perhaps the most well-known heat transfer medium. Second, moving high temperature gas with either high pressure blowers or compressors introduces additional maintenance and operational concerns associated with precision rotating equipment working in extreme conditions. Third, the TRISO fuel will be functioning in an entirely inert environment provided by an

argon pressurized atmosphere. Argon is the third most abundant gas in the atmosphere and is readily available in large quantities. Since the argon will only be applied to the small interstitial volume surrounding the fuel elements, large quantities of argon will not be required. Finally, in addition to the inherent capability of the TRISO fuel to contain fuel and fission products, the steam tube walls will separate the fuel from the flowing steam offering a secondary containment to the possibility of fission product release. The model schematic that will be assumed in this research is illustrated in Figure 6.

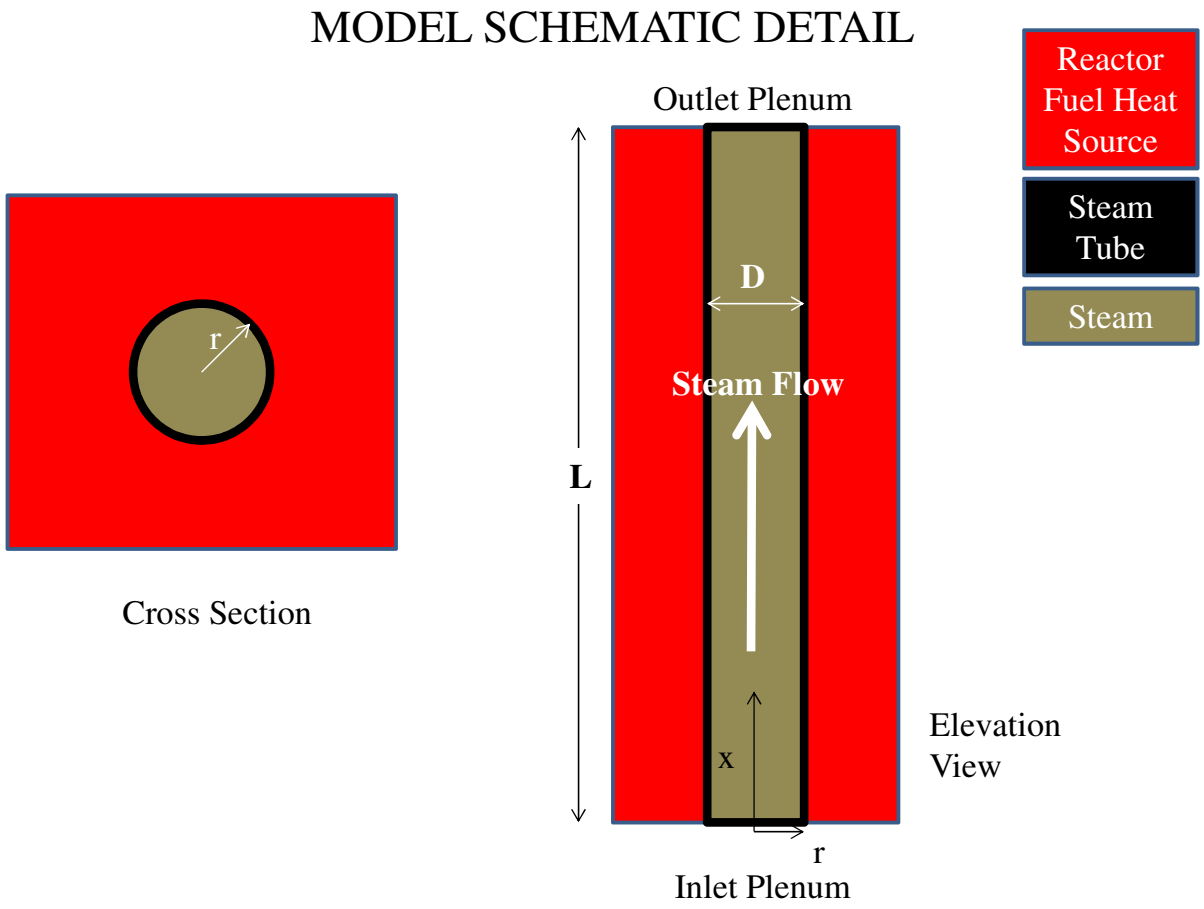

Figure 6. HTGR Heat Transfer Model

Given the significant thermodynamic and operational advantages of integrating modular HTGR technology to reheat PWR/BWR generated steam, there are several technical challenges which must be analyzed and evaluated to determine the feasibility of this design concept. The scope of analysis included in this research is summarized as follows:

1. Use the inlet steam conditions provided in Table 2, state point **(1)**, and steam flow generated by a typical commercial PWR/BWR rated at 1.0 GW_{th};
2. Target exit steam conditions are defined as state point **(1')** in Table 2;
3. Conduct sizing calculations utilizing a Log Mean Temperature Difference (LMTD) analysis. Calculate HTGR steam tube dimensions diameter (*D*) and length (*L*), and total number of steam tubes (*N*). This design analysis assumes a uniform power density typical of the average core power for the TRISO fuel system, and does not account for any two phase fluid effects;
4. Select a the computer code capable of analyzing steady state two phase steam flow with non-uniform axial heat flux boundary conditions. A detailed review of the "two fluid" model equations of motion will be conducted in order to appreciate the assumptions and limitations of the code. The computer code selected will be capable of calculating accurate results for the steam flow regimes that are expected to transition from annular film boiling with entrained droplets, through CHF wall dry out, to single phase steam flow at the steam tube exit. Heat transfer modes considered include convection and thermal radiation;

5. A computer model specific to this study will be constructed. This will require gaining proficiency with all applicable aspects of the code including developing input, running the computer code and analyzing the calculated results. Well documented example problems will be completed as available to gain confidence with this process and with code results;
6. The axial heat flux boundary condition, simulating reactor fission power generation, varies in the axial direction and will be developed based on available TRISO fuel data. The method for applying this boundary condition appropriately in the computer model will also be derived;
7. Computer model results will be evaluated for reasonability and be compared to results from approximate calculations; and
8. The computer model will then be used to calculate the thermal performance of the assumed conditions and the capacity to achieve target exit steam conditions. The steam tube sizing will be based on the LMTD analysis in step 3 above. A range of inlet steam quality conditions will be considered as a parameter study (i.e., 75%, 80%, 85%, 90% and 95% inlet steam quality).

Although interesting, further design concepts and details, such as the argon pressurization providing an inert atmosphere and structural relief to the outside surface of the steam tubes, is beyond the scope of this dissertation and will not be discussed further. Likewise, power density, power shape, from available sources will be utilized, and additional reactor neutron kinetics and system dynamics analyses and calculations are assumed to be outside the scope of this study.

Chapter 2

Literature Review

The concept of reheating steam to obtain superheated steam conditions and improved thermodynamic power cycle efficiency is not new (Holman 1980). The reheat process can be integrated into a Rankine cycle such as in fossil fired power plants as a method to return the steam to superheated conditions following the first high pressure (HP) steam turbine section. Steam exiting the HP turbine is returned to the boiler where it is "reheated" to a temperature approaching the maximum boiler temperature. This additional capital investment in piping to route steam back and forth from the steam turbine to the boiler, and additional boiler tubes in the superheating section, provides maximum temperature superheated steam to medium pressure (MP) and low pressure (LP) steam turbine sections. The results of this process are improved thermodynamic power cycle efficiency and superheated "dry" steam throughout the majority of the steam turbine sections, eliminating operational and maintenance issues associated with liquid droplet erosion. As mentioned previously, steam generated from PWR/BWR cycles is not superheated, and can benefit significantly from a reheat process.

The concept of applying a reheat process to a nuclear reactor power cycle has been previously suggested utilizing several different approaches. For the purposes of this research, these different approaches have been categorized as: fossil fuel integration, multiple- pass single reactor, and dual cycle systems.

Fossil fuel integration involves routing the steam generated from the PWR/BWR to a secondary heat source which derives its energy from combustion of fossil fuel. The

concept is similar to the concept proposed in this study, except it utilizes a fossil fuel fired boiler as the secondary heat source instead of a HTGR.

The earliest example of the application of fossil fuel reheat of steam generated from a nuclear reactor is believed to be a German design that utilized natural gas as a fuel source. However, this current research effort did not identify a specific reference for this design. It is believed that this reference may be unavailable in the public domain.

Two examples of reactor designs with fossil fired reheat of nuclear plant generated steam are presented. One example of a reactor design with this type of reheat application re-routed steam from the exhaust of the HP turbine to the fossil fired (oil) boiler where it was reheated (Schluderberg 1987). The reheat process, in this example, is patented and is very similar to a standard fossil fueled boiler reheat process. The second reactor design example of this concept was used at the Indian Point I PWR in New York (Forsberg 2007), where saturated steam was heated to superheated conditions in a fossil fired superheater. This approach has not been widely accepted in application; however several more recent publications suggest this approach as viable and worth future consideration.

A thermodynamic and thermo-economic evaluation of the Indian Point I reactor is presented in (Lior 1997). The evaluation points out the positive aspects of the design concept including improvement opportunities for thermal and economic areas. The negative aspects of the reactor operation center around the inadequate design and integration of the fossil fired superheater component itself. However with adequate design, these negative aspects “appear to be easily avoidable”.

Idaho National Laboratory compiled a report (Gibbs 2010) which provides a synopsis of the future generation nuclear power plant concepts being considered by the Department of Energy (DOE). Two concepts presented integrate a fossil fired (gas) superheater to reheat steam from nuclear reactors. One concept reheats steam from a light water reactor, and one reheats steam from a liquid metal reactor. Thermodynamic and economic evaluations are provided for both designs.

Finally, the most recent work identified in this research proposing the integration of fossil fired reheat to nuclear power generated steam is was conducted in Russia (Zaryankin 2011). This work was completed in response to the Fukushima accident, and resulting loss of international political support for nuclear power. It defines the fossil fire reheat as the "hybrid" system, i.e., using fossil fuel heating to superheat wet steam. Due to thermodynamic and economic improvements, it views this as a very positive alternative and a way to regain international political support for nuclear power. "A smart response to the political and economic pressures would be to re-engineer currently operational reactors to produce extra output. One way of doing this is to develop hybrid nuclear power plants".

Multi-pass single reactor designs involve the generation of wet steam (not superheated) from a first pass through the reactor core, followed by a second pass back through the core where increased second pass channel temperatures are capable of generating superheated steam. The earliest example of this design type was identified for a uranium-graphite reactor (Dolleszhal 1958). This design utilized a uranium-graphite reactor as a heat source. Liquid water is circulated from the bottom of the steam drum to

the reactor, where it is heated in direct contact with the uranium-graphite to produce saturated steam conditions. In the second loop, saturated steam from the top of the steam drum is routed back through the reactor, where it is reheated in direct contact with the uranium graphite to produce superheated steam conditions. The major concern with this design is the carryover of radioactive materials from the uranium-graphite directly to the steam plant. The reference (Dolleszhal 1958) states that this concern "can be made several times less by proper ventilation". Obviously, this arrangement would not be considered acceptable today.

The next example of the multi-pass type design was the "Pathfinder" reactor constructed by Northern States Power Company and manufactured by Allis-Chalmers (Kok 2009). Its design involved the integration of a superheater into the reactor and its operation was plagued by mechanical and safety issues (Lund 2011), "The plant was never successful and never passed full power tests". The reactor ran between 1966 and 1967 and was shut down.

A later example of a multi-pass design utilizes a BWR design with two passes (Ferrara 2007) where the first pass generated saturated steam and the second pass produces superheated steam.

As can be surmised, the complexities associated with the multi-pass designs include the design of two different flow channels to deal with the physical changes in the steam from liquid to vapor, the challenge of the nuclear physics in order to provide the required heat flux, control and temperature profiles required for the two channels, and, the mechanical issues associated with multiple penetrations of a pressure vessel.

The dual cycle designs appear to be garnering the most attention as a method for capitalizing on the high temperature capabilities of new nuclear fuel systems. These designs combine a high temperature gas cycle, usually utilizing helium, and a secondary Rankine steam cycle as a secondary, or bottoming cycle. The earliest commercial application of this type of HTGR design was the Peach Bottom reactor (Gibbons 1974). In this design, high temperature helium is circulated through the core as the primary coolant and then through a steam generator which produces superheated steam. More recent dual cycle designs first utilize the high temperature helium in a Brayton cycle to produce electric power directly from the hot gas, then, reject heat to a Rankine steam cycle to produce superheated steam (Kim 1980). The DOE is considering the dual cycle design as well, primarily the helium HTGR (Gibbs 2010).

There has been considerable interest in small modular nuclear power plant designs. The modular concept provides many economic advantages including construction of power producing capacity as it is needed, reduced construction costs and reduced time for construction and startup (Shimizu 2011). In order to meet the needs of this new market, a dual cycle design capable of producing 120 $MW_{thermal}$ (compared to > 1,000 $MW_{thermal}$) has been developed which couples a primary circulating helium loop with a Rankine superheated steam cycle (Shimizu 2011).

The research documented in this dissertation focuses on the concept of integrating HTGR technology as a heat source to reheat saturated steam to superheated steam, for the overall objectives of improving thermodynamic power cycle efficiency and reduction of operational and maintenance issues associated with saturated steam. Based on a thorough

review of existing literature, the concept presented in this dissertation is considered to be novel.

Chapter 3

Methods of Analysis

Thermodynamic Power Cycle Thermal Efficiency

Power plants are a complex arrangement of systems designed to ultimately produce the maximum quantity of electric power for a given input of fuel. In this research, this concept is quantified as the thermodynamic power cycle thermal efficiency, η_{thermal} , which is a ratio measured in percent of the desired effect, divided by the total input required for the effect. Essentially, the percentage of work output, for the total amount of heat input. In thermodynamic terms, η_{thermal} can be derived from the state points illustrated in Figure 1 as:

$$\eta_{\text{thermal}} = \frac{W_{\text{net}}}{Q_{\text{in}}} \cdot 100\% = \frac{(h_1 - h_2)_{turbine} - (h_4 - h_3)_{pump}}{(h_1 - h_4)} \times \qquad (1)$$

100%

where : W_{net} = Net Work Output from system, (kJ/s)

Q_{in} = Total Heat Input, (kJ/s)

$h_{\#}$ = Enthalpy at state #, (kJ/kg)

The most significant aspects of two thermodynamic power cycles can be assessed quantitatively with Equation 1 and compared on an equivalent basis. In this research, all of the expansion and pumping processes are assumed to occur isentropically. The system feedwater, state **3**, (see Figure 1), is assumed equivalent for each case since this value is a function of the environmental conditions surrounding the location operating power

plant. Also, the pumping process, state **3** to **4**, is assumed to be the same for each case since the overall system flow is maintained at a constant throughout the research. Therefore, the significant parameter of $\eta_{thermal}$ is the $h_1$state point, which is precisely why the reheat process is of interest.

Exergy Analyses

The previous discussion identifies the improvement of a thermodynamic cycle in terms of the "quantity" of energy improvement. This type analysis is referred to as a "First Law of Thermodynamics" analysis. The First Law states, "The energy of an isolated system remains constant" (Holman 1980). The Second Law of Thermodynamics is more axiomatic, and is based on several experimental observations such as:

- Heat flows from high temperature to a low temperature;
- Two gases, when placed in an isolated chamber, will mix uniformly and will not separate spontaneously once mixed; and
- It is not possible to construct a machine or device which will operate continuously while receiving heat from a single reservoir and producing an equivalent amount of work.

Therefore, the second law relates to the "direction" in which an energy transfer or conversion may take place; some transfers are allowed and others are not. An analysis based on "Second Law of Thermodynamics" uses exergy to quantify the "quality" of the energy available for transfer. Exergy is employed to quantify the causes of the thermodynamic imperfection of a process under consideration (Hepbasli 2008). Exergy

is a measure of the maximum useful work that can be done by a system interacting with an environment. This analysis identifies and quantifies the irreversibilities of a power cycle for comparison to another, but does not provide any information concerning the economic cost saving that will result. The second law analysis points to possible alternatives which can result in saving in fuel or equipment costs. The flow of specific exergy is calculated as follows:

$$\psi = (h - h_0) - T_0(s - s_0) \qquad (2)$$

Where, ψ, exergy, is calculated as an intrinsic property. The subscript zero indicates properties at the "dead" or "zero" state. The zero state is assumed to be the conditions of the surrounding environment. This means that, when the cycle conditions are brought to equilibrium conditions with the surrounding environment, the ability of the system or cycle to produce work, no longer exists.

Exergy analyses are a primary tool for addressing the impact of energy resource utilization on the environment, an effective method using the conservation of mass and energy principles together with the second law of thermodynamics for the design and analysis of energy systems and is a key component in obtaining sustainable development (Hepbasli 2008).

The present thermodynamic cycle improvement will be evaluated with respect to total system exergy in order to quantify the improvement opportunity available for one

cycle compared to another. A system producing significantly higher exergy produces higher quality energy with a greater ability to perform work with reduced irreversibility.

Log Mean Temperature Difference Analysis

A heat exchanger is defined as a device in which the process of heat exchange between two fluids that are at different temperatures separated by a solid wall occurs (Bergman 2011). The purpose of the HTGR is to transfer sufficient nuclear fission generated heat energy to reheat the steam flow such that the incoming saturated steam becomes superheated at the exit. The HTGR can be considered as meeting the definition of a heat exchanger since the steam is a fluid at a lower temperature that is heated by the heat generated by the nuclear reaction. The nuclear fission heat source is being used in the present application as the energy source for boosting the incoming steam temperature to the desired exit value. In this analysis, the HTGR is assumed to approach the design concept of a single pass tube and shell heat exchanger. Steam is flowing through the tubes. The nuclear fission heat source is the heat source on the shell side. As such, the Log Mean Temperature Difference (LMTD) heat exchanger design analysis method will be applied to establish the steam tube sizing of the reheat HTGR including the tube diameter and length, and the total number of steam tubes. The dimensions form the basis for the detailed analysis.

The derivation of the LMTD equations specific to this research begins with the model presented in Appendix B . The outcome of the derivation results in the following equation:

$$q = -\frac{UA(\Delta T_2 - \Delta T_1)}{ln\left(\frac{\Delta T_2}{\Delta T_1}\right)} = -UA\Delta T_{lm} \qquad \text{(B.3)}$$

Equation B.3 (see Appendix B) is the heat exchanger equation. In this analysis, the steam temperature at the inlet is T_{ci} , and the exit steam temperature is T_{co}. T_{hi} and T_{ho} are the temperature of the nuclear fission reaction, and are assumed to be equal. ΔT_{lm} is referred to as the Log Mean Temperature Difference (LMTD), which will be used as a basis for design calculations to develop steam tube dimensions diameter (*D*) and length (*L*), and total tube number (*N*) estimates, used to size the steam reheat HTGR.

Specific Details and Constraints

The LMTD method will be used for sizing the HTGR with the following assumptions:

1. Host PWR/BWR power output is 1.0 GW_{th};
2. Inside tube wall temperature is constant at 1,000 ^{0}C;
3. Working fluid is single phase steam;
4. Steam conditions are known for the steam turbine (inlet and outlet), and the target HTGR outlet (states **1**, **2** and **1'** illustrated in Figure 1, respectively); and
5. Properties of the steam within the steam tube are assumed constant calculated at 450 ^{0}C and 8 MPa.

LMTD Solution Scheme

The following analysis provides a method for sizing the HTGR required to provide the reheat capacity to achieve target outlet steam conditions. Using the assumptions listed above and the thermodynamic properties in Table A.1, the required steam flow to produce 1.0 $GW_{thermal}$ in the host PWR/BWR is calculated as follows:

$$P_{thermal} = (h_1 - h_2) \qquad (3)$$

where: $P_{thermal}$ = PWR/BWR thermal power (GW)

□ = steam flow (kg/s)

h_1 = enthalpy at state **1** (kJ/kg)

h_2 = enthalpy at state **2** (kJ/kg)

Rearranging,

$$= P_{thermal}/(h_1 - h_2) \qquad (4)$$

Now that the steam flow rate has been established for the host PWR/BWR power plant, this now represents the flow rate of steam that will be reheated by the HTGR. The heat input rate supplied by the HTGR to increase the enthalpy from state **1** to state **1'** is:

$$q_{input} = (h_{1'} - h_1) \qquad (5)$$

The LMTD method of sizing the HTGR will utilize the assumptions and quantities calculated above to obtain the dimensions and number of the HTGR steam tubes required. In the LMTD method, the heat transfer required is equal to the overall heat transfer coefficient times the heat transfer area and the average temperature as defined in Equation B.3 (see Appendix B). Assuming that the reactor power can provide adequate heat generation for a constant internal tube surface temperature of 1000^0C, then, using the thermodynamic data in Table A.1, ΔT_{lm} can be calculated, and remains constant throughout the remainder of the analysis since the assumed inlet and outlet temperatures of the steam, and the temperature of the nuclear fission reaction do not change.

Now, the only unknowns are *U* and *A*. However, since *U* and *A* are both functions of the assumed tube dimensions, an iterative solution must be obtained. The iterative scheme is as follows:

1. Initial guess of tube dimensions (diameter, length and total number of tubes), calculate total heat transfer area (*A*):

$$A = \pi DLN \qquad (6)$$

where: *A* = total tube heat transfer area (m^2)

D = inside tube diameter (m)

L = tube length (m)

N = number of tubes

2. Calculate Reynolds Number (*Re*) from assumed tube dimensions and fluid properties at an average temperature of 450^0C and 8 MPa.

$$Re = v \rho D/\mu \quad (7)$$

where: v = steam velocity (m/s)

ρ = density (kg/m^3)

D = tube inside diameter (m)

μ = viscosity (kg/m s)

3. Calculate Nusselt Number (*Nu*) from Reynolds Number (*Re*) and Prandtl Number (*Pr*) assuming turbulent flow (Bergman 2011):

$$Nu_D = 0.023 Re^{4/5} Pr^{0.4} \quad (8)$$

4. Calculate *U* from Nusselt Number (*U* is the convective heat transfer coefficient between the inside tube surface and the steam in this analysis, since the steam tube wall thickness is small, as is the thermal resistance across it, and, there is no convective heat transfer on the outside of the tube):

$$h_i = U = Nu(\frac{k}{D}) \quad (9)$$

where: k = thermal conductivity of steam (W/m K)

5. Finally, calculate "*A*" by rearranging Equation B.3:

$$A = q_{input}/\Delta T_{lm} U \quad (10)$$

6. Compare "*A*" from step 1 and step 5. Adjust tube dimensions and repeat iterations until the "*A*" from step 1, is equal to the "*A*" calculated in step 5 to within a specified tolerance.

Flow Boiling Considerations

The following discussion provides some introductory background on flow boiling and the two phase boiling flow regimes and transitions expected with the application of an HTGR to saturated steam, with a quality in the range of 0.75 (75%) to 1.0 (100%) and inlet conditions provided in Table 2 (state **1**).

Flow Boiling Regimes in a Heated Vertical Tube

The general sequence of the two-phase flow regimes in upward flow boiling in a vertical tube are liquid (single phase), sub-cooled boiling, bubbly flow, slug flow, churn flow, annular flow, mist flow and vapor flow (single phase)(Carey 1992). The flow

characteristics of each regime are quite different as are the heat transfer mechanisms. These regimes are illustrated in Figure 7:

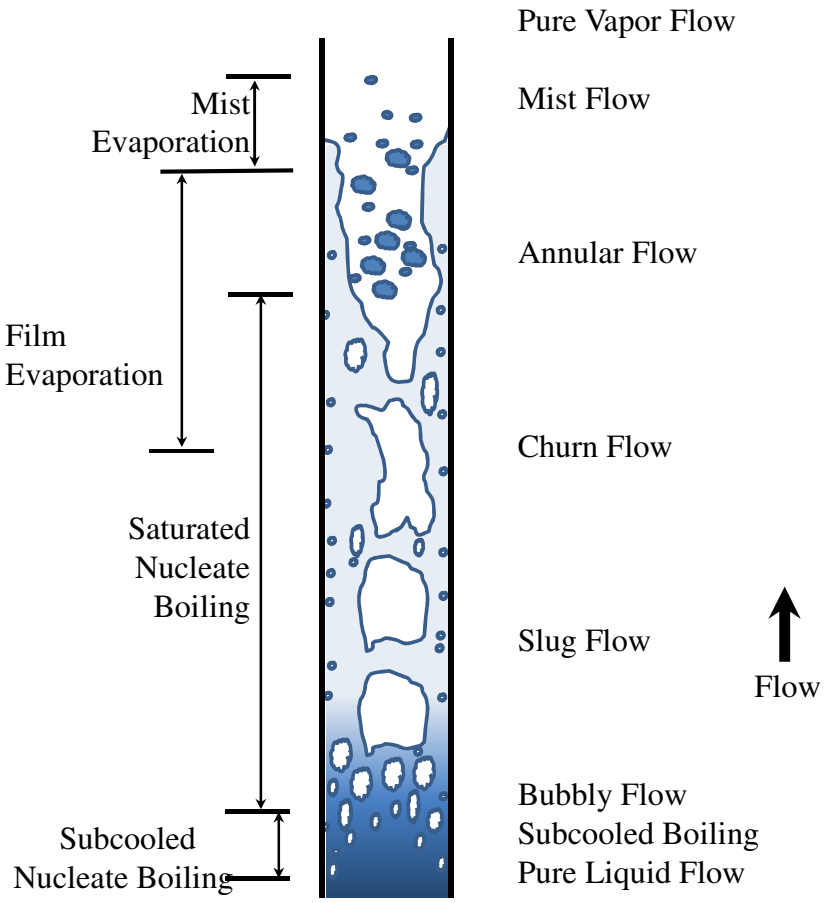

Figure 7. Boiling Flow Regimes (Carey 1992)

Each of the distinct flow regimes is provided with a descriptive title and a corresponding set of qualitative characteristics. The flow in the vertical tube starts as a single phase fluid (water), and transitions to single phase vapor (steam). The objective of the HTGR is to heat the inlet steam with a quality in the range of 0.75 to 0.95, to a superheated condition. Figure 8 illustrates the trends of wall temperature and fluid temperature as a function of quality across the boiling flow regimes.

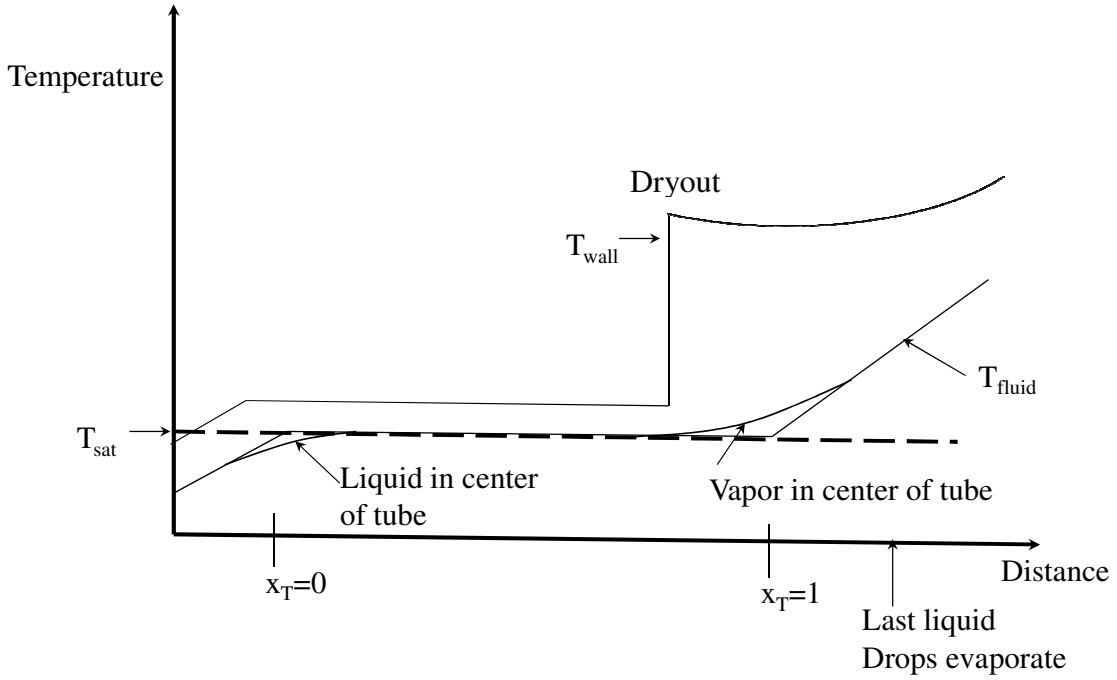

Figure 8. Wall and Fluid Temperature in Flow Boiling (Whalley 1987)

As can be seen, "dryout" occurs at a quality higher than 0.5 and less than 1.0. "Dryout" is a term describing the absence of the liquid phase on the surface of the tube wall. This can occur at two points as the flow transitions from single phase liquid to single phase vapor. The first occurs in the sub-cooled (bulk temperature less than saturation) boiling regime where the dominant heat transfer mechanism is nucleate

boiling. Local high temperature points on the surface of the tube exceed the saturation temperature of the bulk liquid and steam bubbles form and move from the wall to the liquid. There they collapse as the heat is transferred to the lower temperature bulk liquid. The nucleate boiling heat transfer mechanism is very efficient and results in high convective heat transfer coefficients. If the heat flux is high enough in this scenario, the rate of bubble formation at the tube surface will generate a film of steam that will separate the liquid from the wall. This condition would therefore meet the definition of dryout, and the heat flux is referred to as Critical Heat Flux (CHF). This condition is illustrated as curve 1 in the Figure 9.

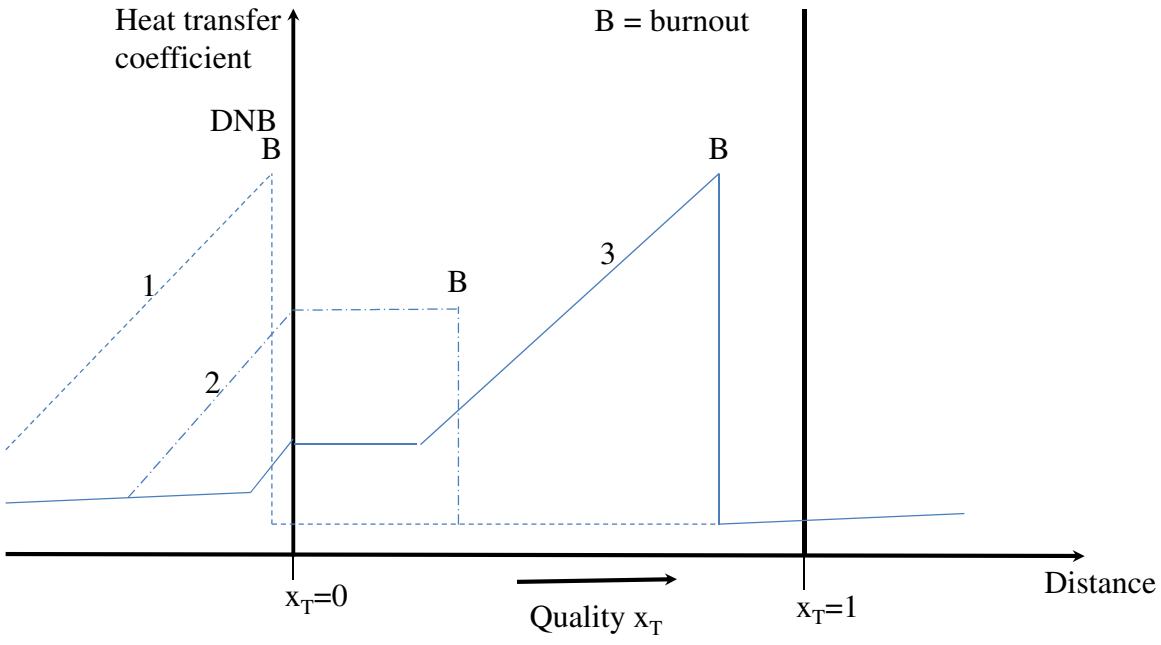

Figure 9. Heat Transfer Coefficient Transition with Quality (Whalley 1987)

Note that the liquid is sub-cooled at the dryout point B, and the heat transfer coefficient drops significantly due to the transition from nucleate to this film boiling regime. This dryout condition is referred to as the Departure from Nucleate Boiling (DNB).

The second dryout condition occurs during the annular flow regime where the liquid is entirely evaporated from the wall surface. In this regime, all of the remaining liquid is entrained in the flow as droplets. This is illustrated in Figure 10.

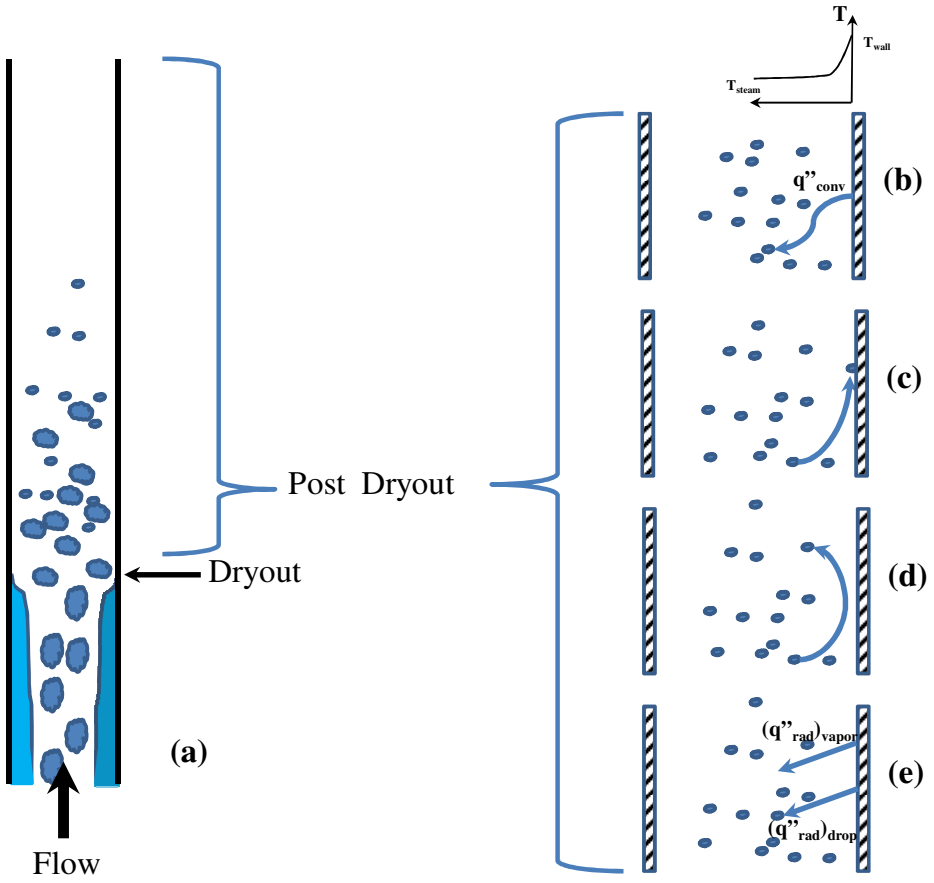

Figure 10. Post Dryout CHF Heat Transfer Mechanisms – Mist Flow (Carey 1992)

From Figure 9, the heat transfer coefficient will follow curve 3, and drop significantly at dryout, but not as dramatically as for DNB. This regime merges into the single-phase vapor regime.

Based on the range of inlet steam quality, DNB is not a consideration. However, it is expected that all of the cases investigated in this research will exhibit dryout (CHF). The actual physical location of the dryout point in the steam tube will vary vertically, based on the inlet conditions for the specific case. It is expected that the dryout location will occur closer to the inlet as the inlet steam quality increases.

Post Dryout (CHF)

After dryout, the flow contains all of the remaining liquid as entrained droplets, and is characterized as Mist flow. Figure 10 illustrates the dryout condition and several schematics of heat transfer mechanisms that can exist in this flow regime. There are a total of six different heat transfer mechanisms in the Mist flow regime.

The first two are illustrated as (b), and are the convective heat transfer from the wall surface to the vapor, and from the vapor to the droplets. It is assumed that the vapor contacting the droplets is superheated in order to enhance the droplet vaporization as they are swept along with the core flow.

Next, if the droplets have adequate momentum in a direction towards the wall, the droplets can impact the wall and evaporate (c). As with any collision, the impact energy may cause the droplet to break apart into smaller droplets or rebound back into the vapor flow.

Fourth, if the droplets come close to the wall without striking it. This is an interesting phenomenon requiring that the wall temperature (defined as the Leidenfrost temperature) be high enough to create a vaporization rate from the droplet sufficient to generate a repulsive force that is larger than the droplet momentum in the direction toward the wall.

Finally, there are two thermal radiation transport mechanisms from the wall; one from the wall to the vapor; and another from the wall to the droplet. Due to the high wall surface temperature expected, ~1,000 ^{o}C, thermal radiation transport from the wall to the droplets could be significant since the droplets would be expected to be optically "thick" (i.e., the absorption spectrum for the droplet matches some of the emission spectra from the wall surface). If the vapor is optically thick, it will contribute to the overall heat transfer from the wall via thermal radiation transport.

RELAP5 Equations of Motion

The differential equations simplified for the one-dimensional transient, two fluid (liquid and vapor phases) model are presented (NRC 2001). The basic field equations are written for two phases each for mass (continuity), momentum and energy conservation, for a total of six equations. This set of equations is referred to as the six equation model. The differential stream tube form considers time (t) and one space dimension (x), as the independent variables, and in terms of time and volume-average dependent variables.

The model illustrated in Figure 11 provides a visualization of the two fluid model control volume between x and x+dx (dV). The model geometry approximates a vertically oriented cylindrical tube, where A_i is the interfacial area between the liquid and vapor/gas

phases. It is the total phase interface area in the control volume. A_{jk} is the cross sectional flow area for phase k. A_{jl} (two segments) and A_{jg} illustrate liquid and gas phase areas respectively.

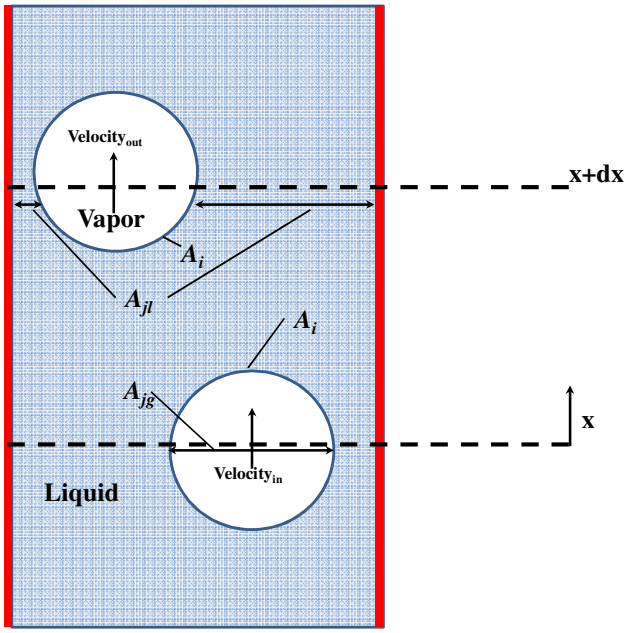

Figure 11. One Dimensional Vertical Two Fluid Model Schematic

The conservation equations in R5 are derived using the Reynolds Transport Theorem and applying volume and area averaging operator techniques as presented in (Todreas 1993). The R5 conservation of mass equation will be derived to demonstrate the approach. The conservation of momentum and energy equations in R5 will be presented without derivation. Some of the approximations made in the R5 formulations have been challenged over the years, however, recent papers evaluating alternative approaches (Mousseau 2004) are still being developed.

Conservation of Mass

The Reynolds Transport field equation for conservation of mass is (Todreas 1993):

$$\frac{\partial}{\partial t}\iiint_{V_k} \rho_k dV + \iint_{S_k} \rho_k(\vec{v}_k - \vec{v}_s)\cdot \boldsymbol{n}\, dS = 0 \qquad (11)$$

where: V_k= volume of each phase in the control volume

ρ_k= density of each phase

dV= differential control volume (gas or liquid)

$S_k = A_{jk} + A_{ik}$= sum of phasic flow area and interfacial flow area

$\vec{v}_k$= velocity of phase

$\vec{v}_s$= velocity of the control volume surface

$\boldsymbol{n}$ = surface unit normal vector

S= interfacial area plus ends of control volume that cuts phase k

In R5, as will be shown later, there is a fixed grid defined by junctions that connect volumes. The A_{jk} is fixed at the control volume boundary and is defined by the code as a junction. A_i is interfacial, and moves with velocity $\vec{v}_s$. The area integrals are split between fixed, at flow cross section, and, interfacial.

$$\frac{\partial}{\partial t}\iiint_{V_k}\rho_k dV + \iint_{A_{jk}}\rho_k(\vec{v}_k - \vec{v}_s)\cdot \boldsymbol{n}\, dS + \iint_{A_{ik}}\rho_k(\vec{v}_k - \vec{v}_s)\cdot \boldsymbol{n}\, dS = 0 \quad (12)$$

Defining Volume Average and Area Average operators:

$$Volume\ Average = \langle c_k\rangle_k \equiv \frac{1}{V_k}\iiint_{V_k} c_k dV \quad (13)$$

$$Area\ Average = \{c_k\}_k \equiv \frac{1}{A_k}\iint_{A_k} c_k dA \quad (14)$$

where: c_k= a material property, ρ_k in this case.

Using these definitions in Equation 12, we produce area and volume averaged formulations of the continuity equation.

$$\frac{\partial}{\partial t}[\langle\rho_k\rangle_k V_k] + \sum_j\{\rho_k\vec{v}_k\}_{jk}\cdot A_{jk} + \{\rho_k(\vec{v}_k - \vec{v}_s)\}_{ik} \times A_{ik} = 0 \quad (15)$$

The second term on the left-hand-side sums over the cross sectional flow, and the third term is the interfacial area. Returning to the inflow and outflow concept for phase *k*, and dropping the volume and area average brackets, we have the following.

$$\frac{\partial}{\partial t}[\rho_k \alpha_k A_{xs} dx] = [\rho_k \vec{v}_k \alpha_k A_{xs}]_{IN} - [\rho_k \vec{v}_k \alpha_k A_{xs}]_{OUT} - \{\rho_k(\vec{v}_k - \vec{v}_s)\}_{ik} \times A_{ik} \quad (16)$$

Note on the left-hand-side that, $V = A_{xs}dx$, and $V_k = \alpha_k A_{xs}dx$. Also, the third term on the right-hand-side is the interfacial mass transfer due to evaporation or condensation. Next, a Taylor expansion (keeping only the linear term) will be used to approximate the outflow ($_{OUT}$) term from Equation 16.

$$[\rho_k \vec{v}_k \alpha_k A_{xs}]_{OUT} \cong [\rho_k \vec{v}_k \alpha_k A_{xs}]_{IN} + \frac{\partial}{\partial x}[\rho_k \vec{v}_k \alpha_k A_{xs}]dx \quad (17)$$

Combining Equation 16 and Equation 17,

$$\frac{\partial}{\partial t}[\rho_k \alpha_k A_{xs} dx] = -\frac{\partial}{\partial x}[\rho_k \vec{v}_k \alpha_k A_{xs}]dx - \{\rho_k(\vec{v}_k - \vec{v}_s)\}_{ik} \times A_{ik} \quad (18)$$

Divide Equation 18 by $V = A_{xs}dx$, and re-arranging,

$$\frac{\partial}{\partial t}[\rho_k \alpha_k] + \frac{\partial}{\partial x}[\rho_k \vec{v}_k \alpha_k] = \frac{-\{\rho_k(\vec{v}_k - \vec{v}_s)\}_{ik} \times A_{ik}}{A_{xs} dx} \quad (19)$$

The term on the right-hand-side of Equation 19 is the interfacial mass transfer and is denoted as Γ_k. Finally, the conservation of mass equations for vapor (g) and liquid (l) are:

$$\frac{\partial(\alpha_g \rho_g)}{\partial t} + \frac{1}{A}\frac{\partial(\alpha_g \rho_g v_g A)}{\partial x} = \Gamma_g \quad (20)$$

$$\frac{\partial(\alpha_l \rho_l)}{\partial t} + \frac{1}{A}\frac{\partial(\alpha_l \rho_l v_l A)}{\partial x} = \Gamma_l \quad (21)$$

Equation 20 and Equation 21 have been written in area average notation where the *L/V* term has been reduced to *1/A*. Subscripts are g for gas/vapor phase, and l for liquid phase and α is the void fraction (ratio of the gas (or liquid) cross-sectional area divided by the total cross sectional area). Since the assumed flow does not include mass sources or sinks, then,

$$\Gamma_g = -\Gamma_l \quad (22)$$

The interfacial mass transfer model assumes that total mass transfer can be partitioned into mass transfer at the vapor/liquid interface in the bulk fluid (Γ_{ig}) and mass transfer at the vapor/liquid interface in the boundary layer near the walls (Γ_w) so that,

$$\Gamma_{g=}\Gamma_{ig} + \Gamma_w \tag{23}$$

Conservation of Momentum

The conservation of momentum equations (NRC 2001) are presented for each phase in an expanded form of momenta per unit volume using velocity variables v_g (x-direction component of gas velocity), and v_l (x-direction component of the liquid velocity). Simplifications include: the phasic pressures are assumed equal, the interfacial pressure is assumed equal to the phasic pressures, interfacial momentum storage is neglected, phasic viscous stresses are neglected, the interface force terms consist of both pressure and viscous stresses, and the normal wall forces are assumed adequately modeled by the variable are momentum flux formulation. The phasic mass continuity equations are multiplied by the corresponding phasic velocity, and are subtracted from the momentum equations, resulting in the following equations (gas and liquid phases respectively):

$$\begin{aligned}\alpha_g\rho_g A\frac{\partial v_g}{\partial t}+\frac{1}{2}\alpha_g\rho_g A\frac{\partial v_g^2}{\partial x}&\\ =-\alpha_g A\frac{\partial P}{\partial x}+\alpha_g\rho_g B_x A&\\ -\left(\alpha_g\rho_g A\right)FWG\left(v_g\right)&\\ +\Gamma_g A\left(v_{gI}-v_g\right)&\\ -\left(\alpha_g\rho_g A\right)FIG\left(v_g-v_l\right)&\\ -C\alpha_l\rho_m A\left[\frac{\partial\left(v_g-v_l\right)}{\partial t}+v_l\frac{\partial v_g}{\partial x}\right.&\\ \left.-v_g\frac{\partial v_l}{\partial x}\right]&\end{aligned} \tag{24}$$

$$\alpha_l \rho_l A \frac{\partial v_l}{\partial t} + \frac{1}{2}\alpha_l \rho_l A \frac{\partial v_l^2}{\partial x}$$
$$= -\alpha_l A \frac{\partial P}{\partial x} + \alpha_l \rho_l B_x A$$
$$- (\alpha_l \rho_l A) FWF(v_l) + \Gamma_g A (v_{ll} - v_l)$$
$$- (\alpha_l \rho_l A) FIF(v_l - v_g) \qquad (25)$$
$$- C \alpha_l \rho_m A \left[\frac{\partial (v_l - v_g)}{\partial t} + v_g \frac{\partial v_l}{\partial x} \right.$$
$$\left. - v_l \frac{\partial v_g}{\partial x} \right]$$

The force terms on the right sides of Equation 24 and Equation 25 (NRC 2001) are the pressure gradient, the body force (i.e., B_x is the body force in the x-direction, (m/s^2)), wall friction, momentum transfer due to interface mass transfer, interface frictional drag, and force due to virtual mass, respectively. Terms FWG and FWF are components of the wall frictional drag, which are linear in velocity, and are products of the friction coefficient, the frictional reference area per unit volume, and the magnitude of the fluid bulk velocity. The interfacial velocity in the interface momentum transfer term is the unit momentum with which phase appearance or disappearance occurs. Coefficients FIG and FIF are the interface frictional drag components; two different models (drift flux and drag coefficient) are used for the interface friction drag, depending on the flow regime.

The coefficient C depends on the flow regime. C>1/2 is appropriate for bubbly or dispersed flows, while C=0 may be appropriate for separated or stratified flow. However, a value of C>1/2 is used for all flow regimes. The spatial derivative portion of the virtual mass term listed in the momentum equations is neglected. These terms primarily impact the mixture sound speed calculation, and therefore are significant near the speed of sound. This formulation is also found to be more convenient for development of numerical schemes. The momentum formulation and momentum effects are considered of secondary importance to mass and energy conservation in thermal reactor design. This assumption is correct since nuclear reactor flows are dominated by large sources and sinks of momentum. In this case, the source and sink of momentum is the entire steam plant, which is considered to provide a constant source and sink for the steam. The steam flow is driven by the pressure drop between the primary reactor steam generator and the turbine condenser, and the HTGR tubes offer a relatively small frictional component of pressure drop.

Assuming conservation of momentum at the interface, then the force terms associated with interface mass and momentum exchange sum to zero as follows:

$$\begin{aligned}\Gamma_g A(v_{gI}) - (\alpha_g \rho_g A) FIG(v_g - v_l) \\ - C\alpha_l \rho_m A\left[\frac{\partial(v_g - v_l)}{\partial t}\right] - \Gamma_g A(v_{lI}) \\ - (\alpha_l \rho_l A) FIF(v_l - v_g) \\ - C\alpha_l \rho_m A\left[\frac{\partial(v_l - v_g)}{\partial t}\right] = 0\end{aligned} \tag{26}$$

It is assumed that the interface momentum transfer due to friction and due to mass transfer independently sum to zero:

$$v_{gI} = v_{lI} = v_I \tag{27}$$

and,

$$\alpha_g \rho_g FIG = \alpha_l \rho_l FIF = \alpha_g \alpha_l \rho_g \rho_l FI \tag{28}$$

These conditions are sufficient to ensure that Equation 26 is satisfied.

Conservation of Energy

The phasic thermal energy equations for the gas phase g, and liquid phase l, respectively are (NRC 2001):

$$\frac{\partial(\alpha_g \rho_g u_g)}{\partial t} + \frac{1}{A}\frac{\partial(\alpha_g \rho_g u_g v_g A)}{\partial x} = -P\frac{\partial \alpha_g}{\partial t} - \frac{P}{A}\frac{\partial(\alpha_g v_g A)}{\partial x} + Q_{wg} + Q_{ig} + \Gamma_{ig} h_g^* + \Gamma_w h_g' + DISS_g \tag{29}$$

$$\frac{\partial(\alpha_l \rho_l u_l)}{\partial t} + \frac{1}{A}\frac{\partial(\alpha_l \rho_l u_l v_l A)}{\partial x} = -P\frac{\partial \alpha_l}{\partial t} - \frac{P}{A}\frac{\partial(\alpha_l v_l A)}{\partial x} + Q_{wl} + Q_{il} + \Gamma_{ig} h_l^* + \Gamma_w h_l' + DISS_l \tag{30}$$

The energy equations include the following simplifications: the interfacial energy storage and internal phasic heat transfer is neglected (lumped mass).

In the energy equations, $DISS$ is the energy dissipation function (W/m^3), u is the specific internal energy (kJ/kg), and, $Q_{wg}$and $Q_{wl}$are the phasic wall heat transfer rates per unit volume, and satisfy the following equation (W/m^3):

$$Q = Q_{wg} + Q_{wl} \tag{31}$$

where, Q is the total wall heat transfer rate to the fluid per unit volume. The phasic enthalpies h_g^* and h_l^* associated with the bulk interface mass transfer are defined in such a way that the interface energy jump conditions at the liquid vapor interface are satisfied. Specifically, the h_g^* and h_l^* are chosen to be h_g^s and h_l, respectively, for the case of vaporization and h_g and h_l^s, respectively, for the case of condensation. The same is true for the phasic enthalpies h_g' and h_l' associated with wall (thermal boundary layer) interface mass transfer. This logic will be further developed later.

Vapor Generation

The vapor generation (or condensation) consists of two parts, vapor generation which results in energy exchange (Γ_{ig}) and vapor generation due to wall heat transfer effects (Γ_w). Each of the vapor generation (or condensation) processes involves interface heat transfer effects. The interface heat transfer terms (Q_{ig} and Q_{il}) include heat transfer from the fluid states to the interface due to interface energy exchange in the bulk and in the thermal boundary layer near the wall. The vapor generation (or condensation) rates are established from energy balance considerations at the interface.

The summation of Equation 29 and Equation 30 produces the mixture energy equation from which it is required that the interface transfer terms sum to zero:

$$Q_{il} + Q_{ig} + \Gamma_{ig}\left(h_g^* - h_l^*\right) + \Gamma_w\left(h_g' - h_l'\right) = 0 \qquad (32)$$

The interface heat transfer terms (Q_{ig} and Q_{il}) each consist of two parts for a total of four components; that is, interface heat transfer in the bulk (Q_{ig}^B and Q_{il}^B) and interface heat transfer in the thermal boundary layer near the wall (Q_{ig}^W and Q_{il}^W). This is one situation where the assumption of "no transverse gradients" needs to be supplemented by a special model as illustrated in Figure 12.

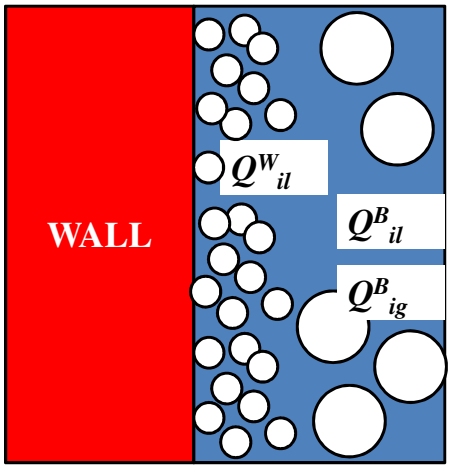

Figure 12. Heat Transfer Model for the Interface in the Bulk and Near the Wall

For subcooled boiling, the two parts are additive:

$$Q_{ig} = Q_{ig}^B + Q_{ig}^W \qquad (33)$$

and,

$$Q_{il} = Q_{il}^{B} + Q_{il}^{W} \tag{34}$$

The bulk interface heat transfer is at the steam-liquid interface in the bulk. This represents thermal energy exchange between the fluid interface (at the saturation temperature T^S corresponding to the local pressure **P**) and the bulk fluid state.

For gas, the bulk interface heat transfer is given by:

$$Q_{ig}^{B} = H_{ig}(T^S - T_g) \tag{35}$$

where H_{ig} is the gas interface heat transfer coefficient per unit volume, and T_g is the gas temperature.

For liquid, the bulk interface heat transfer is given by:

$$Q_{il}^{B} = H_{il}(T^S - T_l) \tag{36}$$

where, H_{il} is the liquid interface heat transfer coefficient per unit volume, and T_l is the liquid temperature.

The terms Q_{ig}^{W} and Q_{il}^{W} are the interface heat transfer rates near the wall and will be defined in terms of the wall vapor generation (or condensation) process. Inserting Equation 35 and Equation 36 into Equation 33 and Equation 34 gives:

$$Q_{ig} = H_{ig}\left(T^{S} - T_{g}\right) + Q_{ig}^{W} \tag{37}$$

and,

$$Q_{il} = H_{il}(T^{S} - T_{l}) + Q_{il}^{W} \tag{38}$$

Although it is not a fundamental requirement, it is assumed that Equation 32 will be satisfied by requiring that the bulk interface energy exchange terms and the near wall interface energy exchange terms each sum to zero independently, so that:

$$H_{ig}\left(T^{S} - T_{g}\right) + H_{il}(T^{S} - T_{l}) + \Gamma_{ig}\left(h_{g}^{*} - h_{l}^{*}\right) = 0 \tag{39}$$

and,

$$Q_{ig}^{W} + Q_{il}^{W} + \Gamma_{W}\left(h_{g}' - h_{l}'\right) = 0 \tag{40}$$

In addition, since it is assumed that vapor appears at saturation, it follows that $Q_{ig}^{W} = 0$ for boiling processes in the boundary layer near the wall. Equation 40 can then be used to solve for the interface vaporization rate in the boundary layer near the walls:

$$\Gamma_W = \frac{-Q_{il}^{W}}{h_g' - h_l'} \tag{41}$$

Similarly, since it is assumed that liquid appears at saturation, it follows that $Q_{il}^{W} = 0$ for condensation processes in the boundary layer near the wall. Equation 40 can then be used to solve for the interface condensation rate in the boundary layer near the walls:

$$\Gamma_W = \frac{-Q_{ig}^{W}}{h_g' - h_l'} \tag{42}$$

Solving Equation 41 and Equation 42 for Q_{il}^{W} and $-Q_{ig}^{W}$, and substituting these terms into Equation 37 and Equation 38, the interface energy transfer terms, Q_{ig} and Q_{il}, can be expressed in a general way as:

$$Q_{ig} = H_{ig}\left(T^S - T_g\right) - \left(\frac{1-\varepsilon}{2}\right)\Gamma_W(h'_g - h'_l) \tag{43}$$

and,

$$Q_{il} = H_{il}(T^S - T_l) - \left(\frac{1+\varepsilon}{2}\right)\Gamma_W(h'_g - h'_l) \tag{44}$$

where ε = 1 for boiling in the boundary layer near the wall, and ε = -1 for condensation in the boundary layer near the wall. Finally, Equation 32 can be used to solve for the interface vaporization (or condensation) rate in the bulk fluid:

$$\Gamma_{ig} = -\frac{Q_{ig} - Q_{il}}{h^*_g - h^*_l} - \Gamma_W \frac{(h'_g - h'_l)}{h^*_g - h^*_l} \tag{45}$$

which, upon substitution of Equation 43 and Equation 44, becomes:

$$\Gamma_{ig} = \left[\frac{H_{ig}\left(T^S - T_g\right) + H_{il}(T^S - T_l)}{h^*_g - h^*_l}\right] \tag{46}$$

The phase change process that occurs at the interface is envisioned as a process in which bulk fluid is heated or cooled to the saturation temperature and phase change occurs at the saturation state. The interface energy exchange process from each phase must be such that at least the sensible energy change to reach the saturation state occurs. Otherwise, it can be shown that the phase change process implies energy transfer from lower temperature to a higher temperature. This is avoided by properly selecting h_g^* and h_l^* for bulk interface mass transfer as well as h_g' and h_l' for near wall interface mass transfer. In particular, it can be shown that h_g^* and h_l^* should be (NRC 2001):

$$h_g^* = \frac{1}{2}\left[\left(h_g^S + h_g\right) + \eta(h_g^S - h_g)\right] \tag{47}$$

and,

$$h_l^* = \frac{1}{2}\left[(h_l^S + h_l) - \eta(h_l^S - h_l)\right] \tag{48}$$

where,

$$\begin{aligned} \eta \quad &= 1 \; for \; \Gamma \geq 0 \\ &= -1 \; for \; \Gamma < 0 \end{aligned} \tag{49}$$

For flashing or isothermal cases η = 1, $h_l^* = h_l$ and $h_g^* = h_g^S$. For condensing cases, η = -1, $h_l^* = h_l^S$ and $h_g^* = h_g$. It can also be shown that h_g' and h_l' should be (NRC 2001):

$$h_g' = \frac{1}{2}\left[\left(h_g^S + h_g\right) + \varepsilon(h_g^S - h_g)\right] \tag{50}$$

and,

$$h_l' = \frac{1}{2}\left[(h_l^S + h_l) - \varepsilon(h_l^S - h_l)\right] \tag{51}$$

where,

$$\begin{aligned} \varepsilon \quad &= 1 \; for \; \Gamma_W \geq 0 \\ &= -1 \; for \; \Gamma_W < 0 \end{aligned} \tag{52}$$

For flashing or isothermal cases, $\Gamma_W \geq 0$, $h_l' = h_l$ and $h_g' = h_g^S$. For condensing cases, $\Gamma_W < 0$, $h_l' = h_l^S$ and $h_g' = h_g$.

Substituting Equation 46 into Equation 23 gives the final expression for the total interface mass transfer as:

$$\Gamma_g = -\frac{H_{ig}\left(T^S - T_g\right) + H_{il}(T^S - T_l)}{h_g^* - h_l^*} + \Gamma_W \tag{53}$$

Dissipation Terms

The phasic energy dissipation terms, $DISS_g$ and $DISS_l$, are the sums of wall friction and pump effects. The dissipation effects due to interface mass transfer, interface friction, and virtual mass are neglected. This is reasonable since these terms are small in magnitude in the energy equation. In the mass and the momentum equations, interface mass transfer, interface friction, and virtual mass are important and are not neglected.

Equations of State

The six equations of motion model, uses five independent state variables. The independent state variables are chosen to be **P**, α_g, u_g, u_l, and x_n. All the remaining thermodynamic variables (temperatures, densities, partial pressures, qualities, etc.) are expressed as functions of these fine independent state variables. In addition to these variables, several state derivatives are needed for some of the linearizations used in the numerical scheme.

Constitutive Equations

The constitutive relations include models for defining flow regimes and flow regime related models for interphase drag and shear, the coefficient of virtual mass, wall frictions, wall heat transfer, interphase heat and mass transfer, and direct (sensible) heat transfer. Heat transfer regimes are defined and used for wall heat transfer.

RELAP5 Solution Scheme

The semi-implicit numerical solution scheme utilized in R5 is based on replacing the system of differential equations with a system of finite difference equations partially implicit in time. The terms evaluated implicitly are formulated to be linear in the dependent variables at new time. This results in a linear time advancement matrix that is solved by direct inversion using a sparse matrix routine. An additional feature of the scheme is that implicitness is selected such that the equations of motion can be reduced to a single difference equation per fluid control volume or mesh cell, which is in terms of the hydrodynamic pressure. Thus, only an N x N system of equations must be solved simultaneously at each time step. N is the total number of control volumes used to simulate the fluid system. The difference equations are based on the concept of a control volume (or mesh cell) in which mass and energy are conserved by equating accumulation to the rate of mass and energy incoming through the cell boundaries, minus the rate of mass and energy outgoing through the cell boundaries plus the source terms. This model results in defining mass and energy volume average properties and requiring knowledge of velocities at the volume boundaries. The velocities at boundaries are most

conveniently defined through use of momentum control volumes (cells) centered on the mass and energy cell boundaries. This approach results in a numerical scheme having a staggered spatial mesh. The scalar properties (pressure, energies, and void fraction) of the flow are defined at cell centers, and vector quantities (velocities) are defined on the cell boundaries. The resulting one-dimensional spatial noding is illustrated in Figure 13. The term cell means an increment in the spatial variable, x, corresponding to the mass and energy control volume.

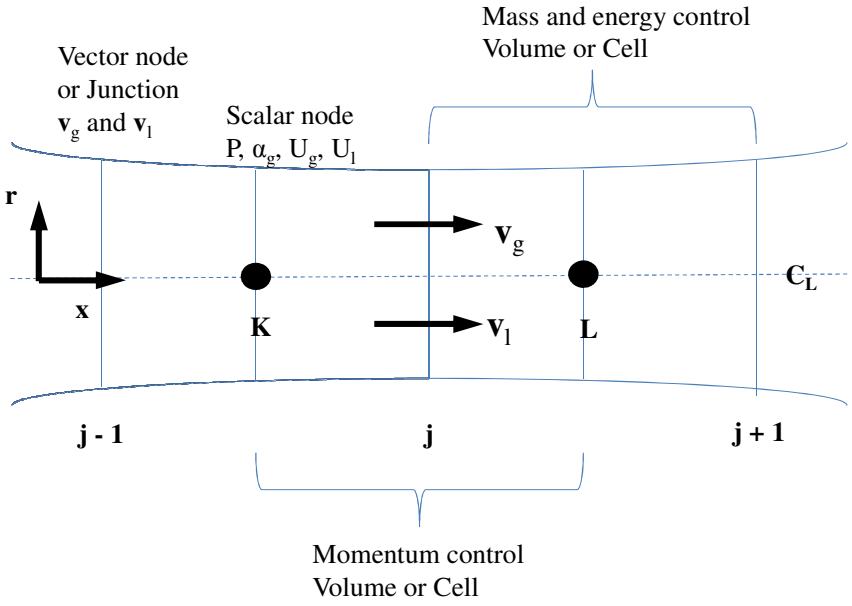

Figure 13. Nodalization Scheme

The difference equations for each cell are obtained by integrating the mass and energy equations with respect to the spatial variable x, from junction at x_j to x_{j+1}. The momentum equations are integrated with respect to the spatial variable from cell center to adjoining cell center (x_K to x_L). When the mass and energy equations are integrated with

respect to the spatial variable from junction j to j+1, differential equations in terms of cell-average properties and cell boundary fluxes are obtained.

Alternative Conservation of Momentum and Energy Calculations

The calculation methods presented in this section are considered alternative in the sense that they can be completed by hand; however, they are based on reasonable first principal assumptions, and as such, produce results which can be utilized to compare with the computer generated solutions for validation purposes.

Momentum Balance – Frictional Pressure Drop

Applying Reynolds Transport Theorem to momentum (steady):

$$\iint \rho \boldsymbol{v}\boldsymbol{v} \cdot \boldsymbol{n} d\boldsymbol{S} = \iiint \rho \boldsymbol{g} dV + \iint (\boldsymbol{\tau} - \boldsymbol{P}) \cdot \boldsymbol{n} d\boldsymbol{S} \qquad (54)$$

where: ρ= fluid density, kg/m^3

$\boldsymbol{v}$= fluid velocity vector, m/s

$\boldsymbol{S}$= control volume surface, m

V= control volume, m^3

$\boldsymbol{\tau}$ = surface shear stress component, Pa

$\boldsymbol{P}$ = normal pressure stress component, Pa

$\boldsymbol{n}$ = unit surface normal vector

The simplified momentum balance includes the convective momentum exchange in and out of the control volume (on left), balanced with body forces and surface friction and pressure terms (on right).

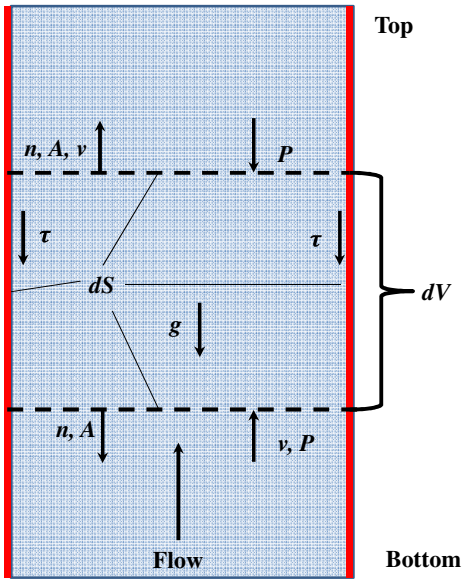

Figure 14. Vertical Channel Model (Tube)

A schematic of the vertical channel model for this analysis is provided in Figure 14. Analyzing the convective term on the left, we assume a vertical channel with liquid inlet conditions, and a mixture of liquid and vapor for the outlet conditions. The left hand side (lhs) term is:

$$-\iint \rho v|v| dA_{bottom} + \iint \rho v|v| dA_{top} = lhs$$

At the bottom of the channel:

$$-\iint \rho v^2\, dA_{bottom} = -\iint \rho v^2\, dA_{vapor\ bottom} - \iint \rho v^2\, dA_{liquid\ bottom}$$

$$= \left(-v_{vapor} - v_{liquid}\right)_{bottom}$$

The same analysis can be completed for the top of the channel, and remembering that:

$$_{vapor} = x$$

where: x = steam quality, (fraction)

and,

$$_{liquid} = (1 - x)$$

Therefore,

$$\iint \rho \boldsymbol{vv} \cdot \boldsymbol{n} d\boldsymbol{S} = \left(x v_{vapor} + (1-x) v_{liquid}\right)_{top} - \qquad (55)$$

$$\left(x v_{vapor} + (1-x) v_{liquid}\right)_{bottom}$$

Evaluating the first term on the right hand side of Equation 54:

$$\iiint \rho \boldsymbol{g} dV = -\rho_{channel\ average} \boldsymbol{g} V_{channel} \qquad (56)$$

now the second term on the right hand side of Equation 54:

$$\iint (\boldsymbol{\tau} - \boldsymbol{P}) \cdot \boldsymbol{n} d\boldsymbol{S} = (\tau A)_{wall} - \left(P_{bottom} - P_{top}\right) \times \qquad (57)$$

$A_{cross\ section}$

We can consider a friction factor (*f*), so that for a tubular channel with diameter, *D*, and length, *L*:

$$\tau_{wall}(\pi DL) = \left(\frac{1}{2}\right)\rho v^2(fL/D)\pi D^2/4$$

Defining mass flux $G = \square/A$, and rewriting Equation 54 with all of the simplified terms, we arrive at:

$$P_{bottom} - P_{top} = \Delta P_{channel} = \frac{1}{2}\frac{G^2}{\rho}\frac{L}{D}f + G\left(xv_{vapor} + (1-x)v_{liquid}\right)_{top} - G\left(xv_{vapor} + 1-xvliquidbottom+\rho L\boldsymbol{g}\right) \quad (58)$$

Equation 58 can be further reduced in order to apply empirical factors that have been developed experimentally. One such set of correlations is available (Todreas 1993) that utilizes an equation similar to Equation 58 with factors r_2, r_3 and r_4 determined from empirical results, and provided as graphical data. Hence, Equation 59 can be used to estimate the channel pressure drop. The empirical data presented in the graphs (Todreas 1993) is based on inlet steam with a quality of 0.0. The factors r_2, r_3 and r_4 are selected corresponding to the channel inlet pressure, and desired channel exit quality, and are then used in the pressure drop calculation:

$$\Delta P_{channel} = \frac{1}{2}\frac{G^2}{\rho}\frac{L}{D} f r_3 + \frac{G^2}{\rho} r_2 + L\boldsymbol{g}\rho r_4 \qquad (59)$$

Energy Balance

The approach taken to calculate the exit steam temperature that can be compared to the computer solution is based on a thermodynamic energy balance. Using the known inlet steam conditions, total channel heat input and total channel mass flow, the exit channel enthalpy can be calculated using the following equation:

$$q^{"} A = (h_{out} - h_{in}) \qquad (60)$$

re-arranging,

$$h_{out} = h_{in} + \frac{q^{"} A}{} \qquad (61)$$

Assume that the channel pressure approximately equal to the inlet, i.e., $\boldsymbol{\Delta P_{channel}}$ is small compared to the total fluid pressure, and, the exit steam is superheated. Then the exit steam temperature can be found directly by using the superheated steam tables along with the state of the steam defined by h_{out} and channel pressure.

Axial Power Distribution and Heat Flux Boundary Condition Development

The axial (vertical z-direction) heat flux boundary condition applied to the steam tube essentially models the heat input resulting from the nuclear fission reaction in the HTGR core. This heat generation is not uniform, and is actually a function of spatial location, radial and axial, in the core (assuming cylindrical reactor core and coordinates with axis-symmetry, i.e., no gradient in the θ direction). A steady state power density profile (Strydom 2011) calculated for the TRISO fuel system at a radial location (r=15 cm) was available, therefore, it was selected for use in this analysis. The basis for this selection is the assumption that the axial power density profile will provide a reasonably accurate approximation of the axial power distribution expected in an actual reactor loaded with TRISO fuel. Any gradients in the radial direction across the tube are assumed to be small, since the $D << L$.

Non-Dimensional Development

The axial power density used in this analysis is from figure 3(Strydom 2011). In order to use the graphical data presented in that reference in a spreadsheet format, the data was manually transferred from graphical to tabular form. Axial power density values for 23 axial locations were specifically read from the graph. The axial, or z dimension was easily transferred since 23 specific axial data points were provided in the graph. The maximum axial dimension, z_{max}, for the reactor core provided ((Strydom 2011)Table 3) was 943 cm. The z coordinates for the power density distribution were calculated as multiples of (943 cm (total length)/22 cm (length between each data point)). The power density values corresponding to these z values were measured directly from the graph in

millimeters and then converted by a graphical scale factor in the spreadsheet. The spreadsheet is included in Appendix C , and the resulting transferred axial power density appears to replicate the data reasonably well as illustrated in Figure 15.

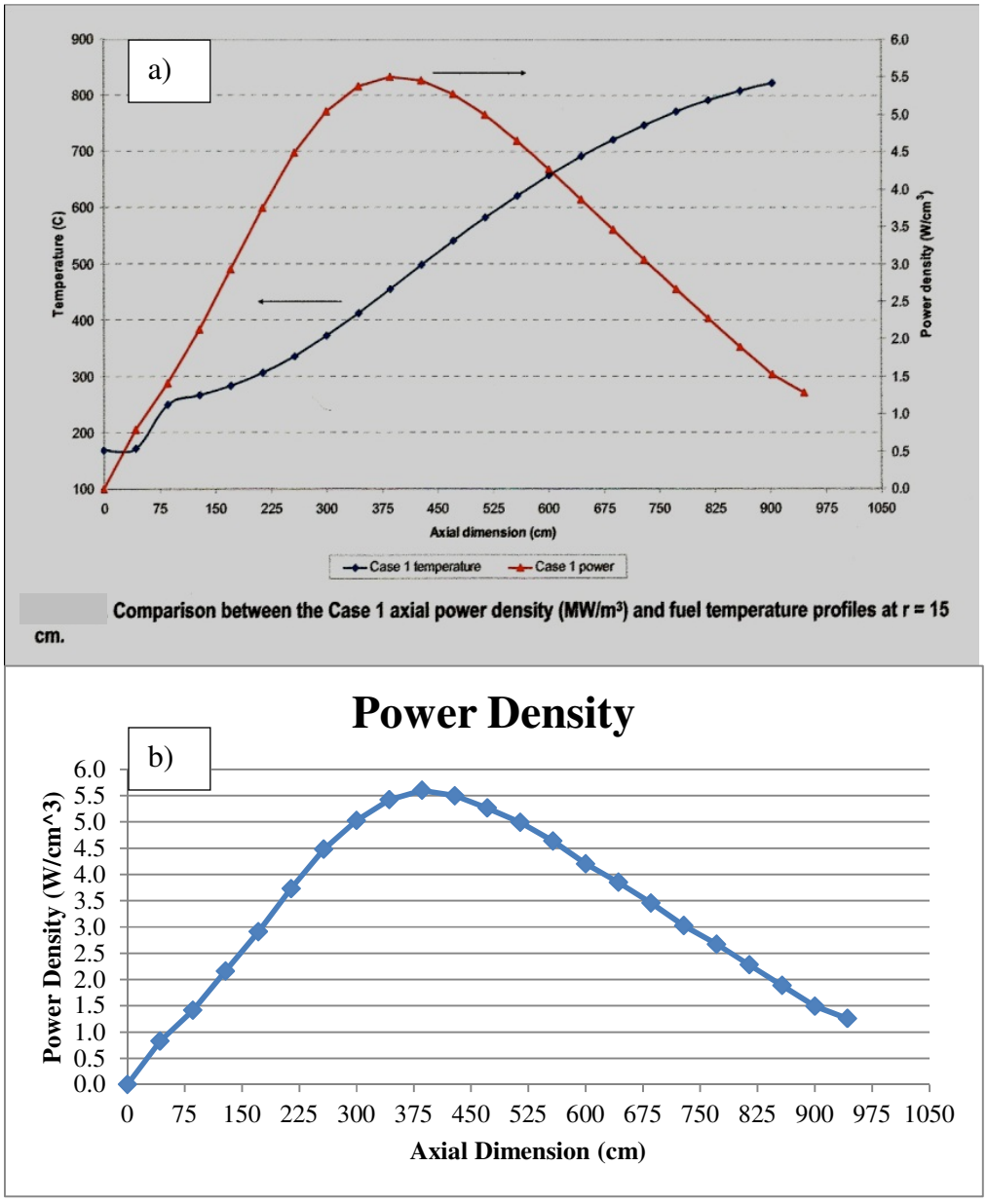

Figure 15. Comparison of Axial Power Density Profiles – a) (from(Strydom 2011)) and b) Data Transferred to Spreadsheet

The next objective is to develop a non-dimensional representation of the axial power density profile that can be used to generate axial heat flux boundary conditions for reactors with different total power levels and different physical (axial) dimensions. First, define the non-dimensional Power Factor at location *z (PF(z))* as follows:

$$PF(z) = P(z)/P_{avg} \tag{62}$$

where: *PF(z)* = Power Factor at location z (non-dimensional)

P(z) = Power Density at location z (W/cm^3)

P_{avg} = Average Power Density (W/cm^3)

and,

$$P_{avg} = 1/z_{max}\left(\int_0^{z_{max}} P(z)dz\right) \tag{63}$$

The power density curve developed above is utilized as *P(z)*, and a numerical integration process (simple trapezoidal method) is used in a spreadsheet to calculate P_{avg} from *P(z)*.

The axial dimension z is non-dimensionalized as follows:

$$Z = z/z_{max} \tag{64}$$

where: Z = non-dimensional axial location

z = axial dimension (cm)

z_{max} = maximum axial dimension (cm)

Data from (Strydom 2011) has been non-dimensionalized, and is illustrated in Figure 16. Now that the *PF(Z)* is defined, it can be used to develop an axial heat flux distribution boundary condition for a single tube in a reactor of any size (length, L), or total power utilizing TRISO fuel. As a test, the *PF* curve was numerically integrated to calculate PF_{avg}. As expected, the result was 1.0 (see Appendix C , PF Integration Check).

The approach for developing the axial heat flux boundary condition starts by calculating the total core power, then dividing by the number of steam tubes in the core to yield the total power for each tube. Total power is defined as the power required to heat the steam from inlet conditions, to the target outlet conditions (state **1** to **1'** in Figure 1).

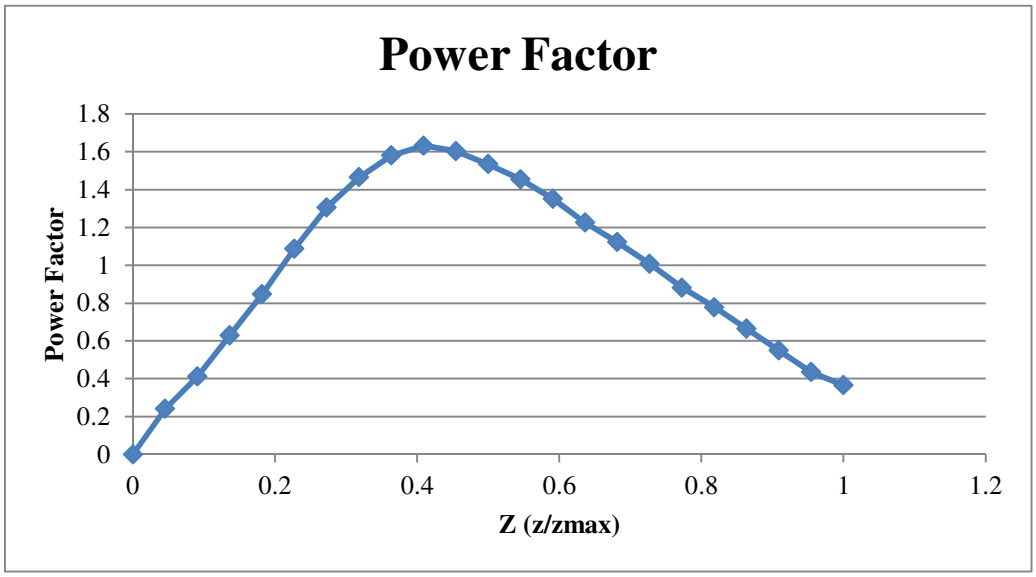

Figure 16. Non-dimensional Axial Power Factor (PF(Z))

Reactor Specific Boundary Condition

Knowing the average power per tube and the physical dimensions of the tube ($L = z_{max}$), the *PF* equation, Equation 62, can be re-arranged and used to develop the power density distribution *P(z)* specific to the core; and finally, the axial heat flux boundary condition can be defined.

The *PF(z)* profile specific to the actual core dimensions must first be calculated from the non-dimensional *PF(Z)*. This is accomplished in the spreadsheet by simply multiplying the non-dimensional *Z* by the actual z_{max} to determine z_{actual}:

$$z_{actual} = Z * z_{max} \tag{65}$$

where: z_{actual} = axial coordinates, actual reactor (cm)

Z = non-dimensional axial location

z_{max} = maximum axial dimension, also L, (cm)

Knowing P_{avg} per tube, Equation 62 is re-arranged to calculate the actual $P(z)$ for the actual tube, from the $PF(Z)$:

$$P(z)_{actual} = P_{avg} * PF(Z) \tag{66}$$

Now, the PF values adjacent to the z_{actual} dimensions in the spreadsheet are the corresponding $PF(z)_{actual}$.

Finally, dividing both sides of the equation by the area of the tube ($A_{tube}=\pi D\ell$) yields the axial heat flux profile boundary condition:

$$\begin{aligned} q"(z) = P(z)/A_{tube} &= P_{avg} * PF(z)/A_{tube} \\ &= P_{avg} * PF(z)/(\pi D\ell) \end{aligned} \tag{67}$$

where: $q"$ = average tube element heat flux at z (W/cm^2)

D = tube diameter (cm)

ℓ = length of tube element (cm)

$A_{tube} = \pi D\ell$

The dimensionally specific heat flux boundary condition, as illustrated in Figure 17, can be applied to the outside of an individual tube in order to approximate the heat

provided to the tube from the fission reaction heat generated by the reactor. The derived boundary condition illustrated in this section forms the basis for the heat flux applied to each hydrodynamic cell via its associated heat structure in R5. This specific boundary condition modeling refinement will be discussed further in the RELAP5 Research Model section.

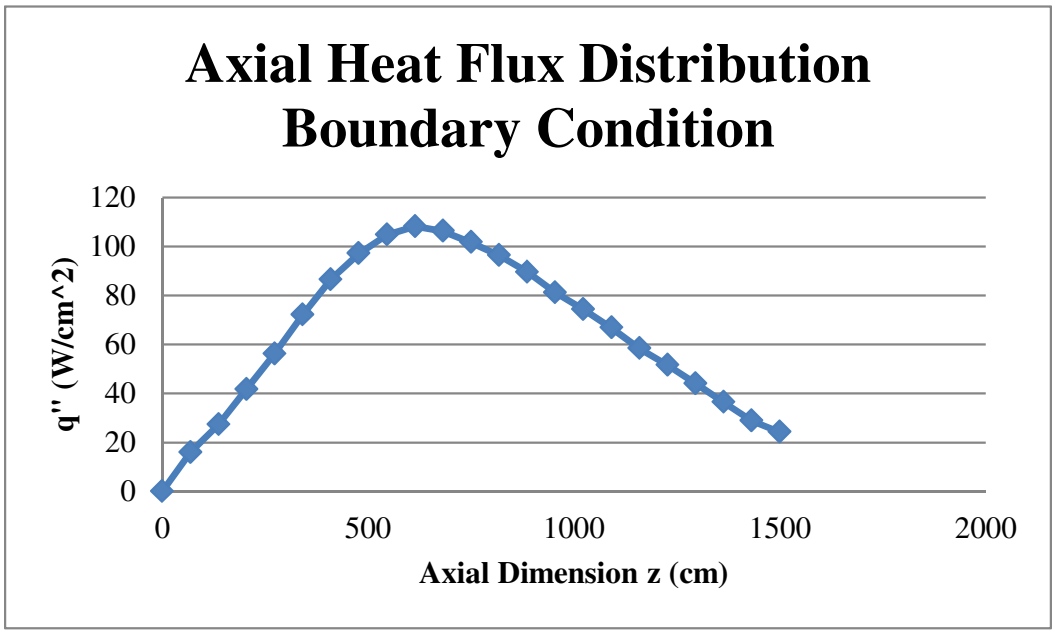

Figure 17. Axial Heat Flux Boundary Condition for a Reactor with L=1500 cm and q”avg = 66.2 W/cm^2

RELAP5 Research Model

R5 is fully capable of working with the one dimensional, cylindrical axis-symmetric reheat steam tube geometry, two fluid (vapor (steam) and liquid (water)), non-uniform axial heat flux (power shape) problem as defined. R5 calculates a balance of

momentum, mass and energy using six conservation equations (set of three for each fluid). A significant quantity of documentation exists in the R5 user manuals (NRC 2001) pertaining to all aspects of the equation development, discretization, and solution scheme of these and other constitutive equations as summarized in the RELAP5 Equations of Motion section. After review of the information, including well documented detailed descriptions, it was concluded that the R5 capabilities are well suited for this research problem as defined.

A single channel R5 model was selected for further development to analyze the complex two phase flow and boiling heat transfer mechanisms expected to occur within the reheat steam tube. Axis-symmetric cylindrical modeling geometry and coordinates were selected based on the cylindrically shaped steam tube. General guidance provided in the R5 user manual (NRC 2001), as well as R5 modeling results from previous modeling work (Nilsson 1993), were used as the basis for the initial modeling scheme including selection of the initial number of hydrodynamic cells and nodalization.

Utilization of a HTGR to reheat steam results in the internal tube surface temperatures approaching and possibly exceeding 1,000 ^{o}C. At this condition, the thermal radiation transport models included within R5 may not be adequate. The film boiling model in R5 ((NRC 2001) Volume IV) considers the vapor liquid mixture to be an optically thin medium, which means the vapor and liquid do not self-absorb emitted thermal radiation. The radiative exchange, as coded, between wall and vapor, and vapor to liquid, is neglected. In order to quantify the efficacy of this assumption, and to

determine the conditions at which it is no longer adequate, an analysis is provided later in this Chapter which assumes that the vapor in the steam tube is optically thick.

Following model construction, inlet and outlet hydrodynamic conditions, and heat transfer boundary conditions were specified.

Hydrodynamic Cells and Nodalization

The channel model utilizes the "pipe" component structure available in R5. It streamlines the connection of several hydrodynamic cells with similar geometric dimensions such as diameter. A pipe component with 47 hydrodynamic cells was selected as the initial model refinement, and a schematic of the model is provided in Figure 18.

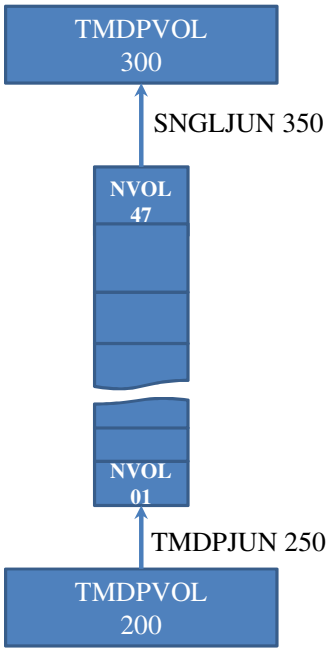

Figure 18. RELAP5 Hydrodynamic Model

Dimensionally, the assumed total tube length of 15 m and a diameter of 0.08 m for each of the 47 hydrodynamic cells provides a *L/D* of ~4 (*L/D*=15/47/0.08=3.99), which is greater than 1 (recommended (NRC 2001) Manual Appendix A). In order to evaluate the adequacy of the initial nodalization scheme, the number of hydrodynamic cells was decreased from 47 to 22, and then increased to 57, and 77. Results of the nodalization sensitivity are presented in Chapter 4.

In addition to the channel modeled using the pipe structure, the hydrodynamic part of the model also included the inlet time dependent volume (TMDPVOL 200) which defined the flow and thermodynamic state of the inlet steam. The source element 200 was connected to the pipe by using a time dependent junction (TMDPJUN 250) as recommended. The outlet of the pipe structure is connected to a regular non-time dependent junction (SNGLJUN 350) which is recommended to provide the characteristics of an infinite sink for the pipe output. The final reservoir for the system is a time dependent volume (TMDPVOL 300) which is connected to the output of the pipe outlet junction.

Heat Structures

A heat structure is associated with each hydrodynamic cell in the pipe structure. This modeling scheme allows the specification of a non-uniform heat flux condition for each hydrodynamic cell in the pipe. Each heat structure is dimensioned and nodalized as illustrated in Figure 19. The heat flux boundary condition is applied on the right side surface of the heat structure at “RCOORD”. An insulated boundary condition, i.e., zero

temperature gradient, is specified on the outside of RCOORD. The convective boundary condition is applied to the left side boundary surface at LCOORD. Since the axial power shape is non-uniform, a normalized power factor was derived for each heat structure.

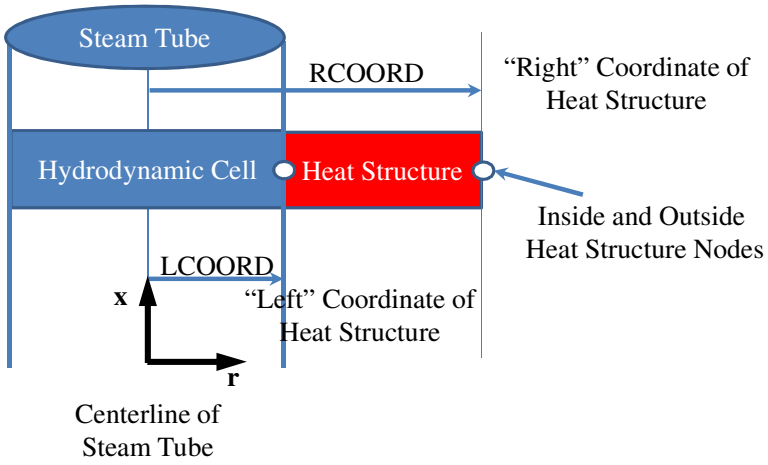

Figure 19. Heat Structure Association with the Hydrodynamic Cell

The total reactor length L is assumed fixed at 15 m (based on LMTD results), and the number of hydrodynamic cells selected defines the actual length (ℓ) dimension of each hydrodynamic cell. Since this number of cells in the R5 may be greater than the heat flux profile defined points derived previously, a method to increase this refinement was developed. Basically, linear interpolation between two known data points is used to calculate the power factor at any point between the known points. The accuracy of this heat flux boundary condition refinement method is checked by comparing the total power applied to the steam tube, calculated in R5, with the total power of each tube calculated and presented as 1.686E+6 W in Appendix C .

Annotated input of the 47 hydrodynamic cell "base" model is included in Appendix D along with notations for significant model defining input parameters.

Thermal Radiation Transport

The following analysis provides an approximate method for quantifying the additional heat transfer of thermal radiation transport to the vapor/steam from the wall, assuming that the medium is optically thick. This analysis will be conducted utilizing an extension to the Rosseland Approximation (Viskanta 1966). The spectral radiant energy flux vector is defined as the net flow of radiant energy in a given direction **s** per unit area, time and frequency interval due to radiation from all directions:

$$\boldsymbol{\mathcal{F}}_{\nu} = \int_{\Omega=4\pi} I_{\nu} \boldsymbol{s}\, d\Omega \tag{68}$$

where: $\boldsymbol{\mathcal{F}}_{\nu}$ = Radiant energy flux vector, (W/m^2)

Ω = Solid Angle, (sr)

$\boldsymbol{\nu}$ = frequency, (s^{-1})

$\boldsymbol{s}$ = Unit vector in the direction of the pencil rays

I_{ν} = Intensity of radiation, (W/μm sr m^2)

For the Rosseland approximation to be valid in the interior of a non-gray medium, it is necessary to introduce the definition of the mean extinction coefficient. In the case of an optically thick media, the intensity of scattered radiation approaches $n_{\nu}^2 I_{b,\nu}$ whenever the condition $\int_0^L \beta_{\nu}\, ds \gg 1$ is satisfied for all important frequencies. Here, n_{ν} is the index of refraction, β_{ν} is the mean extinction coefficient, and $I_{b,\nu}$ is the intensity of radiation of a black body. Making a Taylor expansion about $n_{\nu}^2 I_{b,\nu}$, yields:

$$I_\nu = n_\nu^2 I_{b,\nu} - \frac{1}{\beta_\nu}(\boldsymbol{s}\cdot\nabla)n_\nu^2 I_{b,\nu} + \frac{1}{\beta_\nu}(\boldsymbol{s}\cdot\nabla)\left[\frac{1}{\beta_\nu}(\boldsymbol{s}\cdot\nabla)n_\nu^2 I_{b,\nu}\right] - \cdots \tag{69}$$

Substituting Equation 69 into Equation 68 and retaining the first three terms of the expansion:

$$\boldsymbol{\mathcal{F}}_\nu = -({}^{4\pi}/_{3\beta_\nu})\nabla\left[n_\nu^2 I_{b,\nu}(T)\right] \tag{70}$$

Integration of Equation 70 over the entire spectrum yields:

$$\boldsymbol{\mathcal{F}} = -({}^{4}/_{3\beta_R})\nabla[n^2 E_b(T)] \tag{71}$$

where β_R is the Rosseland mean extinction coefficient defined by:

$$\frac{1}{\beta_R} = \int_0^\infty \frac{d(n_\nu^2 I_{b,\nu})\,d\nu}{\beta_\nu\,dT} \Bigg/ \int_0^\infty \frac{d(n_\nu^2 I_{b,\nu})\,d\nu}{dT} \tag{72}$$

The difficulty resulting from this approximation near the boundary can be removed by introducing a temperature-jump boundary condition. The resulting expressions for the radiative heat flux obtained by using the Rosseland Approximation with temperature boundary conditions were found to agree with a wide range of optical depths with the exact numerical calculations (Abu-Romia 1967). Assuming that the index of refraction is independent of temperature, and considering the emitting process in the vapor can be written in terms of black-body emissive power:

$$E_b(T) = \sigma T^4$$

where σ is the Stefan-Boltzmann constant; then, Equation 71 reduces to:

$$\boldsymbol{\mathcal{F}} = -\frac{16n^2\sigma T^3}{3\beta_R}\nabla T \tag{73}$$

The black-body assumption is reasonable for derivation purposes. Calculations will be performed with correlations based on empirical data. For optically thick media, the radiation flux vector is similar to the Fourier-Biot law of heat conduction with the radiative conductivity component given by:

$$k_r = \frac{16n^2\sigma T^3}{3\beta_R} \tag{74}$$

Therefore, if the medium is assumed to be optically thick, then the thermal conductivity of the medium, k_{steam}, is enhanced by the addition of k_r such that:

$$k_{total} = k_{steam} + k_r \tag{75}$$

k_{steam} and β_R are calculated utilizing correlations from (Mohanty 1987):

$$k_{steam} = 0.0592(0.8302 - 0.0320\,\theta^1 + 0.4903\,\theta^2 \tag{76}$$

$$\beta_R = 574.0(2.8 - 2.428\,\theta^1 + 0.6286\,\theta^2)$$

for T < 1115 K; (77)

β_R = 260

for T > 1115 K

where: k_{steam} = Steam thermal conductivity, (W/m K)

β_R = Rosseland mean extinction coefficient, $(atm \cdot m)^{-1}$

θ = T (K) / 555

As noted in (Abu-Romia 1967), for many practical applications, a gas/vapor can be optically thick in some parts of the infrared spectrum and optically thin or transparent in the rest. The spectral data used as the basis for this analysis of water vapor are 2.7 μm, 6.3 μm (fundamental) bands, and 20 μm (rotational) band. Thus, the channel diameter

dimension of the modeled steam tube of the order of ~0.08 m, is much larger than the wavelengths of the "strong" bands considered.

The values of the Rosseland mean extinction coefficient (β_R) were calculated for specific "strong" bands for water vapor (noted for water vapor previously). β_R values are calculated, and presented in (Abu-Romia 1967) as a function of temperature and pressure, on the basis of selecting average values for the line intensity-spacing ratio and the line half-width-spacing ratio for each band at each temperature. Correlations provided in (Mohanty 1987) and presented as Equation 76 and Equation 77 were developed from this data.

Chapter 4

Results and Discussion

The LMTD results form the basis for the sizing of the HTGR reactor and the individual steam tubes modeled using the R5 computer code. R5 model results are presented and compared to approximate calculation results using simplified models for pressure drop and total heat transfer. Steady state conditions were obtained by initiating the computer calculations from an isothermal condition, then increasing channel power from zero to 100% from 5.0 to 10 second. Isothermal conditions were established during the initial 5.0 seconds. Then, this input power condition is held constant for the remainder of the 600 second run, at which point steady state conditions exist.

LMTD Results

As previously presented in Equations 7, 8 and 9, the convective heat transfer (U) calculation is essentially a power function of inner steam tube diameter D. Since q_{input} and ΔT_{lm} are constant, plotting U as a function of D results in a curve, as shown in Figure 20.

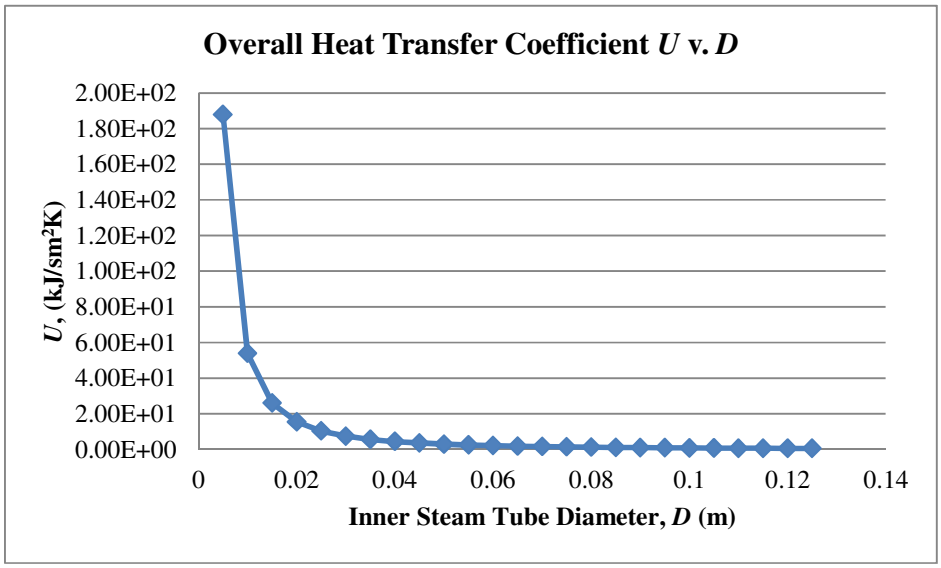

Figure 20. Functionality of U

As presented in Equation 10, A is proportional to $1/U$ in the LMTD equation. Area A calculated using the assumed tube dimensions, i.e., $A = \pi D L$, is a linear function of D. The LMTD iterative solution exists where the two "A" curves intersect. Based on the mathematical characteristics of the two equations, one intersection, or solution, is expected for each set of tube dimensions as shown in the Figure 21.

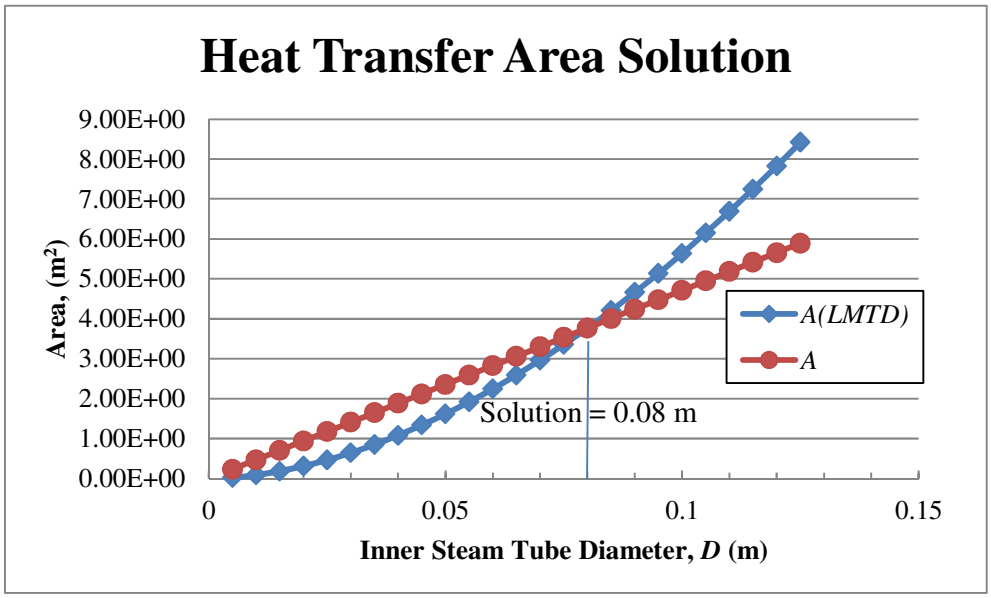

Figure 21. LMTD Iterative Solution Graphical Representation

This scenario lends itself to a parameterization type of analysis where a set of solution curves is developed by setting one parameter constant, such as *L*, then generating a curve by calculating the total number of tubes *N*, as a function of *D*. Repeating this process for different *L*'s results in a set of solution curves which provide insight for the selection of reasonable tube dimensions based on other considerations such as pressure drop.

The dimensions of the steam tube in this research were determined by conducting a parameter study using the LMTD iterative spreadsheet. There are three primary steam tube dimensional variables investigated in the parameter study: Tube Length (*L*), Inner Tube Diameter (*D*) and Number of Tubes (*N*). As mentioned previously, each curve was developed for an assumed *L*, then, for each *D*, an iterative solution was used to determine *N*.

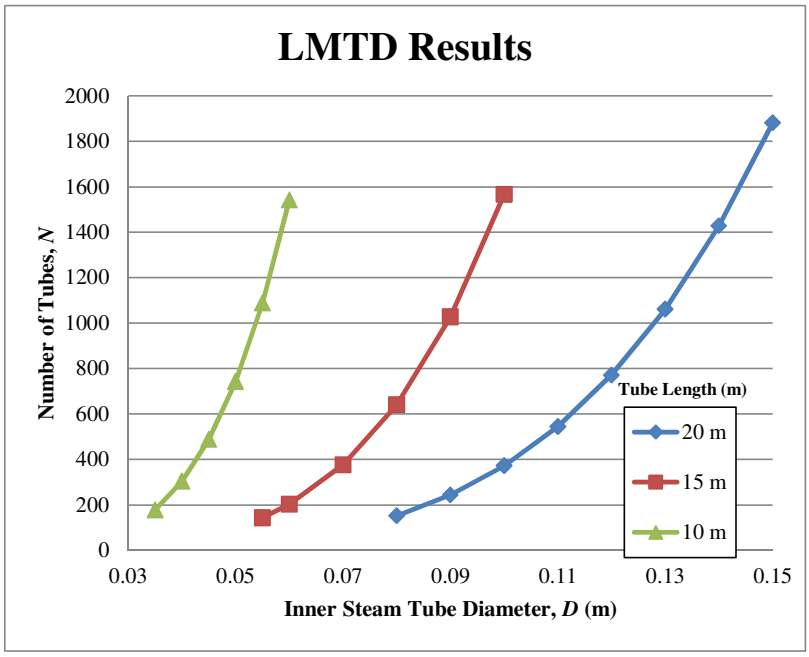

Figure 22. Iterative Results

As shown in Figure 22, iterative solutions were calculated for several cases. The equations are sensitive to *D* (i.e., affects heat transfer area, *Re* and velocity), *L* (i.e., effects heat transfer area), and *N* (i.e., affects total heat transfer area). The next step is to evaluate pressure drop as a function of dimension change.

The steam tube pressure drop was calculated utilizing the single phase vapor equations as presented in Appendix E with r2, r3, and r4 equal to 1.0. This is assumed reasonable since the functionality of pressure drop with diameter was important only as a relative selection factor. An accurate value of pressure drop was not important as a selection factor.

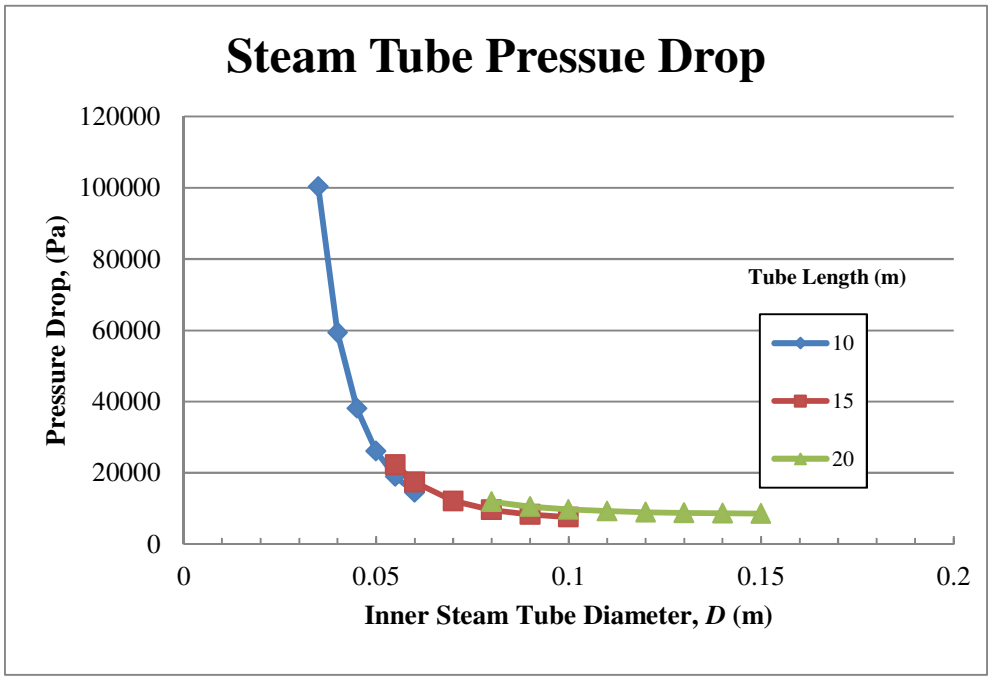

Figure 23. Steam Tube Pressure Drop Varying *L, D* and *N*

Pressure drop was calculated over the range of tube diameters derived in the previous analysis, for each of the range of the three *L* dimensions considered, and are illustrated in Figure 23. As can be seen, pressure drop increases rapidly with $D < 0.05$ m, but is relatively constant at $D > 0.08$ m. For information, standard sized tube internal diameters are available in the range considered (Kanthal 2011).

The tube dimensions were selected on a qualitative review of the parameter study results, and basically arrived at a reasonable middle point: $L = 15$ m, $D = 0.08$ m, and $N = 641$. The total cross sectional area of the tubes is 7.3% of the total cross sectional area of the HTGR assuming a reactor diameter of 7.5 m (2:1 reactor *L* to *D* ratio). The LMTD calculations and results for the base case are presented in Appendix B . In order to reheat the total steam mass flow of 1,109 kg/s from thermodynamic condition **1** to **1'**,

1,081,496.8 kJ/s of heat input is required. This calculation also sets the mass flow rate per steam tube at 1.73 kg/s, which is used as an inlet boundary condition for other calculations in this research.

RELAP5 Results

The first step in the R5 analysis was to determine the length of run time required for the problem to achieve steady state conditions. Several initial de-bug runs were made during the initial stages of the R5 analysis and they indicated that a 600 second long run time was adequate to achieve steady state for the defined problem. The base 47 cell R5 model (75% inlet steam quality) output results are presented in the following figures for inlet and outlet mass flow, inlet and outlet channel pressure (i.e., channel total pressure drop), inside steam tube surface temperatures at cell 20, 25, 30 and 35, and inlet and outlet steam temperature. As can be seen in Figure 24, steady state conditions occur well before the 600 second time frame.

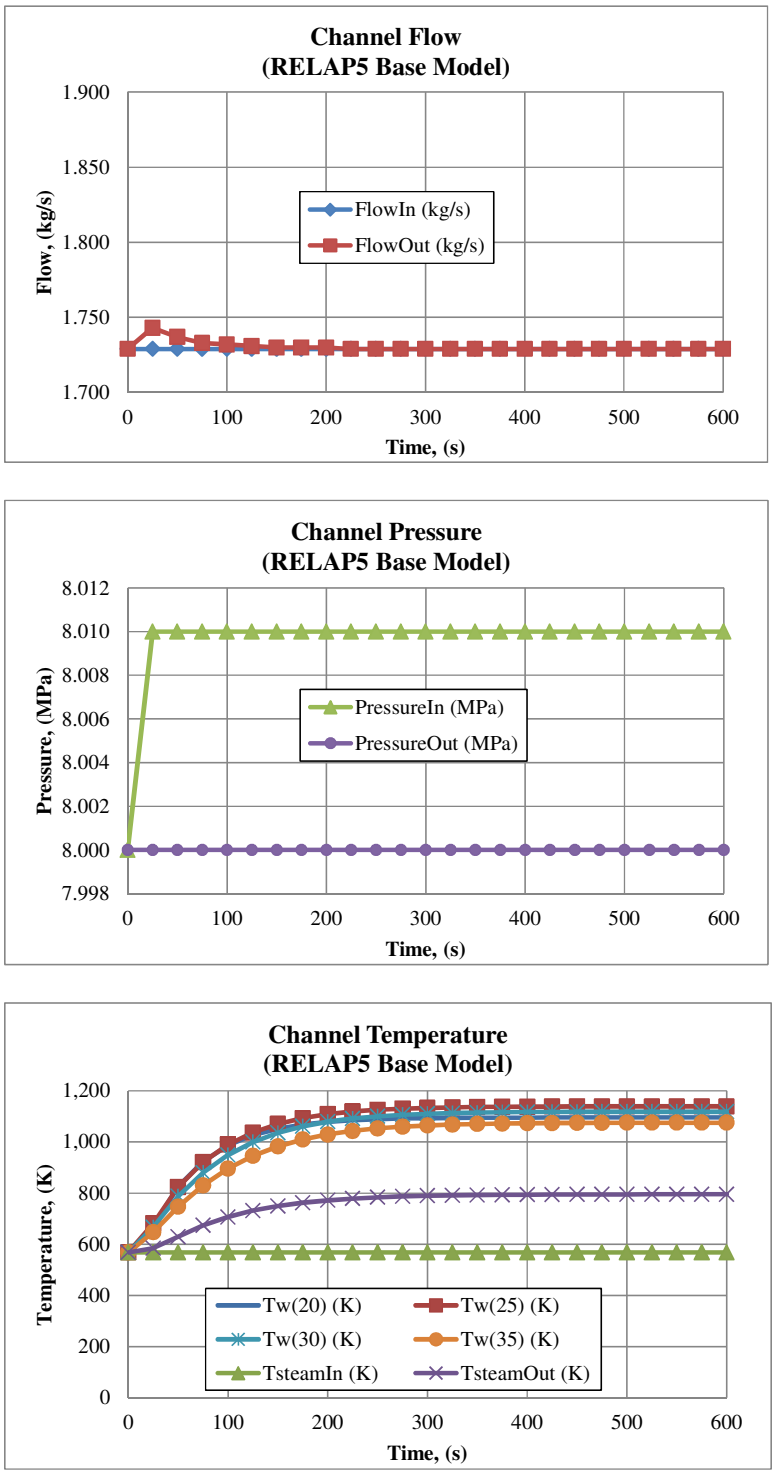

Figure 24. RELAP5 Results (Base 47 cell model, 75% Inlet Steam Quality)

Initially the channel mass flow in, and mass flow out differ slightly. The peak transient difference in mass is ~0.8% of the total. This imbalance is considered an acceptable numerical variation due do initial transient conditions. Therefore mass conservation equations have achieved acceptable steady state conditions. The steady overall pressure drop indicates that the overall momentum equations have achieved a steady state condition. Finally, the steady tube wall surface temperatures as a function of length up the steam tube, and the inlet and outlet steam temperatures are steady indicating that the overall energy equations have achieved steady state. The model run time could have been reduced; however, the actual computer run time was on the order of a couple of minutes and did not appear to tax computing resources in any way, therefore, it was decided to keep the run time set at 600 seconds for all of the computer runs.

Since steady state conditions were demonstrated to exist at 600 seconds, the tabulated output for the 600 second major edit is used for the results of each model run considered.

Nodalization

In order to determine if the number of hydrodynamic cells assumed for the model is adequate, a nodalization sensitivity analysis was conducted. The sensitivity analysis is a comparison of R5 results using models with both increased and decreased number of cells (nodes) from the base assumption of 47. The objective is to quantify the variability of the model results as a function of the number of hydrodynamic cells, and determine which model nodalization is sufficient.

NVOL defines the total number of hydrodynamic cells (cells) in the R5 model. Four total cases were considered for this analysis (cells equal NVOL): 22 cells, 47 cells (base case), 57 cells, and 77 cells. Changing the number of hydrodynamic cells is a fairly involved process requiring modification to several lines of the input deck. In each case, the following inputs were modified:

- Plotting variable definitions – due to exit cell number changes
- Minor edit cell number changes
- NVOL several places
- Length (ℓ) of hydrodynamic cell
- Re-calculation of power shape factors
- Power input (as a function of time) per hydrodynamic cell volume

In order for the total channel power to remain constant, each nodalization case required re-dimensionalizing the power shape data to fit the new size cells. This was a very tedious process and was completed using a separate spreadsheet which is provided in Appendix D . The check to ensure this was completed accurately is demonstrated by the comparison of total (integrated) channel power for each case. Results for the nodalization analysis are presented in Table 3 and Figure 25.

Table 3. RELAP5 Nodalization Analysis Results

NVOL	Total Channel Power (W)	Pin-Pout (Pa)	Tsteam (K)
22	1.694E+06	13183.2	802.19
%Diff.	0.44%	3.54%	0.86%
47	1.686E+06	13650.0	795.31
%Diff.	0.02%	0.07%	0.66%
57	1.686E+06	13660.0	790.06
%Diff.	0.07%	0.88%	0.18%
77	1.685E+06	13780.0	791.46

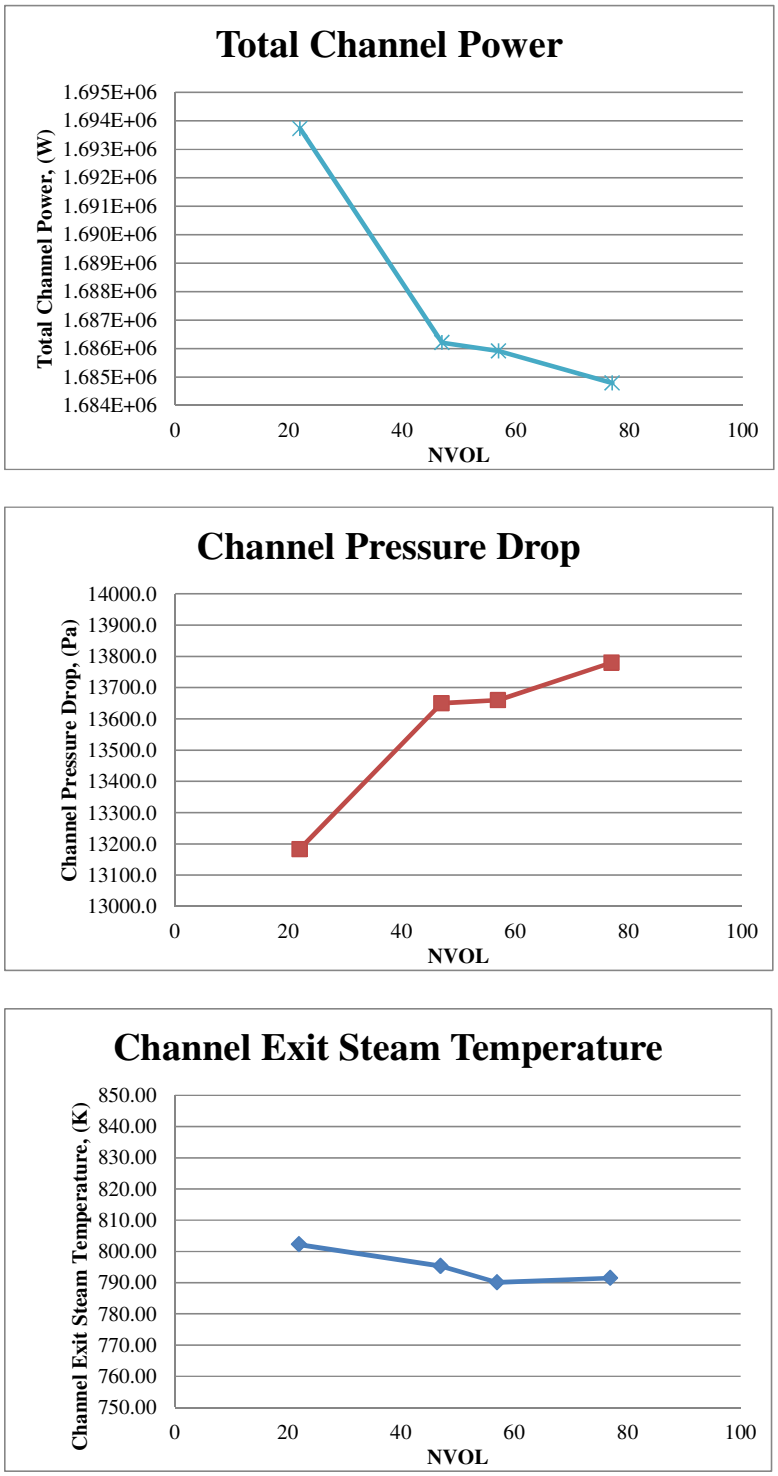

Figure 25. RELAP5 Nodalization Analysis Results

Parameters selected for comparison for the cases are presented in Figure 25 and include total channel power in Watts (W), total channel pressure drop in Pascal (Pa), and channel exit steam temperature (^{o}C). There appears to be some benefit to increase the nodalization from 22 to 47 since the maximum % difference between the 22 cell and 47 cell models is pressure drop. The maximum % difference between the 47 cell, 57 cell and 77 cell cases for all three of these key parameters is on the order of <1.0%, therefore the assumed nodalization of the base 47 cell case is considered adequate.

Time Step

An additional parameter analysis was conducted to determine if the initially assumed calculation time step of 0.0125 seconds is sufficient to produce stable numerical results. The calculation time step in the 47 cell base model was reduced to 0.005 seconds and re-run. The R5 results calculated for both cases were virtually identical; therefore, the 0.0125 second calculation time step is considered appropriate to produce stable numerical results.

Pressure Drop Calculation

Three approximate confirmation calculations were performed in order to assess the R5 results for reasonableness. The confirmation calculations are presented in Appendix E .

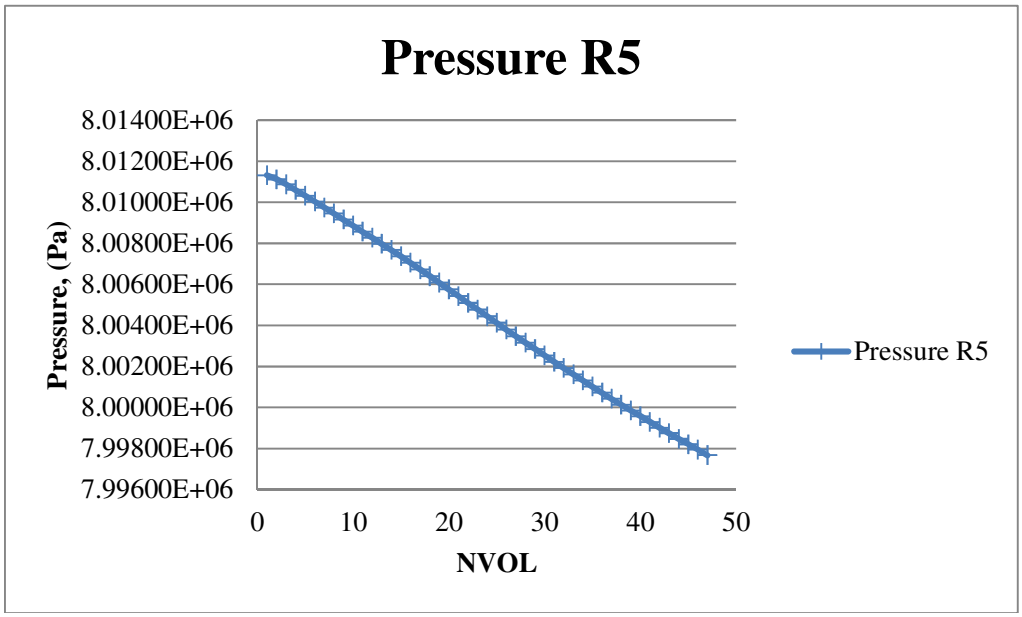

Figure 26. R5 Channel Pressure Drop Results

The R5 channel pressure drop at steady state conditions, i.e., 600 seconds, is plotted as a function of hydrodynamic cell number in Figure 26. The pressure drop appears to be a smooth decreasing function as the steam flows up the channel.

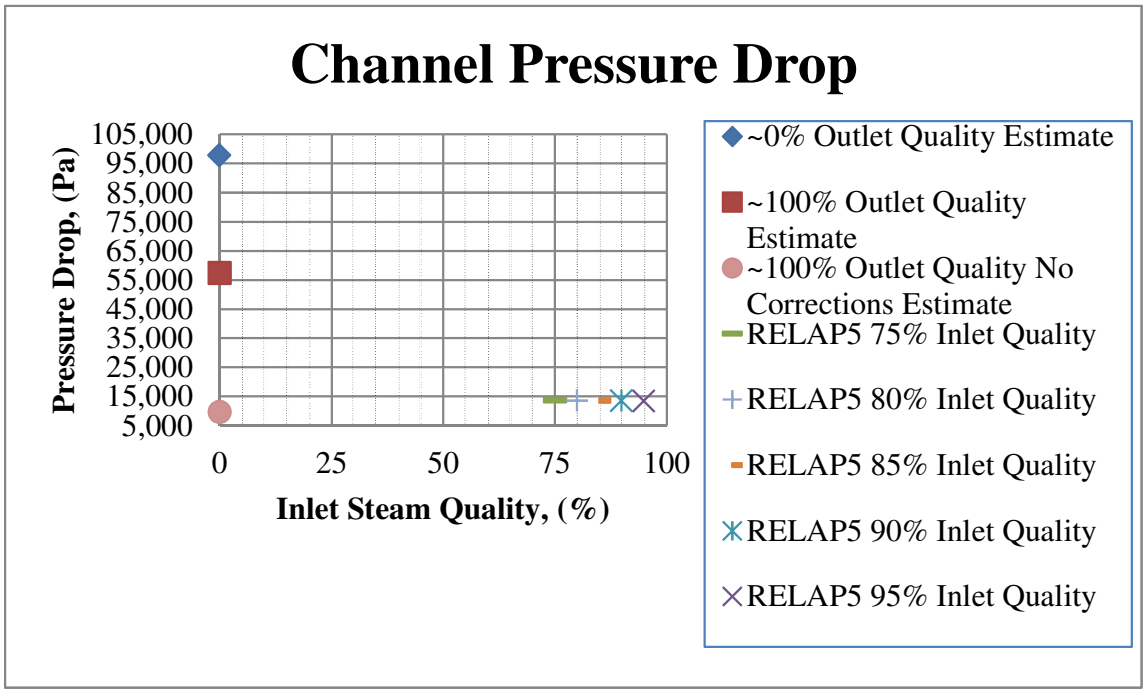

Figure 27. Approximate Channel Pressure Drop Calculation Results Compared to R5

The data plotted as a function of inlet channel quality in Figure 27, compares the R5 calculated total channel pressure drop, with the results of three approximate calculations provided in Appendix E The first observation is that all three R5 pressure drop results are very similar. The pressure drop does not appear to vary as a function of inlet channel quality in the 75% to 95% range. The channel exit quality is ~100% in each of the R5 cases.

The three approximate results are all based on empirical correlations with an inlet channel quality of 0.0%. The case with ~0% channel outlet quality exhibits the largest pressure drop. This is primarily due to the assumption that the flow consists mostly of liquid, and the liquid density is assumed in this calculation. As a result, the hydrostatic component of pressure drop makes up 99.9% of the total pressure drop, and is the

dominant of the three pressure drop components (i.e., frictional (due to wall and interfacial shear), acceleration (due to density change since the channel cross sectional area is constant) and hydrostatic (weight)). The density assumption in this case is somewhat contrived and not very realistic; however, it provides a worst case maximum upper bound channel pressure drop.

The second case is more realistic with the 100% exit quality assumption, however, still results in significantly higher channel pressure drop than calculated by the R5. As with the previous case, the 0.0% channel inlet quality conditions are significantly different than the R5 inlet conditions of >75%, i.e., less water content. As expected, the second case yields a decreased pressure drop compared to the first case, but a higher pressure drop compared to the R5 results. In the second case, the acceleration pressure term dominates the pressure drop calculation (87.4% of the total pressure drop). In the third case, the 2-phase correction factors in the correlation calculation, r_2, r_3 and r_4, are set to 1.0. Here, the total channel pressure drop appears to correlate reasonably. This assumption implies that the friction, acceleration and hydrostatic terms are weighted equally, and as a result, the acceleration and hydrostatic pressure drop components are 28.9% and 64.9% of the total channel pressure drop respectively.

In any of the cases reviewed, approximate calculation or R5, the significant channel pressure drop components are attributable to flow acceleration and hydrostatic terms, and not wall shear/friction.

Boiling Flow Regimes

The flow regime is expected to be dynamic as the inlet steam flows up through the heated steam channel. R5 calculates the flow regime for each hydrodynamic cell so that the appropriate heat transfer correlation is utilized for each cell. These heat transfer modes are referenced by number and the boiling flow regime is referenced by a descriptive title as discussed previously. As illustrated in Figure 28, the initial heat transfer (HT) mode is sub-cooled nucleate boiling. Next is saturated nucleate boiling. Beyond cell 15 the HT mode is saturated film boiling, then, the final HT mode is single phase vapor. The flow regimes are depicted as annular mist flow and mist flow. A physical interpretation of the calculated results would be that, initially, liquid is coating the tube surface and mist (small droplet) is flowing in the core of the channel. As the steam progresses up the channel, the liquid reaches saturation and boils off, resulting in mist flow and finally single phase vapor. As can be seen, the transitions occur sooner, up the steam tube, as the inlet steam quality increases.

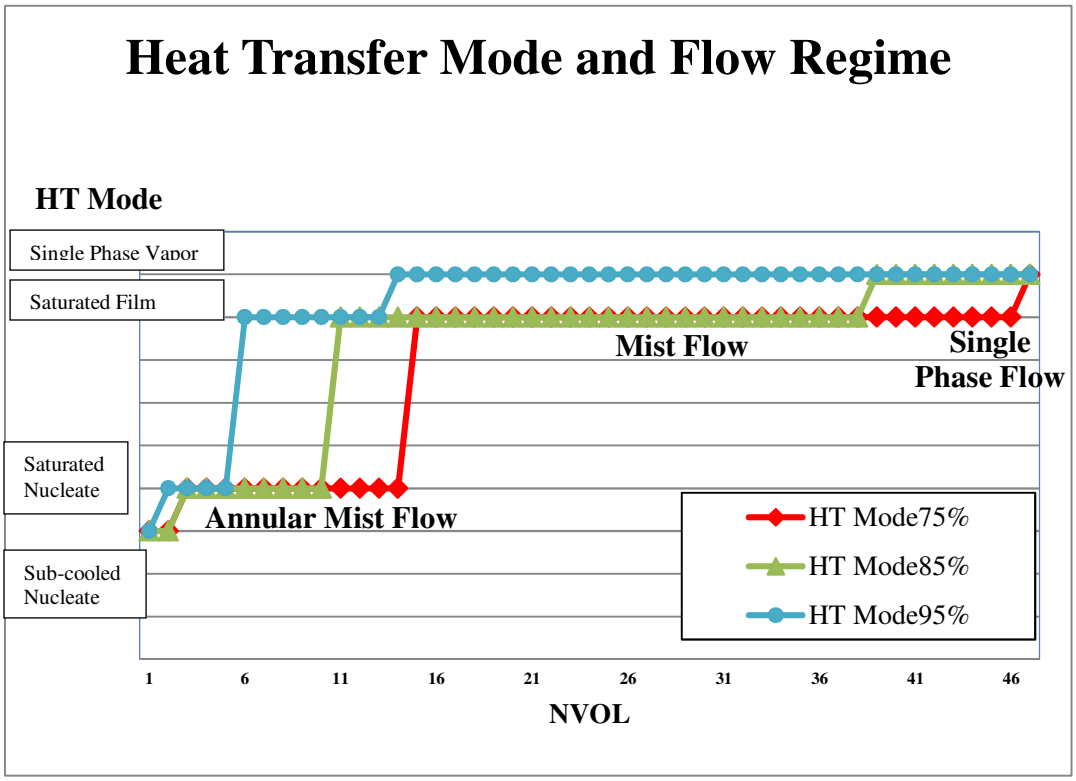

Figure 28. RELAP5 Heat Transfer Modes and Flow Regimes

Exit Steam Temperature Comparison with Approximate Calculation

A heat balance is provided in Appendix F . Knowing the channel mass flow, inlet steam conditions and total channel heat input, the exit enthalpy and exit steam temperature can be calculated. Using this overall heat balance thermodynamic approach, the calculated exit steam temperature is 488.4 ^{o}C. This compares to within 6.9% of the R5 exit steam temperature of 522.3 ^{o}C calculated for the 47 cell base model.

Thermal Performance

The objective of this research is to evaluate the improved thermodynamic power cycle efficiency with the addition of the HTGR reheat process. Exit steam temperature results from R5 illustrated in Figure 29 for a range of inlet qualities between 75% and 95%. An exit steam temperature of 600 ^{o}C was established as a target to demonstrate the efficacy of the HTGR reheat concept. This target is not intended to portray a maximum capability. Maximizing the design would require detailed optimization analyses which are outside the scope of this research. As expected, exit steam temperature increases with increased inlet steam quality. Given the dimensions and power boundary conditions assumed, the target exit steam temperature is achieved with an inlet steam quality of ~92%.

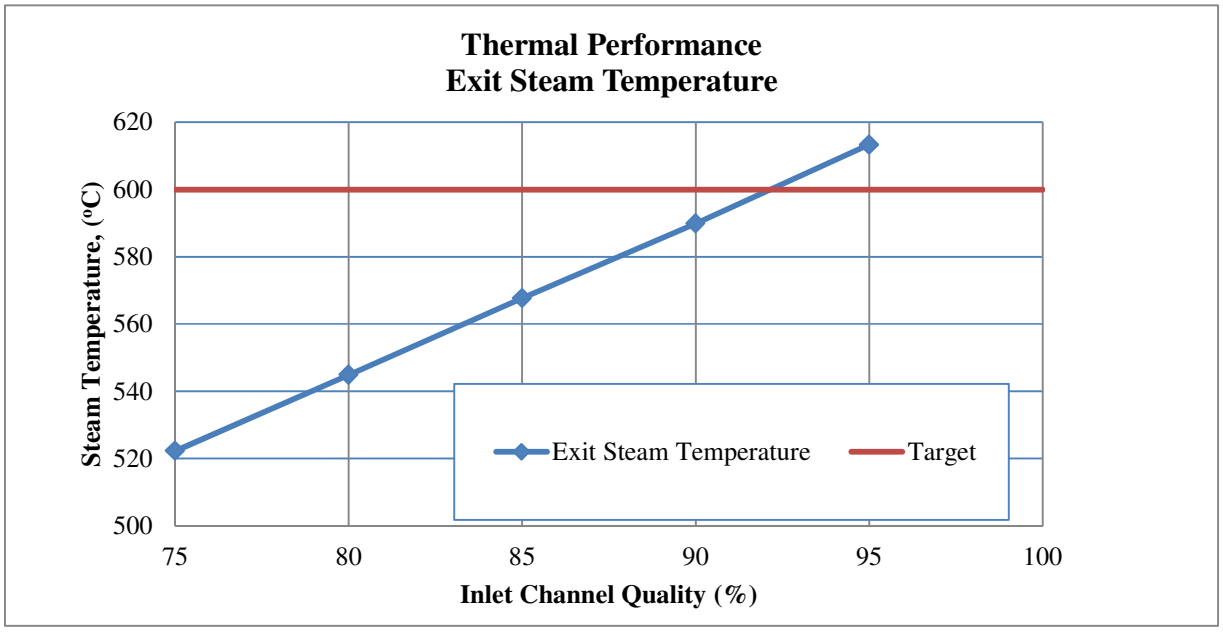

Figure 29. Thermal Performance as a Function of Inlet Steam Quality

The thermodynamic power cycle thermal efficiency values and calculations for the same range of inlet steam quality are presented in Appendix A and illustrated in Figure 30. Also as expected, the thermodynamic power cycle thermal efficiency improves as the reheat process increases the exit steam temperature.

The thermal efficiency calculations indicate the relative quantification of First Law of Thermodynamics analysis. Clearly, the HTGR reheat process increases thermal efficiency significantly. The Second Law quantification of the quality of energy using the exergy calculation produces even more impressive increases as presented in Appendix A and illustrated graphically in Figure 31.

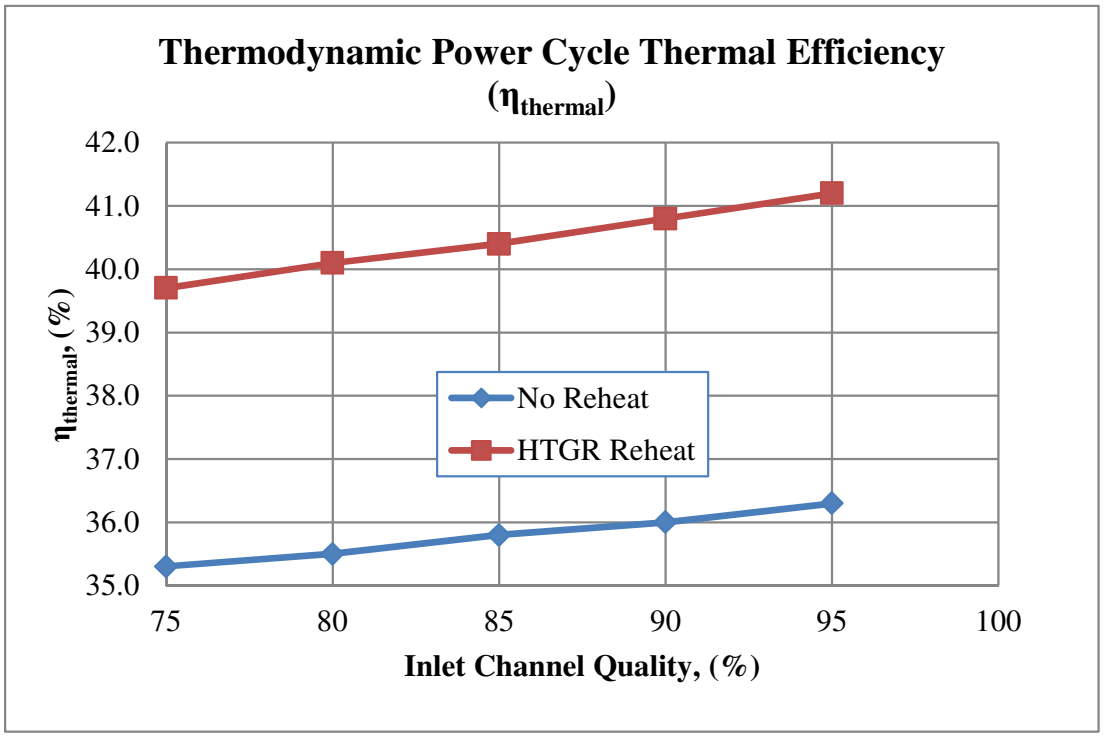

Figure 30. Thermodynamic Power Cycle Efficiency Improvement with HTGR Reheat

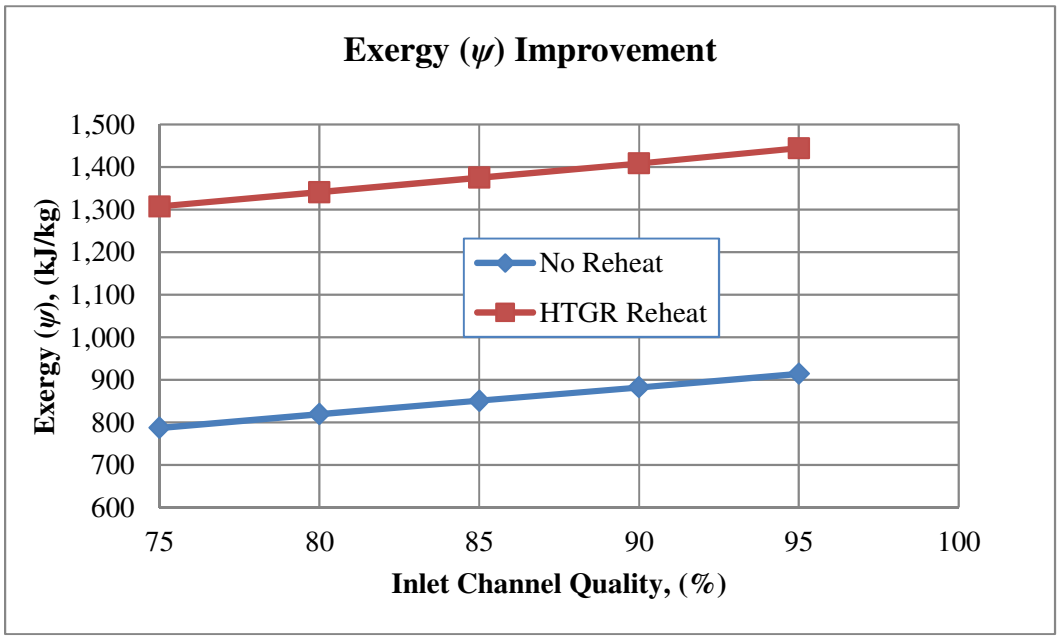

Figure 31. Exergy Improvement with the Addition of HTGR Reheat

Thermal performance improvements, in terms of thermodynamic power cycle efficiency and exergy, have been demonstrated. There is an additional significant outcome from the addition of the HTGR reheat. Recall that the initial starting point of this research was to improve the efficiency of a commercial nuclear power plant with an output of 1.0 GW_{th}. Adding the HTGR provides the improvements demonstrated, and, at the same time, increases the total output of the power plant. Using the thermodynamic values provided in Appendix A for the 75% inlet quality steam case, the actual thermal power outputs without reheat, Equation 78, and with reheat, Equation 79, respectively, compare as follows:

$$P_{out} = (h_1 - h_2) = 1109\,{}^{kg}/_{s}\left(783.2\,{}^{kJ}/_{kg}\right) \quad (78)$$

$$= 868{,}568.8\,{}^{kJ}/_{s} = 0.9\,GW$$

$$P_{out} = (h_{1'} - h_{2'}) = 1109\,{}^{kg}/_{s}\left(1{,}301.6\,{}^{kJ}/_{kg}\right) \quad (79)$$

$$= 1{,}443{,}474.4\,{}^{kJ}/_{s} = 1.4\,GW$$

The addition of HTGR reheat increases the total power plant output by 66%.

The addition of HTGR reheat can be viewed from two perspectives. The first perspective shown above, presents the case of adding a HTGR to an existing ~1 GW power plant, and increasing its output 66%. The second perspective would be to reduce

the size of the host commercial nuclear power plant output, then add an appropriately sized HTGR to provide a total output of ~1 GW. The second perspective is examined further in Chapter 5 in order to outline potential initial capital/economic advantages.

Thermal Radiation Transport – Optically Thick Approximation

As previously discussed in the R5 research model description, the assumption to neglect thermal radiation transport between the wall and the vapor has been quantified using the assumption that the vapor is "optically thick". The specific calculation makes use of the Rosseland Approximation (results are included in Table G.1). The Rosseland Approximation essentially arrives at a thermal conductivity enhancement (k_r), which is added to the thermal conductivity of the steam, (k_{steam}). The enhanced thermal conductivity, $k_{total} = k_{steam} + k_r$, then provides a mechanism to approximate the thermal radiation transport from the wall to the vapor, assuming that the vapor is optically thick. The thermal conductivity of steam, with and without the Rosseland Approximation is illustrated as a function of temperature in Figure 32 and tabulated in Table G.1.

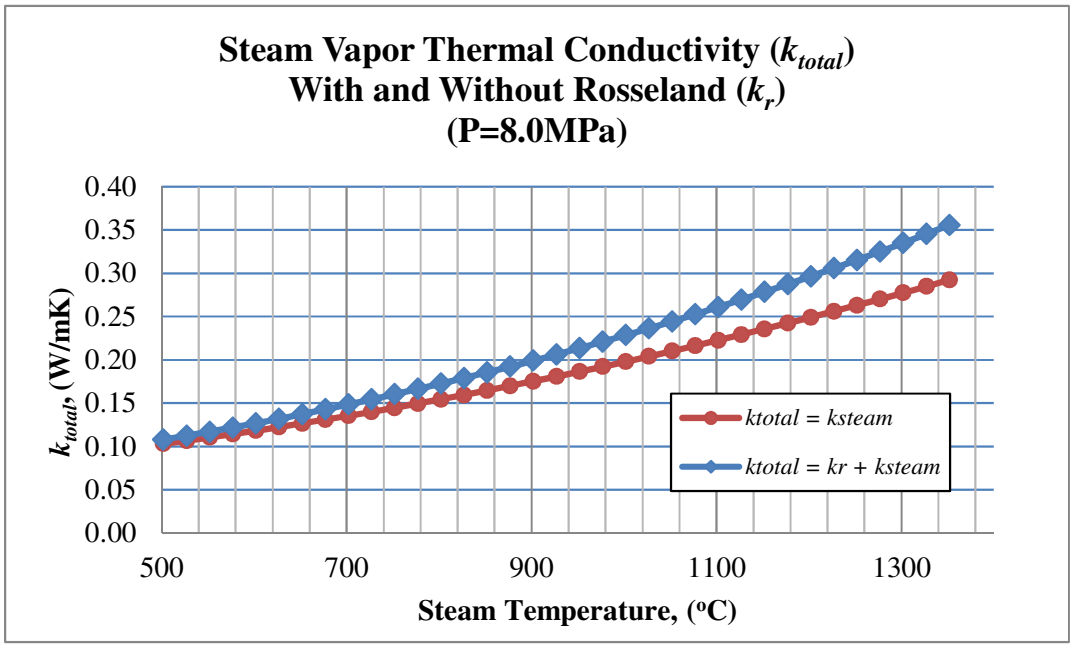

Figure 32. Conductivity of Steam Comparison, With and Without Rosseland Optically Thick Assumption

At the target steam temperature of ~600 °C, the k_{steam} is 0.12 W/m K, compared to $k_{total} = k_{steam} + k_r$ of 0.13 W/m K. This represents an 8% increase in the steam conductivity. At a steam temperature of 1,000 °C, the k_{steam} is 0.20 W/m K, compared to $k_{total} = k_{steam} + k_r$ of 0.23 W/m K. This represents a 15% increase in the steam conductivity. It is recommended that, as the temperatures of a steam design approach and exceed 1,000 °C, the optically thin steam vapor approximation should be challenged and the optically thick Rosseland approximation should be further evaluated. This research provides a method for this evaluation.

Rosseland Mean Extinction Coefficient Uncertainty Evaluation

The uncertainties associated with the steam conductivity (k_{steam}), and Rosseland mean extinction coefficient (β_R) correlations, Equation 76 and Equation 77, respectively, are evaluated.

The steam thermal conductivity (k_{steam}) correlation, provided in Equation 76 at temperatures >700 K exhibits <1% deviation (Mohanty 1987).

The Equation 77 correlation for β_R (Mohanty 1987), was based on graphical data presented in (Abu-Romia 1967). In order to quantify the deviation between the correlation and the graphical data presented for water vapor, selected points were read from the graph, and the results were then compared with the results calculated from the correlation provided in Equation 77. The results of the comparison are presented in Table 4. Since the steam thermal conductivity is an integral part of the convective heat transfer calculations, it is difficult to quantify the significance of the overall thermal performance improvement.

Table 4. Rosseland Mean Extinction Coefficient Uncertainty

				Rosseland Mean Extinction Coefficient (β_R)			
Temperature			Pressure	From Graph		Correlation	(% change)
(R)	(^{o}C)	(K)	(ATM)	(ATM-FT)$^{-1}$	(ATM-m)$^{-1}$	(ATM-m)$^{-1}$	(%)
1,000	283	556	>10	180	591	580	2
2,000	838	1,111	>10	80	262	262	0
3,000	1,394	1,667	>10	75	246	260	6
4,000	1,949	2,222	>10	83	272	260	4

As can be seen, the deviation presented as (% change) in Table 4 between graphical data and the correlation presented in Equation 77 is small and on the order of ~0% in the 800 ^{o}C temperature range. The uncertainty associated with the Rosseland

Mean Extinction Coefficient correlation is well within what would be expected for graphical methods.

Future Thermal Radiation Transport Investigation

The overall change in heat transfer from the wall to the steam, assuming an optically thick medium scenario, can be evaluated by R5 directly if the thermal conductivity of the steam used by the R5 code can be modified to include the enhanced thermal conductivity effect. This would require modification to the computational routines associated with the material property calculations for the steam vapor and liquid.

An alternate approach to simulating the increased thermal conductivity was attempted in R5 which involved inserting a calculated flow rate of hydrogen to increase the thermal conductivity of the mixture to match the increase in thermal conductivity expected from the thermal radiation enhancement. R5 has the capability of including hydrogen as a non-condensable gas. Due to the high thermal conductivity of hydrogen compared to steam, approximately four times, the presumption was that the mass flow of hydrogen would not affect the overall flow regimes and heat transfer calculations. The mass flow rate of the hydrogen was calculated to be ~2% of the total flow in order to achieve the required enhanced thermal conductivity. This approach did not produce reasonable results. The mass fraction of hydrogen was significant enough such that the corresponding reduction in steam flow in the tube and reduce the overall heat transfer from the tube to the steam. The net result was a decrease in exit steam temperature due to

the reduced heat transfer. This is counter to the expected result of increased exit steam temperature from the hydrogen enhanced thermal conductivity.

Chapter 5

Conclusions and Recommendations

Several conclusions can be made based on the research conducted:

- LMTD heat transfer sizing analyses produced a set of dimensions that accomplished the research objectives;
- Alternative calculations determined that the R5 results are reasonable; and
- The addition of HTGR Reheat Process technology provides the potential for significant improvement in the following areas:
    - Thermodynamic power cycle thermal efficiency (>13% increase)
    - Exergy (>57% increase)
    - Power Output Increase (66%)
    - Reduced Initial Capital Cost
    - Environmental Impact (>17% reduction).

Based on the conclusions listed, it is recommended that further study be conducted to maximize the thermodynamic power cycle efficiency and the exergy with the HTGR reheat concept. As mentioned previously, it is recommended that the optically thin vapor approximation be further evaluated as part of the HTGR application development since it is expected that temperatures will exceed 600 ^{o}C.

A preliminary economic and environmental assessment is provided below as a summary. Based on these preliminary results, a detailed capital cost estimate should be conducted for the addition of the HTGR reheat process as this will quantify the overall economic advantages of this concept.

Economic and Environmental Improvement Assessment

First and Second Law Thermodynamic analyses quantify the technical improvement in the power cycle with the addition of the HTGR reheat process. Since the viability of implementation is largely dependent on economics and environmental impacts, an approximate determination for each is provided.

The cost of nuclear power is determined primarily by the initial capital cost of the project (equipment and construction costs) (von Hippel 2010). As a result, the decision to move forward with the development, licensing and construction of a nuclear power project is based on the initial capital cost. The range of capital cost is $2,300 to $6,000 per kW of generating capacity, with a median of $4,000 per kW worldwide. An economic value summary is provided in Table 5.

Table 5. Economic Value of HTGR Reheat

	Comparison Cases			
	Base Case	**1**	**2**	**3**
Capital Cost / kW	Host = $6,000/kW	HTGR=$6,000/kW	HTGR=$4,000/kW	HTGR=$2,300/kW
PWR/BWR Power (GW_{th})	0.9	0.5	0.5	0.5
HTGR Reheat Power (GW_{th})	0.0	0.4	0.4	0.4
Total Reactor Power (GW_{th})	0.9	0.9	0.9	0.9
Total Steam Flow (kg/s)	1109	665	665	665
Total Reject Heat (kJ/s)	2461	2038	2038	2038
Total Cycle η_{th} (%)	35	40	40	40
Construction Capital ($B)	5.4	5.4	4.6	3.9
Percent Cost Reduction from Base	0	0	15%	27%
		(no cost change assumed)		
Note: 75% Quality Inlet Steam results from Appendix A.				

The Base Case is assumed to be a host PWR or BWR with a total thermal power output of 0.9 GW_{th}. No HTGR power is included in this case, and the thermodynamic performance values, consistent with the 75% quality inlet steam, are provided from

Appendix A . The initial capital cost of $6.0 B is based on the maximum value of the cost range from (von Hippel 2010). All of the Cases presented for comparison also generate a total power output of 0.9 GW_{th}.

A reheat HTGR is added in Case 1. The thermodynamic improvements are presented for comparison. Due to these improvements, production of a total of 0.9 GW_{th}, allows the size of the host PWR or BWR to be reduced from 0.9 to 0.5 GW_{th}, with the added HTGR providing the remaining 0.4 GW_{th}. The reduction in host power is determined by applying the ratio of the specific power output of the Base Case PWR/BWR, 783.2 kJ/kg (state **1** to state **2**, Figure 1), and the specific power output from the addition of the HTGR maintaining the same steam flow, 1301.6 kJ/kg (state **1'** to state **2'**, Figure 1) (see Appendix A).

In Case 1, it is assumed that the capital cost of the additional HTGR is the same as the host PWR/BWR, i.e., $6,000 per kW. The resulting total capital cost will be the same, $6.0B. However, this cost assumption is considered overly conservative. The addition of a reheat HTGR requires only the cost of the additional reactor system along with steam piping/valve modifications. Costs to include the HTGR will **not** include the following major cost components:

- Reactor Coolant Pumps (2 to 4 (or more) depending on design);
- Steam Generators;
- Primary Coolant Valves and Piping;
- Steam Turbine;
- Generator;

- Condensers;
- Feedwater Heaters;
- Feedwater Pumps;
- Ultimate Heat Sink System (e.g., Cooling Towers); and
- Facility Siting and Environmental Impact Study.

Based on this, Cases 2 and 3 provide capital cost estimates assuming that the initial capital cost of the HTGR will be lower than that of the host PWR/BWR. In Case 2, the international median cost of $4,000 per kW is assumed, and in Case 3, the lower range cost of $2,300 per kW is assumed. In actuality, these costs could still be conservatively high since it is expected that there will be more cost "overlap" than noted above. The cost assumptions made for Cases 2 and 3 yield 15% and 27% reductions in initial capital respectively.

As expected from the previous discussion on thermodynamic power cycle efficiency and exergy increase, the environmental impact of the HTGR addition results in a >17% reduction in the quantity of heat rejected to the environment. This will reduce the "environmental footprint" of the power generating facility, as well as reduce the size and cost of the ultimate heat sink system required. The initial capital cost savings of a 17% reduction in the size of the ultimate heat sink system was not included in this preliminary analysis.

List of References

Abu-Romia, M., and Tien, C. (1967). "Appropriate mean Absorption Coefficients for Infrared Radiation in Gases." Journal of Heat Transfer **89**: 321-327.

Article (2011, March 25, 2011). "Advanced Nuclear Power Reactors." News. Retrieved May 9, 2011, from http://www.world-nuclear.org/info/inf08.html.

ASME (2010). ASME Power Boilers, Chapter 17, A Guide to Section I of the ASME Boiler and Pressure Vessel Code.

Ball, S. (2010). High temperature gas-cooled reactors –some history, what's going on, and why the US should build some NOW. Friends of ORNL. Oak Ridge National Laboratory Conference.

Bendixen, K. (2003). Experience with Coal Fired USC Boilers in Denmark. Power-Gen Europe. Dusseldorf, Burmeister&Wain Energy A/S.

Bergman, T. L., Lavine, A.S., Incropera, F.P., DeWitt, D.P. (2011). Fundamentals of Heat and Mass Transfer, John Wiley & Sons.

Cabet, C., A. Terlain, et al. (2006). "High temperature corrosion of structural materials under gas-cooled reactor helium." Materials and Corrosion **57**(2): 147-153.

Carey, V. P. (1992). Liquid - Vapor Phase - Change Phenomena, Taylor and Francis.

ChemGoodie (March 2011). Excel Spreadsheet Add-In Steam Calculator**:** Calculates Steam Properties.

Dolleszhal, N. A. (1958). "The Uranium-Graphite Reactor and Superheated Steam Power Stations." Nuclear Energy **7**(1).

Ferrara, Z. (2007). "Conceptual Design of a Superheat Boiling Water Reactor." Nuclear Science and Engineering **97**(1): 809-813.

Fitzpatrick, T. (2007) Helium supplies endangered, threatening science and technology. Washington University Web Newsroom

Forsberg, C. W. (2007). "A Nuclear-Fossil Combined Cycle Power Plant for Base-Load and Peak Electricity." Nuclear Science and Engineering **96**(1): 683-684.

FosterWheeler (2002). FWPG Benson VT Boiler Process and Operational Description, Foster-Wheeler Power Group. **TP-PC-04-02.DOC**.

Fujita, M., Domoto, K., Yoshikawa, Y. (2010). Mitsubishi Latest Coal Fired USC Boiler Technology (CFE Pacifico 700 MW), Mitsubishi Heavy Industries Ltd.

Gibbons, J. P. (1974). "The Design of 2300 MW(e) Twin High Temperature Gas-Cooled Reactors for the Philadelphia Electric Company." Nuclear Engineering and Design **26**(1): 27-37.

Gibbs, G. (2010). Considerations Associated with Reactor Technology Selection for the Next Generation Nuclear Plant Project. Idaho National Laboratory Next Generation Nuclear Plant Project, Idaho National Laboratory. **INL/EXT-10-19838**.

Hepbasli, A. (2008). "A key review on exergetic analysis and assessment of renewable energy resources for a sustainable future." Renewable and Sustainable Energy Reviews **12**: 593-661.

Holman, J. P. (1980). Thermodynamics. New York, McGraw-Hill Book Company.

Hurd, P., Thamm, M., Neef, M., Truckenmiller, F., Pollak, H., Deckers, M. (2005). Moder Reaction HP/IP Turbine Technology Advances and Experiences. PWR2005 ASME Power.

Iwamoto, H. (2001). Experiences in Designing and Operating the Latest 1050 MW Coal Fired Boiler, Babcock-Hitachi K.K. **50 Number 3**.

Jonas, O. (2008). Tutorial Paper - Steam Turbine Corrosion and Deposits Problems and Solutions. Thirty-Seventh Turbomachinery Symposium.

Kanthal (2011). "Kanthal APMT Ferritic FeCrAlMo Alloy." Retrieved 10/27/2012, from www.kanthal.com/products/material-datasheets/tube/kanthal-apmt/.

Kim, R. L. (1980). "Optimization of Helium-Steam Binary Cycles for HTGRs." Annals of Nuclear Energy **7**(11): 611-622.

Knief, R. (1992). Nuclear engineering : theory and technology of commercial nuclear power. Washington, DC, Hemisphere.

Kok, K., Ed. (2009). Nuclear Engineering Handbook, Taylor and Francis Group.

Leizerovich, A. (2005). Wet steam turbines for nuclear power plants. Tulsa, Okla., PennWell Corp.

Lior, L. (1997). "Energy, Exergy and Thermoeconomic Analysis of the Effects of Fossil-Fuel Superheating in Nuclear Power Plants." Energy Convers. Mgmt. **38**(15-17): 1585-1593.

Lund, D. (2011). Pathfinder Atomic Power Plant - Sioux Falls, South Dakota. blog.keloland.com/lund/blog/2011/03/19/sioux-falls-nuclear-experiment. **10/27/2012**.

Mohanty, A. K., and Viskanta, R. (1987). "Buoyancy-dominated laminar convection and radiation transfer in rod arrays." Heat and Fluid Flow **8**(4): 277-286.

Moore, T. (1985). "Robots for Nuclear Power Plants." EPRI **IAEA Bulletin** (Autumn): 8.

Mousseau, A. A. (2004). "Implicitly balanced solution of the two-phase flow equations coupled to nonlinear heat conduction." Journal of Computational Physics **200**: 104-132.

Naidin, M., Pioro, I., Zirn, U., Chophla, K. (2009). Supercritical water Reactor NPP Concept: No-Reheat Cycle Option. Proceedings of the 17th International Conference on Nuclear Engineering, ASME.

Nilsson, L. (1993). Assessment of RELAP5/MOD3 Against Twenty Five Post Dryout Experiments Performed at the Royal Institute of Technology, Swedish Nuclear Power Inspectorate.

NRC (2001). RELAP5/MOD3.3 CODE MANUAL. U. S. N. R. Commission. Washington, DC. **1-8**.

Planta, J., Huston, D. (1997). Upgrade Superheaters Restore Lost Boiler Capacity. Power-Gen '97.

Retzlaff, K. M., Ruegger, W.A. (1996). Steam Turbines for Ultrasupercritical Power Plants, General Electric. **GER-3945A**.

Schluderberg, D. (1987). Nuclear power plant and apparatus for superheating steam. Courier Press. E. P. Office. England.

Shimizu, K. (2011). "Small-sized high temperature reactor (MHR-50) for electricity generation: Plant concept and characteristics." Progress in Nuclear Enery **53**(7): 846-854.

Strydom, G. (2011). Reactor Physics Characterization of the HTR Module with UCO Fuel, Idaho National Laboratory. **INL/EXT-10-20521**.

TAN, C. (2009). The Numerical Study on the Flow Characteristics of the Last Stage Hollow Stationary Blades with Suction Slot of Nuclear Power Plant Turbine. The International Conference on Electrical Engineering. Wuhan University.

Todreas, N. E. a. K., M. (1993). Nuclear Systems 1: Thermal Hydraulic Fundamentals, Hemisphere.

Viskanta, R. (1966). Radiation Transfer and Interaction of Convection with Radiation Heat Transfer. Advances in Heat Transfer. T. F. Irvine, Academic Press. **3:** 175-251.

von Hippel, F. (2010). The Uncertain Future of Nuclear Energy. Research Report 9, International Panel on Fissile Material.

Whalley, P. B. (1987). Boiling, Condensation, and Gas - Liquid Flow, Clarendon Press.

Wikimedia. "Water Steam Temperature Entropy Diagram." Retrieved 10/31/2012, from http://en.wikipedia.org/wiki/File:TS-Wasserdampf_engl.png

Zaryankin, A., et.al. (2011). "Super powerful steam superheaters and turbines for hybrid nuclear power plants." Journal of Power Technologies **91**(4): 191-197.

Zirn, U. (2008). "Hitachi Turbine Generator Technology for Nuclear Applications." Retrieved April 4, 2011, from www.powergenu.com.

Appendices

Appendix A : Thermodynamic Power Cycle Analysis

The following analyses quantify the potential improvement in thermodynamic power cycle efficiency utilizing reheat from an HTGR integrated into a PWR/BWR steam cycle. Both First Law (thermal cycle efficiency) and Second Law (exergy) calculations are presented.

THERMODYNAMIC POWER CYCLE COMPARISON

Base Case	**T**	**P**	**h**	**s**	**v**		**Process**		**hin**	**hout**	**Q**	**W**
State Point	**C**	**kpa**	**kJ/kg**	**kJ/kgK**	**m^3/kg**		**Unit**	**State**	**kJ/kg**	**kJ/kg**	**kJ/kg**	**kJ/kg**
1	295.0091	8000	2667.8	5.58501	0.02213		Pump	3 to 4	191.8	199.9	0.0	-8.0
2	45.80755	10	1766.1	5.58501	9.65536		Boiler	4 to 1	199.9	2667.8	2467.9	0.0
3	45.80755	10	191.8	0.64922	0.00101	X=0.0	Turbine	1 to 2	2667.8	1766.1	0.0	901.7
4	46.06925	8000	199.9	0.64922	0.00101		Condenser	2 to 3	1766.1	191.8	-1574.3	0.0
										Sums =	893.6	893.6
										η =	36.2	%
With Reheat	**T**	**P**	**h**	**s**	**v**		**Process**		**hin**	**hout**	**Q**	**W**
State Point	**C**	**kpa**	**kJ/kg**	**kJ/kgK**	**m^3/kg**		**Unit**	**State**	**kJ/kg**	**kJ/kg**	**kJ/kg**	**kJ/kg**
1'	600.2361	8000	3643.0	7.02319	0.04848		Pump	3 to 4	191.8	199.9	0.0	-8.0
2'	45.80755	10	2224.8	7.02319	12.46843		Boiler	4 to 1	199.9	3643.0	3443.1	0.0
3	45.80755	10	191.8	0.64922	0.00101	X=0.0	Turbine	1 to 2	3643.0	2224.8	0.0	1418.2
4	46.06925	8000	199.9	0.64922	0.00101		Condenser	2 to 3	2224.8	191.8	-2033.0	0.0
										Sums =	1410.1	1410.1
										η =	41.0	%

*Notes: Turbine expansion and pump compression processes are assumed to be isentropic.

Thermodynamic State Defining Input

Power Cycle Efficiency

% Improvement = 13.1 %

Figure A.1 Rankine Power Cycle Efficiency Calculation

Thermodynamic state properties presented in this section are calculated using Steam Calculator 3.0 from ChemGoodie (ChemGoodie March 2011). Steam Calculator is an engineering tool built as an MS Excel add-in used to calculate thermodynamic and transport properties of steam. It calculates properties such as: Temperature, Pressure, Enthalpy, Entropy, Density, Internal Energy, Isobaric Heat Capacity, Isochoric Heat Capacity, Specific Volume, Speed of Sound, Thermal Conductivity, Viscosity, Surface

Tension, Helmholtz Free Energy, Gibbs Free Energy, Compressibility Factor, Isothermal Compressibility, Joule Thompson Coefficient, Isothermal Joule Thompson Coefficient, Thermal Expansion Coefficient, Prandtl Number, Static Dielectric Constant, etc. The calculator works within MS Excel. Two input conditions, defining the thermodynamic state of the steam, are entered into the cells outlined by borders. The steam properties are then calculated and conveniently entered into the output cells selected by the user. For example, for state point **1**, pressure and enthalpy are provided by the user to define the state of the steam. Temperature, entropy, and specific volume are calculated and entered into the selected cells for that state. For each case considered, channel exit temperature was calculated by R5 model runs. Enthalpy was adjusted, assuming a constant pressure of 8.0 MPa, the temperature corresponding to the R5 channel exit temperature was reached in the spreadsheet. This defined the steam properties.

The thermodynamic power cycle efficiency is calculated utilizing Equation 1 for each case as follows (the "without reheat" case is presented below as an example):

$$\eta = \frac{W_{out}}{Q_{in}} = \frac{(h_1 - h_2)}{(h_1 - h_4)} \cdot 100\% = \frac{\left(2667.8\,{}^{kJ}/_{kg} - 1766.1\,{}^{kJ}/_{kg}\right)}{\left(2667.8\,{}^{kJ}/_{kg} - 199.9\,{}^{kJ}/_{kg}\right)} \cdot 100 = 36.2\%$$

The thermodynamic power cycle results from the RELAP5 analysis as a function of inlet quality are presented in Table A.1.

Table A.1 Thermodynamic Power Cycle Comparison

THERMODYNAMIC POWER CYCLE COMPARISON - 75% Inlet Quality												
Base Case	**T**	**P**	**h**	**s**	**v**		**Process**		**hin**	**hout**	**Q**	**W**
State Point	**C**	**kpa**	**kJ/kg**	**kJ/kgK**	**m^3/kg**		**Unit**	**State**	**kJ/kg**	**kJ/kg**	**kJ/kg**	**kJ/kg**
1	295.0091	8000	2397.6	5.10944	0.01798		Pump	3 to 4	191.8	199.9	0.0	-8.0
2	45.80755	10	1614.4	5.10944	8.72515		Boiler	4 to 1	199.9	2397.6	2197.7	0.0
3	45.80755	10	191.8	0.64922	0.00101	X=0.0	Turbine	1 to 2	2397.6	1614.4	0.0	783.2
4	46.06925	8000	199.9	0.64922	0.00101		Condenser	2 to 3	1614.4	191.8	-1422.6	0.0
										Sums =	775.1	775.1
							ψ =	787.4	kJ/kg	η =	35.3	%
With Reheat	**T**	**P**	**h**	**s**	**v**		**Process**		**hin**	**hout**	**Q**	**W**
State Point	**C**	**kpa**	**kJ/kg**	**kJ/kgK**	**m^3/kg**		**Unit**	**State**	**kJ/kg**	**kJ/kg**	**kJ/kg**	**kJ/kg**
1'	522.3097	8000	3454.3	6.79686	0.04330		Pump	3 to 4	191.8	199.9	0.0	-8.0
2'	45.80755	10	2152.7	6.79686	12.02573		Boiler	4 to 1	199.9	3454.3	3254.4	0.0
3	45.80755	10	191.8	0.64922	0.00101	X=0.0	Turbine	1 to 2	3454.3	2152.7	0.0	1301.6
4	46.06925	8000	199.9	0.64922	0.00101		Condenser	2 to 3	2152.7	191.8	-1960.8	0.0
										Sums =	1293.6	1293.6
							ψ =	1307.5	kJ/kg	η =	39.7	%
*Notes: Turbine expansion and pump compression processes are assumed to be isentropic.									**Power Cycle Efficiency**			
Thermodynamic State Defining Input									**% Improvement =**		**12.7**	**%**

THERMODYNAMIC POWER CYCLE COMPARISON - 80% Inlet Quality												
Base Case	**T**	**P**	**h**	**s**	**v**		**Process**		**hin**	**hout**	**Q**	**W**
State Point	**C**	**kpa**	**kJ/kg**	**kJ/kgK**	**m^3/kg**		**Unit**	**State**	**kJ/kg**	**kJ/kg**	**kJ/kg**	**kJ/kg**
1	295.0091	8000	2469.6	5.23616	0.01909		Pump	3 to 4	191.8	199.9	0.0	-8.0
2	45.80755	10	1654.9	5.23616	8.97302		Boiler	4 to 1	199.9	2469.6	2269.7	0.0
3	45.80755	10	191.8	0.64922	0.00101	X=0.0	Turbine	1 to 2	2469.6	1654.9	0.0	814.7
4	46.06925	8000	199.9	0.64922	0.00101		Condenser	2 to 3	1654.9	191.8	-1463.0	0.0
										Sums =	806.7	806.7
							ψ =	819.1	kJ/kg	η =	35.5	%
With Reheat	**T**	**P**	**h**	**s**	**v**		**Process**		**hin**	**hout**	**Q**	**W**
State Point	**C**	**kpa**	**kJ/kg**	**kJ/kgK**	**m^3/kg**		**Unit**	**State**	**kJ/kg**	**kJ/kg**	**kJ/kg**	**kJ/kg**
1'	544.9437	8000	3509.5	6.86528	0.04483		Pump	3 to 4	191.8	199.9	0.0	-8.0
2'	45.80755	10	2174.5	6.86528	12.15956		Boiler	4 to 1	199.9	3509.5	3309.6	0.0
3	45.80755	10	191.8	0.64922	0.00101	X=0.0	Turbine	1 to 2	3509.5	2174.5	0.0	1335.0
4	46.06925	8000	199.9	0.64922	0.00101		Condenser	2 to 3	2174.5	191.8	-1982.7	0.0
										Sums =	1327.0	1327.0
							ψ =	1341.0	kJ/kg	η =	40.1	%
*Notes: Turbine expansion and pump compression processes are assumed to be isentropic.									**Power Cycle Efficiency**			
Thermodynamic State Defining Input									**% Improvement =**		**12.8**	**%**

Table A.1 Thermodynamic Power Cycle Comparison (continued)

THERMODYNAMIC POWER CYCLE COMPARISON - 85% Inlet Quality

Base Case	T	P	h	s	v		Process		hin	hout	Q	W
State Point	C	kpa	kJ/kg	kJ/kgK	m^3/kg		Unit	State	kJ/kg	kJ/kg	kJ/kg	kJ/kg
1	295.0091	8000	2541.7	5.36306	0.02020		Pump	3 to 4	191.8	199.9	0.0	-8.0
2	45.80755	10	1695.3	5.36306	9.22124		Boiler	4 to 1	199.9	2541.7	2341.8	0.0
3	45.80755	10	191.8	0.64922	0.00101	X=0.0	Turbine	1 to 2	2541.7	1695.3	0.0	846.4
4	46.06925	8000	199.9	0.64922	0.00101		Condenser	2 to 3	1695.3	191.8	-1503.5	0.0
										Sums =	838.3	838.3
							ψ =	850.9	kJ/kg	η =	35.8	%
With Reheat	**T**	**P**	**h**	**s**	**v**		**Process**		**hin**	**hout**	**Q**	**W**
State Point	**C**	**kpa**	**kJ/kg**	**kJ/kgK**	**m^3/kg**		**Unit**	**State**	**kJ/kg**	**kJ/kg**	**kJ/kg**	**kJ/kg**
1'	567.7337	8000	3564.7	6.93183	0.04635		Pump	3 to 4	191.8	199.9	0.0	-8.0
2'	45.80755	10	2195.7	6.93183	12.28973		Boiler	4 to 1	199.9	3564.7	3364.8	0.0
3	45.80755	10	191.8	0.64922	0.00101	X=0.0	Turbine	1 to 2	3564.7	2195.7	0.0	1369.0
4	46.06925	8000	199.9	0.64922	0.00101		Condenser	2 to 3	2195.7	191.8	-2003.9	0.0
										Sums =	1361.0	1361.0
							ψ =	1375.0	kJ/kg	η =	40.4	%

*Notes: Turbine expansion and pump compression processes are assumed to be isentropic.

Power Cycle Efficiency

Thermodynamic State Defining Input

% Improvement = 13.0 %

THERMODYNAMIC POWER CYCLE COMPARISON - 90% Inlet Quality

Base Case	T	P	h	s	v		Process		hin	hout	Q	W
State Point	C	kpa	kJ/kg	kJ/kgK	m^3/kg		Unit	State	kJ/kg	kJ/kg	kJ/kg	kJ/kg
1	295.0091	8000	2613.8	5.48997	0.02130		Pump	3 to 4	191.8	199.9	0.0	-8.0
2	45.80755	10	1735.8	5.48997	9.46946		Boiler	4 to 1	199.9	2613.8	2413.9	0.0
3	45.80755	10	191.8	0.64922	0.00101	X=0.0	Turbine	1 to 2	2613.8	1735.8	0.0	878.0
4	46.06925	8000	199.9	0.64922	0.00101		Condenser	2 to 3	1735.8	191.8	-1544.0	0.0
										Sums =	869.9	869.9
							ψ =	882.6	kJ/kg	η =	36.0	%
With Reheat	**T**	**P**	**h**	**s**	**v**		**Process**		**hin**	**hout**	**Q**	**W**
State Point	**C**	**kpa**	**kJ/kg**	**kJ/kgK**	**m^3/kg**		**Unit**	**State**	**kJ/kg**	**kJ/kg**	**kJ/kg**	**kJ/kg**
1'	589.925	8000	3618.2	6.99463	0.04781		Pump	3 to 4	191.8	199.9	0.0	-8.0
2'	45.80755	10	2215.7	6.99463	12.41256		Boiler	4 to 1	199.9	3618.2	3418.3	0.0
3	45.80755	10	191.8	0.64922	0.00101	X=0.0	Turbine	1 to 2	3618.2	2215.7	0.0	1402.5
4	46.06925	8000	199.9	0.64922	0.00101		Condenser	2 to 3	2215.7	191.8	-2023.9	0.0
										Sums =	1394.4	1394.4
							ψ =	1408.5	kJ/kg	η =	40.8	%

*Notes: Turbine expansion and pump compression processes are assumed to be isentropic.

Power Cycle Efficiency

Thermodynamic State Defining Input

% Improvement = 13.2 %

Table A.1 Thermodynamic Power Cycle Comparison (continued)

THERMODYNAMIC POWER CYCLE COMPARISON - 95% Inlet Quality												
Base Case	**T**	**P**	**h**	**s**	**v**		**Process**		**hin**	**hout**	**Q**	**W**
State Point	**C**	**kpa**	**kJ/kg**	**kJ/kgK**	**m^3/kg**		**Unit**	**State**	**kJ/kg**	**kJ/kg**	**kJ/kg**	**kJ/kg**
1	295.0091	8000	2685.8	5.61669	0.02241		Pump	3 to 4	191.8	199.9	0.0	-8.0
2	45.80755	10	1776.2	5.61669	9.71733		Boiler	4 to 1	199.9	2685.8	2485.9	0.0
3	45.80755	10	191.8	0.64922	0.00101	X=0.0	Turbine	1 to 2	2685.8	1776.2	0.0	909.6
4	46.06925	8000	199.9	0.64922	0.00101		Condenser	2 to 3	1776.2	191.8	-1584.4	0.0
										Sums =	901.5	901.5
							ψ =	914.3	kJ/kg	η =	36.3	%
With Reheat	**T**	**P**	**h**	**s**	**v**		**Process**		**hin**	**hout**	**Q**	**W**
State Point	**C**	**kpa**	**kJ/kg**	**kJ/kgK**	**m^3/kg**		**Unit**	**State**	**kJ/kg**	**kJ/kg**	**kJ/kg**	**kJ/kg**
1'	613.3484	8000	3674.5	7.05899	0.04933		Pump	3 to 4	191.8	199.9	0.0	-8.0
2'	45.80755	10	2236.3	7.05899	12.53845		Boiler	4 to 1	199.9	3674.5	3474.6	0.0
3	45.80755	10	191.8	0.64922	0.00101	X=0.0	Turbine	1 to 2	3674.5	2236.3	0.0	1438.2
4	46.06925	8000	199.9	0.64922	0.00101		Condenser	2 to 3	2236.3	191.8	-2044.4	0.0
										Sums =	1430.2	1430.2
							ψ =	1444.4	kJ/kg	η =	41.2	%
*Notes: Turbine expansion and pump compression processes are assumed to be isentropic.									**Power Cycle Efficiency**			
Thermodynamic State Defining Input									**% Improvement =**		**13.5**	**%**

For the Second Law analysis, the total exergy is calculated for two cases, with and without reheat, and are compared using Equation 2.

$$\psi = (h - h_0) - T_0(s - s_0)$$

Then,

$$\psi_{without\ reheat} = (h_1 - h_3) - T_0(s_1 - s_3)$$

$$= (2685.8 - 191.8)\frac{kJ}{kg} - (45 + 273)K(5.61669 - 0.64922)\frac{kJ}{kgK}$$

$$= 914.3\frac{kJ}{kg}$$

$$\psi_{with\ reheat} = (h_{1'} - h_3) - T_0(s_{1'} - s_3)$$

$$= (3674.5 - 191.8)\frac{kJ}{kg} - (45 + 273)K(7.05899 - 0.64922)\frac{kJ}{kgK}$$

$$= 1444.4\frac{kJ}{kg}$$

The addition of the HTGR reheat increases the exergy by (1444.4-914.3)/914.3 *100% = 58.0%

Appendix B : Log Mean Temperature Difference Analysis

The derivation of the Log Mean Temperature Difference (LMTD) equations used in this research begins with the model illustrated in Figure B.1 (Bergman 2011). In that reference, heat is transferred from the hot fluid, shown in red, to the cold fluid shown in blue. Heat is transferred from hot to cold fluids across the differential heat transfer surface area dA. The heat transfer in the incremental volume, shown from red to blue, increases the inlet cold fluid temperature T_c, to the temperature T_c+dT_c.

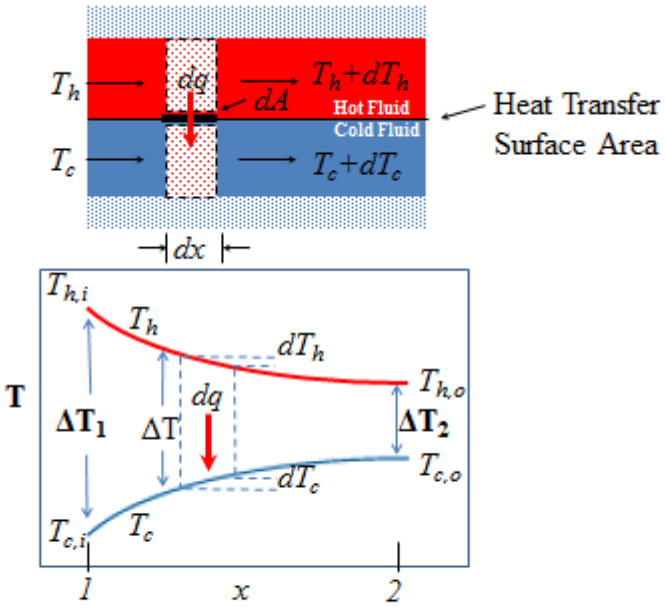

Figure B.1 LMTD Heat Transfer Model

Define:

T_{ci} = inlet cold fluid temperature;

T_{co} = outlet cold fluid temperature;

T_{hi} = inlet hot fluid temperature;

T_{ho} = outlet hot fluid temperature;

□ = mass flow; and

$c_{p,c\ or\ h}$ = heat capacity.

Then, the total heat transferred to the cold fluid will be q:

$$q = {}_{c}\, c_{p,c}(T_{\mathrm{co}} - T_{\mathrm{ci}}) = {}_{h}\, c_{p,h}(T_{\mathrm{ho}} - T_{\mathrm{hi}}) \qquad \text{(B.1)}$$

Applying an energy balance to the differential element in Figure B.1, yields the differential energy balance expressions. The energy transfer between elements must also equal the overall heat transfer across the surface area *dA*:

$$dq = {}_{c}\, c_{\mathrm{p,c}}\, dT_{\mathrm{c}} = {}_{h}\, c_{\mathrm{p,h}}\, dT_{\mathrm{h}} = U\, \Delta T\, dA \qquad \text{(B.2)}$$

where: *U*= overall heat transfer coefficient;

ΔT = Local temperature difference, $T_h - T_c$,

T_h = Local hot fluid temperature,

T_c = Local cold fluid temperature,

Differentiating,

$d(\Delta T) = d(T_h) - d(T_c)$

Re-arranging Equation B.2,

$$d(\Delta T) = d(T_h) - d(T_c) = -dq(1/\square_h\, c_{p,h} + 1/\square_c\, c_{p,c})$$

Substituting from Equation B.2 again, and integrating from inlet (1) to outlet (2),

$$\int_1^2 \frac{d(\Delta T)}{\Delta T} = -(U/(1/_h c_{p,h} + 1/_c c_{p,c}))\int dA$$

And, dA is actually $\pi^* D^* dx$. Following integration, $A = \pi^* D^* L$. Re-arranging using Equation B.1,

$$\ln\left(\frac{\Delta T_2}{\Delta T_1}\right) = -UA\left(1/_h c_{p,h} + 1/_c c_{p,c}\right) = -\frac{UA((T_{ho} - T_{hi}) + (T_{co} - T_{ci}))}{q}$$

Finally,

$$q = -\frac{UA(\Delta T_2 - \Delta T_1)}{ln\left(\frac{\Delta T_2}{\Delta T_1}\right)} = -UA\Delta T_{lm} \qquad \text{(B.3)}$$

where: $\Delta T_2 = T_{ho} - T_{co}$

$\Delta T_1 = T_{hi} - T_{ci}$

Equation B.3 is the heat exchanger equation. In this analysis, the steam temperature at the inlet is T_{ci} , and the exit steam temperature is T_{co}. T_{hi} and T_{ho} are the temperature of the steam pipe due to nuclear fission reaction, and are assumed to be equal. ΔT_{lm} is referred to as the Log Mean Temperature Difference (LMTD), which will be used as a basis for design calculations to develop steam tube dimensions including diameter (D) and length (L), as well as total tube number (N) estimates, used to size the steam reheat HTGR.

The following analysis provides a method for sizing the HTGR required to provide the reheat capacity to achieve target outlet steam conditions. Assuming that the power output from the commercial PWR/BWR, considered for reheat integration, is 1.0 $GW_{thermal}$, then, using the thermodynamic properties in Appendix A , the required steam flow is calculated as follows:

$$P_{thermal} = (h_1 - h_2) \qquad (3)$$

where: $P_{thermal}$ = PWR/BWR thermal power (GW)

□ = steam flow (kg/s)

h_1 = enthalpy at state **1** (kJ/kg)

h_2 = enthalpy at state **2** (kJ/kg)

Rearranging,

$$= P_{thermal}/(h_1 - h_2) \qquad (4)$$

Calculating,

$$= {}^{P_{thermal}}/_{(h_1 - h_2)} = \frac{\left(1.0GW * 10^6 \, {}^{kJ}/_{s\,GW}\right)}{\left(2667.8 \, {}^{kJ}/_{kg} - 1766.1 \, {}^{kJ}/_{kg}\right)} = 1109.0 \, {}^{kg}/_{s}$$

Now that the steam flow rate has been established for the PWR/BWR power plant, this now represents the flow rate of steam that will be reheated by the HTGR. The heat input

rate supplied by the HTGR to increase the enthalpy from state **1** to state **1'** using Equation 5 is:

$$q_{input} = (h_{1'} - h_1) = 1109.0\,{}^{kg}/_{s}\left(3643.0\,{}^{kJ}/_{kg} - 2667.8\,{}^{kJ}/_{kg}\right) = 1081496.8\,{}^{kJ}/_{s}$$

The calculated quantity of heat required to accomplish the desired reheat effect together with the Log Mean Temperature Difference (LMTD) method are used for sizing the HTGR steam tubes required. In the LMTD method, the heat transfer required is equal to the overall heat transfer coefficient times the heat transfer area and the average temperature as defined in Equation B.3. Assuming that the reactor power can provide adequate heat generation for a constant internal tube surface temperature of 1000°C, then, using the thermodynamic data in Table A.1:

$$\Delta T_{lm} = \frac{(\Delta T_2 - \Delta T_1)}{ln\left({}^{\Delta T_2}/_{\Delta T_1}\right)} = \frac{((1000 - 600) - (600 - 295))}{ln\left({}^{(1000 - 600)}/_{(600 - 295)}\right)} = 350.36℃$$

The only remaining unknowns are *U* and *A*. However, since *U* and *A* are dependent on each other, an iterative solution must be obtained. The iterative scheme is as follows:

1. Initial guess of tube dimensions (diameter, length and number); calculate total heat transfer area A.
2. Calculate Reynolds Number (Re) from assumed tube dimensions and fluid properties at an average temperature of 450°C.

3. Calculate Nusselt Number (*Nu*) from Reynolds Number (*Re)* and Prandtl Number (*Pr*) assuming turbulent flow $Nu = 0.023Re^{4/5}Pr^{0.4}$ (Bergman 2011).
4. Calculate *U* from Nusselt Number (*U* is essentially same as the internal convective heat transfer coefficient $h_i = U = Nu\ k/D$)).
5. Finally, calculate *A* by rearranging : $q_{input} = UA\Delta T_{lm}$
6. Compare *A* from step 1 and step 5, guess new tube dimensions. Continue iterations until the *A* from step 1 is equal to the *A* calculated in step 5.

The end result from one of the iterative processes is presented in the following Table B.1

Table B.1 Iterative Reactor Sizing Approach Using LMTD

Steam mass flow rate					
m=	1109 kg/s				
Heat Transfer Rate Required					
q=	1081496.8 kJ/s(Calculated from q=m (h_1-$h_{1'}$))				
Guess Tube Dimensions		**Iteration and Design Checks**			
D_{ID}=	0.08 m	A_T=	2418.1 m^2		
L=	15 m	%Cross Section=	7.30 %		
Number=	641 integer	$Velocity_{tube}$ =	13.1 m/s		
		$Mass\ Flow_{tube}$=	1.729 kg/s		
$A_{tubecross}$=	0.00503 m^2	$Mass\ Velocity_{tube}$ =	344.0 kg/m^2 s		
		$Mach_{tube}$=	625.7 m/s		
Calculate Heat Transfer Area		**Steam Properties**			
Re=	1.03E+06	Temperature (C)	Pressure (MPa)	Density (kg/m3)	
Pr=	1.01E+00	450	8	26.182	
Nusselt=	1.49E+03	Enthalpy (kJ/kg)	Entropy (J/g*K)	Cp (J/g*K)	
h_i=	1.28E+00 kJ/kg m^2 ^{0}C	3273.3	6.5579	2.5827	
U=	1.28E+00 kJ/kg m^2 ^{0}C	Sound Spd. (m/s)	Viscosity (Pa*s)	Cond. (W/m*K)	
LMTD=	350.36 ^{0}C	625.72	2.66E-05	0.068415	
A_T=	2418.1 m^2				

Based on this analysis, the HTGR reactor core would be approximately 15 meters in length, 7.5 meters in diameter (assuming a 2:1 reactor core L to D ratio) and contain 641 steam tubes with a 0.08 meter internal diameter.

Appendix C : Axial Heat Flux Boundary Condition

Table C.1 Axial Heat Flux Calculations

Axial Power Distribution Data from Reference 69, Figure 3.												
	Scaled From	**(5.5W/cm^3/70mm)**										
z	**Figure 3**	**Power Density**				**Average Power Density**		**Z**	**PF(Power Factor)**		**PF Integration Check**	
(cm)	**(mm)**	**(W/cm^3)**				**(W/cm^3)**		**(z/zmax)**				
0	0.0	0.00				**Numerical Integration**		0	0			
43	10.5	0.83				17.68		0.05	0.24		0.01	
86	18.0	1.41				47.99		0.09	0.41		0.01	
129	27.5	2.16				76.61		0.14	0.63		0.02	
171	37.0	2.91				108.60		0.18	0.85		0.03	
214	47.5	3.73				142.28		0.23	1.09		0.04	
257	57.0	4.48				175.96		0.27	1.31		0.05	
300	64.0	5.03				203.74		0.32	1.47		0.06	
343	69.0	5.42				223.94		0.36	1.58		0.07	
386		5.60	Peak Power Density (Table 1 ref. 69)			236.19		0.41	1.63		0.07	
429	70.0	5.50				237.87		0.45	1.60		0.07	
471	67.0	5.26				230.68		0.50	1.53		0.07	
514	63.5	4.99				219.73		0.55	1.45		0.07	
557	59.0	4.64				206.26		0.59	1.35		0.06	
600	53.5	4.20				189.43		0.64	1.23		0.06	
643	49.0	3.85				172.59		0.68	1.12		0.05	
686	44.0	3.46				156.59		0.73	1.01		0.05	
729	38.5	3.03				138.91		0.77	0.88		0.04	
771	34.0	2.67				122.07		0.82	0.78		0.04	
814	29.0	2.28				106.08		0.86	0.66		0.03	
857	24.0	1.89				89.24		0.91	0.55		0.03	
900	19.0	1.49				72.40		0.95	0.44		0.02	
943	16.0	1.26				58.93		1.00	0.37		0.02	
					Total	**3233.79**				**Total**	**1.00**	
					Average	**3.43**				**Average**	**1.00**	

Core				**Calculations**			**Heat Flux Boundary Condition**				
Core Volume=	662.68	m^3		zmax=	1500	cm	Z	PF(Power Factor)		z	q"
Core Power=	1081.5	MW (thermal)		Pavg=	1.63	W/cm^3	(z/zmax)			(cm)	(W/cm^2)
Average Core Power Density=	1.63	MW/m^3 or W/cm^3		Vtube=	1033160.46	cm^3	0	0		0	0
Tube Dimensions				Ptube=	1.6861E+06	W	0.045455	0.240557		68.2	10.75909
D=	0.08	m		q"tube=	447258.1	W/m^2	0.090909	0.412383		136.4	18.44416
L=	15	m			44.726	W/cm^2	0.136364	0.630029		204.5	28.17857
Number=	641	integer		Plinear=	1.12E+05	W/m	0.181818	0.847676		272.7	37.91299
							0.227273	1.088233		340.9	48.67208
							0.272727	1.305879		409.1	58.4065
							0.318182	1.46625		477.3	65.57923
							0.363636	1.580801		545.5	70.7026
							0.409091	1.632869		613.6	73.03141
							0.454545	1.603711		681.8	71.72728
							0.5	1.534981		750.0	68.65325
							0.545455	1.454795		818.2	65.06689
							0.590909	1.351699		886.4	60.45585
							0.636364	1.225693		954.5	54.82013
							0.681818	1.122598		1022.7	50.2091
							0.727273	1.008047		1090.9	45.08572
							0.772727	0.882041		1159.1	39.45
							0.818182	0.778945		1227.3	34.83896
							0.863636	0.664395		1295.5	29.71559
							0.909091	0.549844		1363.6	24.59221
							0.954545	0.435293		1431.8	19.46883
							1	0.366563		1500.0	16.39481

Appendix D : R5 Input

Heat Flux Boundary Condition

Table D.1 Derivation of R5 Heat Flux Boundary Condition

47 Hydrodynamic Cells

NVOL=	47		ZMAX=	15	m			actual				pick z/zmax>z/zmaxactual			
			SRCTYP	MULT	DHL	DHR	HSNR	z/zmax	m	b	PF	Z	PF(Power Factor)	M	B
		11000701	1	0.11	0.0	0.0	1	0.021277	5.292247	0.000	0.112601	(z/zmax)			
		11000702	1	0.23	0.0	0.0	2	0.042553	5.292247	0.000	0.225202	0	0		
		11000703	1	0.31	0.0	0.0	3	0.06383	3.780176	0.069	0.310018	0.045455	0.240557	5.292247	0.000
		11000704	1	0.39	0.0	0.0	4	0.085106	3.780176	0.069	0.390448	0.090909	0.412383	3.780176	0.069
		11000705	1	0.49	0.0	0.0	5	0.106383	4.788223	-0.023	0.486475	0.136364	0.630029	4.788223	-0.023
		11000706	1	0.59	0.0	0.0	6	0.12766	4.788223	-0.023	0.588352	0.181818	0.847676	4.788223	-0.023
		11000707	1	0.69	0.0	0.0	7	0.148936	4.788223	-0.023	0.690229	0.227273	1.088233	5.292247	-0.115
		11000708	1	0.79	0.0	0.0	8	0.170213	4.788223	-0.023	0.792107	0.272727	1.305879	4.788223	0.000
		11000709	1	0.90	0.0	0.0	9	0.191489	5.292247	-0.115	0.898858	0.318182	1.46625	3.528164	0.344
		11000710	1	1.01	0.0	0.0	10	0.212766	5.292247	-0.115	1.011459	0.363636	1.580801	2.520117	0.664
		11000711	1	1.12	0.0	0.0	11	0.234043	4.788223	0.000	1.120648	0.409091	1.632869	1.145508	1.164
		11000712	1	1.22	0.0	0.0	12	0.255319	4.788223	0.000	1.222525	0.454545	1.603711	-0.64148	1.895
		11000713	1	1.32	0.0	0.0	13	0.276596	3.528164	0.344	1.319528	0.5	1.534981	-1.51207	2.291
		11000714	1	1.39	0.0	0.0	14	0.297872	3.528164	0.344	1.394595	0.545455	1.454795	-1.76408	2.417
		11000715	1	1.47	0.0	0.0	15	0.319149	2.520117	0.664	1.468687	0.590909	1.351699	-2.26811	2.692
		11000716	1	1.52	0.0	0.0	16	0.340426	2.520117	0.664	1.522307	0.636364	1.225693	-2.77213	2.990
		11000717	1	1.58	0.0	0.0	17	0.361702	2.520117	0.664	1.575926	0.681818	1.122598	-2.26811	2.669
		11000718	1	1.60	0.0	0.0	18	0.382979	1.145508	1.164	1.602958	0.727273	1.008047	-2.52012	2.841
		11000719	1	1.63	0.0	0.0	19	0.404255	1.145508	1.164	1.62733	0.772727	0.882041	-2.77213	3.024
		11000720	1	1.62	0.0	0.0	20	0.425532	-0.64148	1.895	1.622323	0.818182	0.778945	-2.26811	2.635
		11000721	1	1.61	0.0	0.0	21	0.446809	-0.64148	1.895	1.608674	0.863636	0.664395	-2.52012	2.841
		11000722	1	1.58	0.0	0.0	22	0.468085	-1.51207	2.291	1.583238	0.909091	0.549844	-2.52012	2.841
		11000723	1	1.55	0.0	0.0	23	0.489362	-1.51207	2.291	1.551066	0.954545	0.435293	-2.52012	2.841
		11000724	1	1.52	0.0	0.0	24	0.510638	-1.76408	2.417	1.516214	1	0.366563	-1.51207	1.879
		11000725	1	1.48	0.0	0.0	25	0.531915	-1.76408	2.417	1.47868				
		11000726	1	1.44	0.0	0.0	26	0.553191	-2.26811	2.692	1.437247				
		11000727	1	1.39	0.0	0.0	27	0.574468	-2.26811	2.692	1.388989				
		11000728	1	1.34	0.0	0.0	28	0.595745	-2.77213	2.990	1.338294				
		11000729	1	1.28	0.0	0.0	29	0.617021	-2.77213	2.990	1.279313				
		11000730	1	1.22	0.0	0.0	30	0.638298	-2.26811	2.669	1.221306				
		11000731	1	1.17	0.0	0.0	31	0.659574	-2.26811	2.669	1.173049				
		11000732	1	1.12	0.0	0.0	32	0.680851	-2.26811	2.669	1.124791				
		11000733	1	1.07	0.0	0.0	33	0.702128	-2.52012	2.841	1.071415				
		11000734	1	1.02	0.0	0.0	34	0.723404	-2.52012	2.841	1.017796				
		11000735	1	0.96	0.0	0.0	35	0.744681	-2.77213	3.024	0.959789				
		11000736	1	0.90	0.0	0.0	36	0.765957	-2.77213	3.024	0.900808				
		11000737	1	0.85	0.0	0.0	37	0.787234	-2.26811	2.635	0.849138				
		11000738	1	0.80	0.0	0.0	38	0.808511	-2.26811	2.635	0.800881				
		11000739	1	0.75	0.0	0.0	39	0.829787	-2.52012	2.841	0.749698				
		11000740	1	0.70	0.0	0.0	40	0.851064	-2.52012	2.841	0.696079				
		11000741	1	0.64	0.0	0.0	41	0.87234	-2.52012	2.841	0.642459				
		11000742	1	0.59	0.0	0.0	42	0.893617	-2.52012	2.841	0.58884				
		11000743	1	0.54	0.0	0.0	43	0.914894	-2.52012	2.841	0.53522				
		11000744	1	0.48	0.0	0.0	44	0.93617	-2.52012	2.841	0.481601				
		11000745	1	0.43	0.0	0.0	45	0.957447	-1.51207	1.879	0.430906				
		11000746	1	0.40	0.0	0.0	46	0.978723	-1.51207	1.879	0.398734				
		11000747	1	0.37	0.0	0.0	47	1	-1.51207	1.879	0.366563				
							This spreadsheet uses the non-dimensional PF distribution and linearizes an equation between points so a PF								
							can be specified for a finer mesh size in RELAP5.								

Table D.1 (Continued)

22 Hydrodynamic Cells

NVOL=	22		ZMAX=	15	m			actual				pick z/zmax>z/zmaxactual			
			SRCTYP	MULT	DHL	DHR	HSNR	z/zmax	m	b	PF	Z	PF(Power Factor)	M	B
		11000701	1	0.24	0.0	0.0	1	0.045455	5.292247	0.000	0.240557	(z/zmax)			
		11000702	1	0.41	0.0	0.0	2	0.090909	3.780176	0.069	0.412383	0	0		
		11000703	1	0.63	0.0	0.0	3	0.136364	4.788223	-0.023	0.630029	0.045455	0.240557	5.292247	0.000
		11000704	1	0.85	0.0	0.0	4	0.181818	4.788223	-0.023	0.847676	0.090909	0.412383	3.780176	0.069
		11000705	1	1.09	0.0	0.0	5	0.227273	5.292247	-0.115	1.088233	0.136364	0.630029	4.788223	-0.023
		11000706	1	1.31	0.0	0.0	6	0.272727	4.788223	0.000	1.305879	0.181818	0.847676	4.788223	-0.023
		11000707	1	1.47	0.0	0.0	7	0.318182	3.528164	0.344	1.46625	0.227273	1.088233	5.292247	-0.115
		11000708	1	1.58	0.0	0.0	8	0.363636	2.520117	0.664	1.580801	0.272727	1.305879	4.788223	0.000
		11000709	1	1.63	0.0	0.0	9	0.409091	1.145508	1.164	1.632869	0.318182	1.46625	3.528164	0.344
		11000710	1	1.60	0.0	0.0	10	0.454545	-0.64148	1.895	1.603711	0.363636	1.580801	2.520117	0.664
		11000711	1	1.53	0.0	0.0	11	0.5	-1.51207	2.291	1.534981	0.409091	1.632869	1.145508	1.164
		11000712	1	1.45	0.0	0.0	12	0.545455	-1.76408	2.417	1.454795	0.454545	1.603711	-0.64148	1.895
		11000713	1	1.35	0.0	0.0	13	0.590909	-2.26811	2.692	1.351699	0.5	1.534981	-1.51207	2.291
		11000714	1	1.23	0.0	0.0	14	0.636364	-2.77213	2.990	1.225693	0.545455	1.454795	-1.76408	2.417
		11000715	1	1.12	0.0	0.0	15	0.681818	-2.26811	2.669	1.122598	0.590909	1.351699	-2.26811	2.692
		11000716	1	1.01	0.0	0.0	16	0.727273	-2.52012	2.841	1.008047	0.636364	1.225693	-2.77213	2.990
		11000717	1	0.88	0.0	0.0	17	0.772727	-2.77213	3.024	0.882041	0.681818	1.122598	-2.26811	2.669
		11000718	1	0.78	0.0	0.0	18	0.818182	-2.26811	2.635	0.778945	0.727273	1.008047	-2.52012	2.841
		11000719	1	0.66	0.0	0.0	19	0.863636	-2.52012	2.841	0.664395	0.772727	0.882041	-2.77213	3.024
		11000720	1	0.55	0.0	0.0	20	0.909091	-2.52012	2.841	0.549844	0.818182	0.778945	-2.26811	2.635
		11000721	1	0.44	0.0	0.0	21	0.954545	-2.52012	2.841	0.435293	0.863636	0.664395	-2.52012	2.841
		11000722	1	0.37	0.0	0.0	22	1	-1.51207	1.879	0.366563	0.909091	0.549844	-2.52012	2.841
												0.954545	0.435293	-2.52012	2.841
												1	0.366563	-1.51207	1.879

Table D.1 (Continued)

57 Hydrodynamic Cells

NVOL=	57		ZMAX=	15	m				actual				pick z/zmax>z/zmaxactual				
			SRCTYP	MULT	DHL	DHR	HSNR		z/zmax	m	b	PF	Z	PF(Power Factor)		M	B
		11000701	1	0.09	0.0	0.0	1		0.017544	5.292247	0.000	0.092846	(z/zmax)				
		11000702	1	0.19	0.0	0.0	2		0.035088	5.292247	0.000	0.185693	0	0			
		11000703	1	0.27	0.0	0.0	3		0.052632	3.780176	0.069	0.267687	0.045455	0.240557		5.292247	0.000
		11000704	1	0.33	0.0	0.0	4		0.070175	3.780176	0.069	0.334006	0.090909	0.412383		3.780176	0.069
		11000705	1	0.40	0.0	0.0	5		0.087719	3.780176	0.069	0.400325	0.136364	0.630029		4.788223	-0.023
		11000706	1	0.48	0.0	0.0	6		0.105263	4.788223	-0.023	0.481113	0.181818	0.847676		4.788223	-0.023
		11000707	1	0.57	0.0	0.0	7		0.122807	4.788223	-0.023	0.565117	0.227273	1.088233		5.292247	-0.115
		11000708	1	0.65	0.0	0.0	8		0.140351	4.788223	-0.023	0.649121	0.272727	1.305879		4.788223	0.000
		11000709	1	0.73	0.0	0.0	9		0.157895	4.788223	-0.023	0.733125	0.318182	1.46625		3.528164	0.344
		11000710	1	0.82	0.0	0.0	10		0.175439	4.788223	-0.023	0.817129	0.363636	1.580801		2.520117	0.664
		11000711	1	0.92	0.0	0.0	11		0.192982	4.788223	0.000	0.924043	0.409091	1.632869		1.145508	1.164
		11000712	1	1.00	0.0	0.0	12		0.210526	5.292247	-0.115	0.999606	0.454545	1.603711		-0.64148	1.895
		11000713	1	1.09	0.0	0.0	13		0.22807	4.788223	0.000	1.092051	0.5	1.534981		-1.51207	2.291
		11000714	1	1.18	0.0	0.0	14		0.245614	4.788223	0.000	1.176055	0.545455	1.454795		-1.76408	2.417
		11000715	1	1.26	0.0	0.0	15		0.263158	4.788223	0.000	1.260059	0.590909	1.351699		-2.26811	2.692
		11000716	1	1.33	0.0	0.0	16		0.280702	3.528164	0.344	1.334014	0.636364	1.225693		-2.77213	2.990
		11000717	1	1.40	0.0	0.0	17		0.298246	3.528164	0.344	1.395912	0.681818	1.122598		-2.26811	2.669
		11000718	1	1.46	0.0	0.0	18		0.315789	3.528164	0.344	1.45781	0.727273	1.008047		-2.52012	2.841
		11000719	1	1.50	0.0	0.0	19		0.333333	2.520117	0.664	1.504434	0.772727	0.882041		-2.77213	3.024
		11000720	1	1.55	0.0	0.0	20		0.350877	2.520117	0.664	1.548646	0.818182	0.778945		-2.26811	2.635
		11000721	1	1.59	0.0	0.0	21		0.368421	1.145508	1.164	1.586282	0.863636	0.664395		-2.52012	2.841
		11000722	1	1.61	0.0	0.0	22		0.385965	1.145508	1.164	1.606378	0.909091	0.549844		-2.52012	2.841
		11000723	1	1.63	0.0	0.0	23		0.403509	1.145508	1.164	1.626475	0.954545	0.435293		-2.52012	2.841
		11000724	1	1.63	0.0	0.0	24		0.421053	-0.64148	1.895	1.625196	1	0.366563		-1.51207	1.879
		11000725	1	1.61	0.0	0.0	25		0.438596	-0.64148	1.895	1.613942					
		11000726	1	1.60	0.0	0.0	26		0.45614	-1.51207	2.291	1.601299					
		11000727	1	1.57	0.0	0.0	27		0.473684	-1.51207	2.291	1.574772					
		11000728	1	1.55	0.0	0.0	28		0.491228	-1.51207	2.291	1.548244					
		11000729	1	1.52	0.0	0.0	29		0.508772	-1.76408	2.417	1.519506					
		11000730	1	1.49	0.0	0.0	30		0.526316	-1.76408	2.417	1.488557					
		11000731	1	1.46	0.0	0.0	31		0.54386	-1.76408	2.417	1.457609					
		11000732	1	1.42	0.0	0.0	32		0.561404	-2.26811	2.692	1.418621					
		11000733	1	1.38	0.0	0.0	33		0.578947	-2.26811	2.692	1.37883					
		11000734	1	1.34	0.0	0.0	34		0.596491	-2.77213	2.990	1.336225					
		11000735	1	1.29	0.0	0.0	35		0.614035	-2.77213	2.990	1.287591					
		11000736	1	1.24	0.0	0.0	36		0.631579	-2.77213	2.990	1.238957					
		11000737	1	1.20	0.0	0.0	37		0.649123	-2.26811	2.669	1.196754					
		11000738	1	1.16	0.0	0.0	38		0.666667	-2.26811	2.669	1.156963					
		11000739	1	1.12	0.0	0.0	39		0.684211	-2.52012	2.841	1.116569					
		11000740	1	1.07	0.0	0.0	40		0.701754	-2.52012	2.841	1.072356					
		11000741	1	1.03	0.0	0.0	41		0.719298	-2.52012	2.841	1.028144					
		11000742	1	0.98	0.0	0.0	42		0.736842	-2.77213	3.024	0.981519					
		11000743	1	0.93	0.0	0.0	43		0.754386	-2.77213	3.024	0.932886					
		11000744	1	0.88	0.0	0.0	44		0.77193	-2.77213	3.024	0.884252					
		11000745	1	0.84	0.0	0.0	45		0.789474	-2.26811	2.635	0.844058					
		11000746	1	0.80	0.0	0.0	46		0.807018	-2.26811	2.635	0.804267					
		11000747	1	0.76	0.0	0.0	47		0.824561	-2.52012	2.841	0.762868					
		11000748	1	0.72	0.0	0.0	48		0.842105	-2.52012	2.841	0.718655					
		11000749	1	0.67	0.0	0.0	49		0.859649	-2.52012	2.841	0.674443					
		11000750	1	0.63	0.0	0.0	50		0.877193	-2.52012	2.841	0.63023					
		11000751	1	0.59	0.0	0.0	51		0.894737	-2.52012	2.841	0.586018					
		11000752	1	0.54	0.0	0.0	52		0.912281	-2.52012	2.841	0.541805					
		11000753	1	0.50	0.0	0.0	53		0.929825	-2.52012	2.841	0.497593					
		11000754	1	0.45	0.0	0.0	54		0.947368	-2.52012	2.841	0.45338					
		11000755	1	0.42	0.0	0.0	55		0.964912	-1.51207	1.879	0.419618					
		11000756	1	0.39	0.0	0.0	56		0.982456	-1.51207	1.879	0.39309					
		11000757	1	0.37	0.0	0.0	57		1	-1.51207	1.879	0.366563					

Table D.1 (Continued)

77 Hydrodynamic Cells

NVOL=	77		ZMAX=	15	m				actual					pick z/zmax>z/zmaxactual			
			SRCTYP	MULT	DHL	DHR	HSNR		z/zmax	m	b	PF		Z	PF(Power Factor)	M	B
		11000701	1	0.07	0.0	0.0	1		0.012987	5.292247	0.000	0.06873		(z/zmax)			
		11000702	1	0.14	0.0	0.0	2		0.025974	5.292247	0.000	0.137461		0	0		
		11000703	1	0.21	0.0	0.0	3		0.038961	5.292247	0.000	0.206191		0.045455	0.240557	5.292247	0.000
		11000704	1	0.27	0.0	0.0	4		0.051948	3.780176	0.069	0.265103		0.090909	0.412383	3.780176	0.069
		11000705	1	0.31	0.0	0.0	5		0.064935	3.780176	0.069	0.314196		0.136364	0.630029	4.788223	-0.023
		11000706	1	0.36	0.0	0.0	6		0.077922	3.780176	0.069	0.36329		0.181818	0.847676	4.788223	-0.023
		11000707	1	0.41	0.0	0.0	7		0.090909	3.780176	0.069	0.412383		0.227273	1.088233	5.292247	-0.115
		11000708	1	0.47	0.0	0.0	8		0.103896	4.788223	-0.023	0.474568		0.272727	1.305879	4.788223	0.000
		11000709	1	0.54	0.0	0.0	9		0.116883	4.788223	-0.023	0.536752		0.318182	1.46625	3.528164	0.344
		11000710	1	0.60	0.0	0.0	10		0.12987	4.788223	-0.023	0.598937		0.363636	1.580801	2.520117	0.664
		11000711	1	0.66	0.0	0.0	11		0.142857	4.788223	-0.023	0.661122		0.409091	1.632869	1.145508	1.164
		11000712	1	0.72	0.0	0.0	12		0.155844	4.788223	-0.023	0.723306		0.454545	1.603711	-0.64148	1.895
		11000713	1	0.79	0.0	0.0	13		0.168831	4.788223	-0.023	0.785491		0.5	1.534981	-1.51207	2.291
		11000714	1	0.85	0.0	0.0	14		0.181818	4.788223	-0.023	0.847676		0.545455	1.454795	-1.76408	2.417
		11000715	1	0.92	0.0	0.0	15		0.194805	5.292247	-0.115	0.916406		0.590909	1.351699	-2.26811	2.692
		11000716	1	0.99	0.0	0.0	16		0.207792	5.292247	-0.115	0.985137		0.636364	1.225693	-2.77213	2.990
		11000717	1	1.05	0.0	0.0	17		0.220779	5.292247	-0.115	1.053867		0.681818	1.122598	-2.26811	2.669
		11000718	1	1.12	0.0	0.0	18		0.233766	4.788223	0.000	1.119325		0.727273	1.008047	-2.52012	2.841
		11000719	1	1.18	0.0	0.0	19		0.246753	4.788223	0.000	1.18151		0.772727	0.882041	-2.77213	3.024
		11000720	1	1.24	0.0	0.0	20		0.25974	4.788223	0.000	1.243694		0.818182	0.778945	-2.26811	2.635
		11000721	1	1.31	0.0	0.0	21		0.272727	4.788223	0.000	1.305879		0.863636	0.664395	-2.52012	2.841
		11000722	1	1.35	0.0	0.0	22		0.285714	3.528164	0.344	1.351699		0.909091	0.549844	-2.52012	2.841
		11000723	1	1.40	0.0	0.0	23		0.298701	3.528164	0.344	1.39752		0.954545	0.435293	-2.52012	2.841
		11000724	1	1.44	0.0	0.0	24		0.311688	3.528164	0.344	1.44334		1	0.366563	-1.51207	1.879
		11000725	1	1.48	0.0	0.0	25		0.324675	2.520117	0.664	1.482615					
		11000726	1	1.52	0.0	0.0	26		0.337662	2.520117	0.664	1.515343					
		11000727	1	1.55	0.0	0.0	27		0.350649	2.520117	0.664	1.548072					
		11000728	1	1.58	0.0	0.0	28		0.363636	2.520117	0.664	1.580801					
		11000729	1	1.60	0.0	0.0	29		0.376623	1.145508	1.164	1.595678					
		11000730	1	1.61	0.0	0.0	30		0.38961	1.145508	1.164	1.610554					
		11000731	1	1.63	0.0	0.0	31		0.402597	1.145508	1.164	1.625431					
		11000732	1	1.63	0.0	0.0	32		0.415584	-0.64148	1.895	1.628704					
		11000733	1	1.62	0.0	0.0	33		0.428571	-0.64148	1.895	1.620373					
		11000734	1	1.61	0.0	0.0	34		0.441558	-0.64148	1.895	1.612042					
		11000735	1	1.60	0.0	0.0	35		0.454545	-0.64148	1.895	1.603711					
		11000736	1	1.58	0.0	0.0	36		0.467532	-1.51207	2.291	1.584074					
		11000737	1	1.56	0.0	0.0	37		0.480519	-1.51207	2.291	1.564437					
		11000738	1	1.54	0.0	0.0	38		0.493506	-1.51207	2.291	1.544799					
		11000739	1	1.52	0.0	0.0	39		0.506494	-1.76408	2.417	1.523526					
		11000740	1	1.50	0.0	0.0	40		0.519481	-1.76408	2.417	1.500615					
		11000741	1	1.48	0.0	0.0	41		0.532468	-1.76408	2.417	1.477705					
		11000742	1	1.45	0.0	0.0	42		0.545455	-1.76408	2.417	1.454795					
		11000743	1	1.43	0.0	0.0	43		0.558442	-2.26811	2.692	1.425339					
		11000744	1	1.40	0.0	0.0	44		0.571429	-2.26811	2.692	1.395883					
		11000745	1	1.37	0.0	0.0	45		0.584416	-2.26811	2.692	1.366427					
		11000746	1	1.33	0.0	0.0	46		0.597403	-2.77213	2.990	1.333698					
		11000747	1	1.30	0.0	0.0	47		0.61039	-2.77213	2.990	1.297697					
		11000748	1	1.26	0.0	0.0	48		0.623377	-2.77213	2.990	1.261695					
		11000749	1	1.23	0.0	0.0	49		0.636364	-2.77213	2.990	1.225693					
		11000750	1	1.20	0.0	0.0	50		0.649351	-2.26811	2.669	1.196238					
		11000751	1	1.17	0.0	0.0	51		0.662338	-2.26811	2.669	1.166782					
		11000752	1	1.14	0.0	0.0	52		0.675325	-2.26811	2.669	1.137326					
		11000753	1	1.11	0.0	0.0	53		0.688312	-2.52012	2.841	1.106233					
		11000754	1	1.07	0.0	0.0	54		0.701299	-2.52012	2.841	1.073505					
		11000755	1	1.04	0.0	0.0	55		0.714286	-2.52012	2.841	1.040776					
		11000756	1	1.01	0.0	0.0	56		0.727273	-2.52012	2.841	1.008047					
		11000757	1	0.97	0.0	0.0	57		0.74026	-2.77213	3.024	0.972045					
		11000758	1	0.94	0.0	0.0	58		0.753247	-2.77213	3.024	0.936044					
		11000759	1	0.90	0.0	0.0	59		0.766234	-2.77213	3.024	0.900042					
		11000760	1	0.87	0.0	0.0	60		0.779221	-2.26811	2.635	0.867313					
		11000761	1	0.84	0.0	0.0	61		0.792208	-2.26811	2.635	0.837857					
		11000762	1	0.81	0.0	0.0	62		0.805195	-2.26811	2.635	0.808401					
		11000763	1	0.78	0.0	0.0	63		0.818182	-2.26811	2.635	0.778945					
		11000764	1	0.75	0.0	0.0	64		0.831169	-2.52012	2.841	0.746217					
		11000765	1	0.71	0.0	0.0	65		0.844156	-2.52012	2.841	0.713488					
		11000766	1	0.68	0.0	0.0	66		0.857143	-2.52012	2.841	0.680759					
		11000767	1	0.65	0.0	0.0	67		0.87013	-2.52012	2.841	0.64803					
		11000768	1	0.62	0.0	0.0	68		0.883117	-2.52012	2.841	0.615301					
		11000769	1	0.58	0.0	0.0	69		0.896104	-2.52012	2.841	0.582573					
		11000770	1	0.55	0.0	0.0	70		0.909091	-2.52012	2.841	0.549844					
		11000771	1	0.52	0.0	0.0	71		0.922078	-2.52012	2.841	0.517115					
		11000772	1	0.48	0.0	0.0	72		0.935065	-2.52012	2.841	0.484386					
		11000773	1	0.45	0.0	0.0	73		0.948052	-2.52012	2.841	0.451657					
		11000774	1	0.43	0.0	0.0	74		0.961039	-1.51207	1.879	0.425474					
		11000775	1	0.41	0.0	0.0	75		0.974026	-1.51207	1.879	0.405837					
		11000776	1	0.39	0.0	0.0	76		0.987013	-1.51207	1.879	0.3862					
		11000777	1	0.37	0.0	0.0	77		1	-1.51207	1.879	0.366563					

RELAP5 Input Re-print

```
=              RELAP 5 MODEL INPUT          *Notes describing inputs are in red.
*
*  Case Description
*
*   Base Case Corrected Power Inlet Quality 0.75
*
*
0000100 new transnt
0000101 run
*
*              CPU     TIME REMAINING CARD
*0000105 10.0 200.0
*              TIME STEP CONTROL CARDS
*              TIME-ENDDT-MIN DT-MAXSSDTT MINED MAJED RES
0000201 600.0 1.0E-7 0.0125 3 81 2000 4000
*       A 600 second run length selected to achieve steady state solution.
*
*
20300011  mflowj 250000000 1
20300012  mflowj 350000000 1
*20300045 httemp 100000101 1
20300031 p 100010000 1
20300032 p 100470000 1               Selected Parameters for Plotting
20300051 tempg 100470000  1
20300052 tempg 100010000  1
20300041 httemp 100002001 1
20300042 httemp 100002501 1
20300043 httemp 100003001 1
20300044 httemp 100003501 1
*20300061 hthtc 100002000 1
*20300062 hthtc 100002500 1
*20300063 hthtc 100003000 1
*20300064 hthtc 100003500 1
*
*              MINOR EDIT REQUESTS
*
*
*
0000301 cputime 0 *cpu-time
0000302 p 100010000 *inlet node pressure
0000303 p 100470000 *outlet node pressure
0000304 voidg 100200000 *outlet node void fraction
0000305 voidgj 350000000 *outlet junc void fraction
0000306 tempf 100470000 *outlet node tempf
0000307 tempg 100470000 *outlet node tempg
0000308 sattemp 100470000 *outlet node tsat
0000309 httemp 100000101 *wall temp t01
0000310 httemp 100000501 *wall temp t05
0000311 httemp 100001001 *wall temp t10      Additional Minor edit information printed
                                             for review
0000312 httemp 100001501 *wall temp t15
0000313 httemp 100002001 *wall temp t20
0000314 httemp 100002501 *wall temp t25
0000315 httemp 100003001 *wall temp t30
0000316 httemp 100003501 *wall temp t35
0000317 httemp 100004001 *wall temp t40
0000318 httemp 100004501 *wall temp t45
0000319 htrnr 100000100 *heat flux
0000320 htrnr 100000500 *heat flux
0000321 htrnr 100001000 *heat flux
0000322 htrnr 100001500 *heat flux
0000323 htrnr 100002000 *heat flux
0000324 htrnr 100002500 *heat flux
0000325 htrnr 100003000 *heat flux
```

```
0000326 htrnr 100003500 *heat flux
0000327 htrnr 100004000 *heat flux
0000328 htrnr 100004500 *heat flux
0000329 htchf 100000100 *chf
0000330 htchf 100000500 *chf
0000331 htchf 100001000 *chf
0000332 htchf 100001500 *chf
0000333 htchf 100002000 *chf
0000334 htchf 100002500 *chf
0000335 htchf 100003000 *chf
0000336 htchf 100003500 *chf
0000337 htchf 100004000 *chf
0000338 htchf 100004500 *chf
0000339 hthtc 100000100 *htc
0000340 hthtc 100000500 *htc
0000341 hthtc 100001000 *htc
0000342 hthtc 100001500 *htc
0000343 hthtc 100002000 *htc
0000344 hthtc 100002500 *htc
0000345 hthtc 100003000 *htc
0000346 hthtc 100003500 *htc
0000347 hthtc 100004000 *htc
0000348 hthtc 100004500 *htc
0000349 floreg 100010000 *flow regime
0000350 floreg 100050000 *flow regime
0000351 floreg 100100000 *flow regime
0000352 floreg 100150000 *flow regime
0000353 floreg 100200000 *flow regime
0000354 floreg 100250000 *flow regime
0000355 floreg 100300000 *flow regime
0000356 floreg 100350000 *flow regime
0000357 floreg 100400000 *flow regime
0000358 floreg 100450000 *flow regime
0000359 mflowj 250000000 *mflow inlet
0000360 mflowj 350000000 *mflow outlet
*
*
*
*              HYDRODYNAMIC COMPONENTS
*
*
1000000 hot-cha pipe
*
*       NVOL
1000001 47
*
*       AREA  NVOL
1000101 5.0E-3 47             Cross Sectional Area of tube with 0.08 m inner
*                             diameter.
*       LENGTH  NVOL
1000301 0.319149 47           Length of cell based on 15 m /47.
*
*
*       V-ANGLE NVOL
1000601 90.0 47
*
*       ROUGH   DHYD NVOL
1000801 20.0E-6 0.08 47
*
*              PIPE VOLUME CONTROL FLAGS
*       TLPVBFE NVOL
1001001 1111000 47
*
*              PIPE JUNCTION CONTROL FLAGS
*       JEFVCAHS NVOL-1
1001101 01000000 46
*
*       PIPE VOLUME INITIAL CONDITIONS
```

```
*       EBT PRES quality D1 D2 D3 NVOL
1001201 002 8.0E+6 0.75 0.0 0.0 0.0 47        Specification of 8.0MPa and 75% inlet
*                                             Quality
*               PIPE JUNCTION DATA
*       CTRL-WRD
1001300 1
*
*               INITIAL CONDITION
*       FLOWF   FLOWG FLOWFG NJUNC
1001301 0.43225 1.29675 0.0 46                Based on total mass flow of 1.729kg/s
*                                             and 75% inlet quality.
*               HEAT STRUCTURE DATA
*
*       NH NP TYPE SS-FL LCOORD               Dimension of the left BC from tube center
11000000 47 2 2 1 4.0E-2                      line, 0.08m/2.
*
*       LOC FMT
11000100 0 1
*
*       NINT RCOORD                           Dimension of the right BC from the tube
11000101 1 4.635E-2                           center line assuming 0.25inch wall thickness
*
*       COMPOSITION INTERVAL
11000201 1 1
*
*       SOURCE INTERVAL
11000301 1.0 1
*
*       TFLG
11000400 0
*
*
*               INITEMP FOR EACH HEAT STRUCTURE
*       INITEMP MESH
11000401 568.0 2                              Initial temperature and 2 node structure.
*
*   Base Model Length is 15m/47=0.319149m
*       BNDVOL    INCR BNDCON SAC FACTOR      HSNR
11000501 100010000 010000 1 1 0.319149 47 *left
*
11000601 0 0 0 1 0.319149 47 *right
*
*          Axial Power Factor
*       SRCTYP MULT DHL DHR HSNR
11000701 1 0.11 0.0 0.0 1
11000702 1 0.23 0.0 0.0 2
11000703 1 0.31 0.0 0.0 3
11000704 1 0.39 0.0 0.0 4
11000705 1 0.49 0.0 0.0 5                     Power multipliers (Power Shape).
11000706 1 0.59 0.0 0.0 6
11000707 1 0.69 0.0 0.0 7
11000708 1 0.79 0.0 0.0 8
11000709 1 0.90 0.0 0.0 9
11000710 1 1.01 0.0 0.0 10
11000711 1 1.12 0.0 0.0 11
11000712 1 1.22 0.0 0.0 12
11000713 1 1.32 0.0 0.0 13
11000714 1 1.39 0.0 0.0 14
11000715 1 1.47 0.0 0.0 15
11000716 1 1.52 0.0 0.0 16
11000717 1 1.58 0.0 0.0 17
11000718 1 1.60 0.0 0.0 18
11000719 1 1.63 0.0 0.0 19
11000720 1 1.62 0.0 0.0 20
11000721 1 1.61 0.0 0.0 21
11000722 1 1.58 0.0 0.0 22
11000723 1 1.55 0.0 0.0 23
11000724 1 1.52 0.0 0.0 24
```

```
11000725 1 1.48 0.0 0.0 25
11000726 1 1.44 0.0 0.0 26
11000727 1 1.39 0.0 0.0 27
11000728 1 1.34 0.0 0.0 28
11000729 1 1.28 0.0 0.0 29
11000730 1 1.22 0.0 0.0 30
11000731 1 1.17 0.0 0.0 31
11000732 1 1.12 0.0 0.0 32
11000733 1 1.07 0.0 0.0 33
11000734 1 1.02 0.0 0.0 34
11000735 1 0.96 0.0 0.0 35
11000736 1 0.90 0.0 0.0 36
11000737 1 0.85 0.0 0.0 37
11000738 1 0.80 0.0 0.0 38
11000739 1 0.75 0.0 0.0 39
11000740 1 0.70 0.0 0.0 40
11000741 1 0.64 0.0 0.0 41
11000742 1 0.59 0.0 0.0 42
11000743 1 0.54 0.0 0.0 43
11000744 1 0.48 0.0 0.0 44
11000745 1 0.43 0.0 0.0 45
11000746 1 0.40 0.0 0.0 46
11000747 1 0.37 0.0 0.0 47
*
*
*       DE HLF  HLR     GRID FACTORS LBF HSNR
11000801 0 20.0 10.0 0.0 0.0 0.0 0.0 1.0 47
*
*
*               HEAT STRUCTURE THERMAL PROPS KENTHAL (Kanthal 2011)
*               MATERIALTYP    FORFLG1 FORFL2
20100100 tbl/fctn 1 1
*20100100 s-steel
*       TEMP    THCOND
20100101 50.0 11.0
20100102 600.0 21.0
20100103 800.0 23.0
20100104 1000.0 27.0
20100105 1200.0 29.0
20100106 5000.0 29.0
*
*
*       TEMP    VOLHEATCAP
20100151 20.0 7.25e+6
20100152 200.0 8.40e+6
20100153 400.0 9.60e+6
20100154 600.0 10.65e+6              PROPS KENTHAL (Kanthal 2011)
20100155 800.0 10.05e+6
20100156 1000.0 10.35e+6
20100157 1200.0 10.5e+6
20100158 5000.0 10.5E+6
*
*
*
*               GENERAL TABLE FOR HEAT STRUCTURE POWER SRCTYP 1
*       TBLTYP  TRIP    FACTORT FACTORP
20200100 power 0 1.0 1.0
*
*       TIME LINEARPOWER(W/m)
20200101 0.0 0.0                     Initial isothermal condition.
20200102 5.0 0.0
20200103 10.0 3.5745E+4              Total power/cell=1.68e6W/15m*0.319149m
20200104 120.0 3.574e+4
*
*               END OF HEAT STRUCTURE DATA
*
*
*               LOWER BOUNDARY CONDITION STEAM INPUT
```

```
*
*
*              TMDPVOL COMPONENT200   SOURCE
*              TMDPJUN COMPONENT250   SOURCE TO PIPE
*
2000000 lo-bndry tmdpvol
*
*       AREA    LENGTH VOL HANGL VANGL EL ROUGH       DHD TLPVBFE
2000101 1.0 1.0 0.0 0.0 90. 1.0 0.0 1.0 0
*
*       EBT TBLNR
2000200 002 0
*
*       TIME Pressure quality
2000201 0.0 8.0E+6 0.75              Inlet 8.0MPa and 75% Quality.
*
*
*
*
2500000 lo-flow tmdpjun
*
*       FROMCODE  TOCODE    AREA
2500101 200000000 100000000 0.0
*
*       CNTRLWRD
2500200 1
*
*       TIME FLOWF  FLOWG   FLOWFG
2500201 0.0 0.43225 1.29675 0.0
*
*
*
****************************************
*
*
*
*              UPPER BOUNDARY CONDITION
*
*
*              TMDPVOL COMPONENT300
*              SNGLJUN COMPONENT350
*
3000000 up-bndry tmdpvol
*
*       AREA    LENGTH VOL HANGL VANGL EL ROUGH       DHD TLPVBFE
3000101 1.0 1.0 0.0 0.0 90. 1.0 0.0 1.0 0
*
*       EBT TBLNR
3000200 003 0
*
*       TIME    PRES    TEMP
3000201 0.0 8.0E+6 568.0
*
*
*
*
3500000 up-flow sngljun
*
*       FROMCODE  TOCODE   AREA FLOSS RLOSS JEFVCAHS COEFS
3500101 100010000 300000000 0.0 0.0 0.0 01000000 1.0 1.0 1.0
*
*
*       CW      FLOWF   FLOWG   FLOWFG
3500201 0.0 0.43225 1.29675 0.0
*
*
*
****************************************
```

```
*
*
.               end of case
```

Appendix E : Pressure Drop Calculations

The pressure drop calculations completed in this section are based on Equation 59, which was previously developed. The objective is to utilize an alternative method to calculate pressure drop in the steam tube and then compare the results with those produced from the R5 model. The following data are assumed:

Table E.1 Pressure Drop Calculation Assumptions

Parameter	**Value**	**Units**	**Parameter**	**Value**	**Units**
Inlet					
□	1.729	kg/s	ρ_l	722.4	kg/m^3
x	0	%	ρ_v	42.52	kg/m^3
P	8.0	MPa	μ_l	8.78e-5	Pa s
T	295.0	^{o}C	μ_v	1.94e-5	Pa s

Calculating the inputs to Equation 59:

$$G = \frac{}{A} = \frac{}{\pi(D^2)/_4} = \frac{1.729kg/s}{\pi(0.08m^2)/4} = 344.0kg/m^2s$$

$$\frac{L}{D} = \frac{15m}{0.08m} = 187.5$$

Then using Equation E.1 and Equation E.2 (Carey 1992) to calculate the friction factors:

$$f_l = 0.079\left(\frac{GD}{\mu}\right)^{-0.25}$$

$$= 0.079\left(\frac{344.0kg/m^2s(0.08m)}{8.78E-5Pa\ s}\right)^{-.025} = 0.0033 \quad \text{(E.1)}$$

$$f_v = 0.079\left(\frac{GD}{\mu}\right)^{-0.25} \quad \text{(E.2)}$$

$$= 0.079\left(\frac{344.0kg/m^2s(0.08m)}{1.94E-5Pa\ s}\right)^{-.025} = 0.0023$$

Three cases are evaluated using appropriate r_2, r_3 and r_4 values (Todreas 1993) at 8.0 MPa and channel inlet quality of 0.0: 0.0% channel exit quality estimate, 100% channel exit quality estimate, and, a 100% channel exit quality estimate with no empirical corrections (i.e., r_2, r_3 and r_4 values all equal 1.0). The first estimate uses the saturated liquid density and assumes the channel exit quality to be 0.0% (r_2=0.1, r_3=1.0 and r_4=0.92):

$$\Delta P_{channel} = \frac{1}{2}\frac{G^2}{\rho}\frac{L}{D}fr_3 + \frac{G^2}{\rho}r_2 + Lg\rho r_4$$

$$= \frac{1}{2}\frac{(344.0kg/m^2s)^2}{722.4kg/m^3}187.5(0.0033)1.0$$

$$+ \frac{(344.0kg/m^2s)^2}{722.4kg/m^3}0.1 \qquad (59)$$

$$+ 15.0m(9.8m/s^2)(722.4kg/m^3)0.92$$

$$= 50.7Pa + 16.4Pa + 97{,}697.4Pa = 97{,}764.8Pa$$

Assuming the saturated vapor density and a channel exit quality of 100% (r_2=18, r_3=10 and r_4=0.2):

$$\Delta P_{channel} = \frac{1}{2}\frac{G^2}{\rho}\frac{L}{D}fr_3 + \frac{G^2}{\rho}r_2 + Lg\rho r_4$$

$$= \frac{1}{2}\frac{(344.0kg/m^2s)^2}{42.52kg/m^3}187.5(0.0023)10$$

$$+ \frac{(344.0kg/m^2s)^2}{42.52kg/m^3}18 \qquad (59)$$

$$+ 15.0m(9.8m/s^2)(42.52kg/m^3)0.2$$

$$= 6{,}001.0Pa + 50{,}095.2Pa + 1{,}250.1Pa$$

$$= 57{,}346.3Pa$$

Finally, the saturated vapor density and a channel exit quality of 100% case with no empirical corrections (r_2=1, r_3=1 and r_4=1):

$$\Delta P_{channel} = \frac{1}{2}\frac{G^2}{\rho}\frac{L}{D}fr_3 + \frac{G^2}{\rho}r_2 + Lg\rho r_4 =$$

$$\frac{1}{2}\frac{(344.0kg/m^2s)^2}{42.52kg/m^3}187.5(0.0023)1 + \qquad (59)$$

$$\frac{(344.0kg/m^2s)^2}{42.52kg/m^3}1 + 15.0m(9.8m/s^2)(42.52kg/$$

$$m3$$

$$1 = 600.1Pa + 2{,}783.1Pa + 6{,}250.4Pa =$$

$$9{,}633.6Pa$$

It should be noted that the calculated frictional, acceleration and hydrostatic pressure drop components change significantly between the cases.

Appendix F : Exit Steam Temperature Heat Balance

The channel exit steam temperature can be estimated utilizing a first law energy, or heat balance. The calculations in this section are based on Equation 59 and Equation 60, which were presented previously. The following data are assumed:

Table F.1 Heat Balance Data Assumptions

Parameter	**Value**	**Units**	**Parameter**	**Value**	**Units**
Inlet					
□	1.729	kg/s	h_{fg}	1441.3	kJ/kg
x	75	%	h_f	1316.6	kJ/kg
P	8.0	MPa	h_{in}	1316.6+0.75(1441.3)=2397.6	kJ/kg
T	295.0	°C	q"A	1.63E3	kJ/s

$$h_{out} = h_{in} + \frac{q"A}{} = 2397.6\,{}^{kJ}/_{kg} + \frac{1.68E3\,{}^{kJ}/_{s}}{1.729\,{}^{kg}/_{s}} = 3369.2\,{}^{kJ}/_{kg} \quad (61)$$

Using the exit enthalpy of 3369.2 kJ/kg, and interpolating in the superheated steam table at 8.0 MPa between 480 °C (h=3348.4 kJ/kg) and 520 °C (h=3447.7 kJ/kg) (Holman 1980), the channel exit temperature is calculated to be 488.4 °C.

Appendix G : Thermal Radiation Transport – Optically Thick Approximation

Table G.1 presents calculated results for k_{steam} and $k_{total} = k_{steam} + k_r$ for comparison (at an assumed pressure of 8.0 MPa).

Table G.1 Steam Conductivity Increase with Optically Thick Assumption

				Thermal Radiation			
Temperature		θ	β_R	k_r	k_r	$k_{total} = k_{steam}$	$k_{total} = k_r + k_{steam}$
(^oC)	(K)	(T/555)	$(atm*m)^{-1}$	(Watm/mK)	(W/mK)	(W/mK)	(W/mK)
227	500	0.901	644.5	0.0587	0.0007	0.0710	0.0717
252	525	0.946	611.7	0.0715	0.0009	0.0733	0.0742
277	550	0.991	580.4	0.0867	0.0011	0.0758	0.0769
302	575	1.036	550.6	0.1044	0.0013	0.0783	0.0797
327	600	1.081	522.2	0.1251	0.0016	0.0810	0.0826
352	625	1.126	495.3	0.1491	0.0019	0.0838	0.0857
377	650	1.171	469.9	0.1767	0.0022	0.0867	0.0890
402	675	1.216	445.9	0.2086	0.0026	0.0898	0.0924
427	700	1.261	423.4	0.2450	0.0031	0.0929	0.0960
452	725	1.306	402.3	0.2864	0.0036	0.0962	0.0998
477	750	1.351	382.8	0.3333	0.0042	0.0996	0.1038
502	775	1.396	364.6	0.3860	0.0049	0.1031	0.1080
527	800	1.441	348.0	0.4449	0.0056	0.1067	0.1124
552	825	1.486	332.8	0.5102	0.0065	0.1105	0.1169
577	850	1.532	319.1	0.5820	0.0074	0.1143	0.1217
602	875	1.577	306.8	0.6603	0.0084	0.1183	0.1267
627	900	1.622	296.0	0.7447	0.0094	0.1224	0.1318
652	925	1.667	286.7	0.8348	0.0106	0.1266	0.1372
677	950	1.712	278.8	0.9299	0.0118	0.1309	0.1427
702	975	1.757	272.4	1.0289	0.0130	0.1354	0.1484
727	1000	1.802	267.5	1.1306	0.0143	0.1400	0.1543
752	1025	1.847	264.0	1.2336	0.0156	0.1447	0.1603
777	1050	1.892	262.0	1.3362	0.0169	0.1495	0.1664
802	1075	1.937	261.4	1.4370	0.0182	0.1544	0.1726
827	1100	1.982	262.3	1.5342	0.0194	0.1594	0.1788
852	1125	2.027	260.0	1.6560	0.0210	0.1646	0.1855
877	1150	2.072	260.0	1.7689	0.0224	0.1698	0.1922
902	1175	2.117	260.0	1.8868	0.0239	0.1752	0.1991
927	1200	2.162	260.0	2.0098	0.0255	0.1807	0.2062
952	1225	2.207	260.0	2.1380	0.0271	0.1864	0.2135
977	1250	2.252	260.0	2.2716	0.0288	0.1921	0.2209
1002	1275	2.297	260.0	2.4107	0.0305	0.1980	0.2285
1027	1300	2.342	260.0	2.5553	0.0324	0.2040	0.2363
1052	1325	2.387	260.0	2.7056	0.0343	0.2101	0.2443
1077	1350	2.432	260.0	2.8616	0.0362	0.2163	0.2525
1102	1375	2.477	260.0	3.0235	0.0383	0.2226	0.2609
1127	1400	2.523	260.0	3.1915	0.0404	0.2291	0.2695
1152	1425	2.568	260.0	3.3655	0.0426	0.2356	0.2783
1177	1450	2.613	260.0	3.5458	0.0449	0.2423	0.2872
1202	1475	2.658	260.0	3.7324	0.0473	0.2491	0.2964
1227	1500	2.703	260.0	3.9254	0.0497	0.2560	0.3058
1252	1525	2.748	260.0	4.1249	0.0522	0.2631	0.3153
1277	1550	2.793	260.0	4.3312	0.0549	0.2702	0.3251
1302	1575	2.838	260.0	4.5441	0.0576	0.2775	0.3351
1327	1600	2.883	260.0	4.7640	0.0603	0.2849	0.3453
1352	1625	2.928	260.0	4.9908	0.0632	0.2924	0.3556

VITA

Paul J. Marotta, P.E. was born in Mineola, New York on October 28, 1958. He graduated from New Lebanon High School in June, 1976. He received his Bachelor of Science degree in Applied Mathematics in 1980 from Siena College, and, his Bachelor of Engineering degree in Mechanical Engineering from Manhattan College in 1981. He then started work for General Electric at Knolls Atomic Power Laboratory in Schenectady, New York. While working full time as a Design Engineer, he completed the Knolls Design Power School in 1983, and received his Master of Science degree in Mechanical Engineering from Union College in 1985.

He went on to work for International Paper in 1988 where he held several positions in several locations including power plant engineer and environmental manager, Ticonderoga, New York, corporate environmental manager, Memphis, Tennessee, manufacturing manager, Clinton, Iowa, plant manager, Kansas City, Kansas, and senior corporate environmental engineer, Cincinnati, Ohio.

In September, 2001, he joined AquAeTer Inc., as the Operations Manager, where he is presently employed. He is a licensed professional engineer in New York, Michigan, Kentucky and Arkansas.

He married the former Margaret Ann Kissel in 1981, and they are the parents of three daughters and two sons.